

HETEROGENEOUS PHOTOCATALYSIS FOR THE TREATMENT OF CONTAMINANTS OF EMERGING CONCERN IN WATER

by

Jose Ricardo Alvarez Corena

A Dissertation

**Submitted to the Faculty
of the**

WORCESTER POLYTECHNIC INSTITUTE

**in partial fulfillment of the requirements for the
Degree of Doctor of Philosophy
in
Civil Engineering**

July 2015

APPROVED:

Dr. John A. Bergendahl, Assoc. Professor, Civil and Environmental Engineering, Worcester Polytechnic Institute,
Major Advisor

Dr. Frederick L. Hart, Professor, Civil and Environmental Engineering, Worcester Polytechnic Institute, Co-Advisor

Dr. Paul Mathisen, Assoc. Professor, Civil and Environmental Engineering, Worcester Polytechnic Institute

Dr. Jeanine D. Plummer, Assoc. Professor, Civil and Environmental Engineering, Worcester Polytechnic Institute

Dr. Robert W. Thompson, Professor, Chemical Engineering, Worcester Polytechnic Institute

**HETEROGENEOUS PHOTOCATALYSIS FOR THE
TREATMENT OF CONTAMINANTS OF EMERGING
CONCERN IN WATER**

By

Jose Ricardo Alvarez Corena

A Dissertation

Submitted to the

Faculty of Civil and Environmental Engineering

WORCESTER POLYTECHNIC INSTITUTE

in Partial Fulfillment of the Requirements for the

Degree of Doctor of Philosophy

in

Civil Engineering

July 2015



Dr. John A. Bergendahl

**Assoc. Professor of Civil &
Environmental Engineering**

Thesis Advisor



Dr. Fred L. Hart

**Professor of Civil & Environmental
Engineering**

Thesis Co-Advisor, Committee Member



Dr. Paul Mathissen

**Assoc. Professor of Civil &
Environmental Engineering**

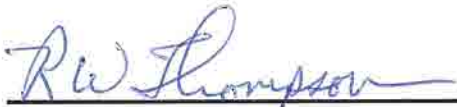
Committee Member



Dr. Jeanine D. Plummer

**Assoc. Professor of Civil &
Environmental Engineering**

Committee Member



Dr. Robert W. Thompson

Professor of Chemical Engineering

Committee Member

Date of Approval: 7/20/2015

ABSTRACT

The simultaneous degradation of five organic contaminants: 1,4 dioxane, n-nitrosodimethylamine, tris-2-chloroethyl phosphate, gemfibrozil, and 17 β estradiol, was investigated using a 1 L batch water-jacketed UV photoreactor utilizing titanium dioxide (TiO₂) nanoparticles (Degussa P-25) as a photocatalyst.

The primary objectives of this research were: (1) to experimentally assess the feasibility of heterogeneous photocatalysis as a promising alternative for the degradation of organic compounds in water; and (2) to model the chemical reactions by the application of two different approaches based on adsorption – surface reactions (Langmuir–Hinshelwood) and its simplification to a first order rate reaction. These objectives were motivated by the lack of information regarding simultaneous degradation of organic compounds in different categories as found in real aqueous matrices, and generation of specific intermediates that could eventually represent a potential risk to the environment. Contaminants were chosen based on their occurrence in water sources, their representativeness of individual sub-categories, and their importance as part of the CCL3 as potential contaminants to be regulated. Contaminant degradation was evaluated over time, and the TiO₂ concentration and solution pH were varied under constant UV irradiation, oxygen delivery rate, mixing gradient, and temperature.

Specific accomplishments of this study were: (1) reaction kinetics data were obtained from the UV/TiO₂ experiments and showed the potential that this UV/TiO₂ process has for effectively removing different types of organic compounds from water; (2) a good fit was obtained between photocatalytic reaction kinetics models and the contaminant data using pseudo first-order and Langmuir-Hinshelwood (L-H) models; (3) results of the analytical methods developed in this study were validated by measurements performed by a certified laboratory; (4) the reaction kinetic parameters obtained in this study were normalized to electrical energy per order, reactor volume and surface area of the photocatalyst in order to provide rate constants with wider applicability for scale-up to more complex systems; and (5) degradation intermediates from the oxidation process and from interaction among compounds were identified and possible pathways for their formation suggested. This research has provided a better understanding of the photocatalytic process for the removal of organic contaminants from complex aqueous matrices.

*I dedicate this thesis to
God, my parents Ana y Benjamin, my lovely wife Carolina and my beloved Sasha
for their constant support, patience and unconditional love.
I love you all deeply*

ACKNOWLEDGMENTS

Although this dissertation has required the effort and full dedication on the part of myself and my advisors it would not have been possible without the generous cooperation of each and every one of the people listed below; their support has been invaluable to me through many ups and downs in this process, both personally and professionally.

First and foremost, I want to thank God for being with me every step along the way, fortifying my heart, enlightening my mind, and providing on my path those companions and teachers who have been so essential and encouraging through the entire journey.

I would like to thank my PhD advisors Professor Fred Hart and Professor John Bergendahl for supporting me during the past four years. Professor Hart is the wisest person I have ever had the opportunity to meet. I am grateful not only for his contributions on a professional level, but beyond that for his wise counsel on a personal level regarding what life is all about. Words are inadequate to express all my gratitude to him for his encouragement to keep moving forward, and for his unconditional and permanent support of my family and myself. Professor Bergendahl is the smartest person I have ever had met. I cannot but admire his depth of experience and dedication to his profession. I am very proud to be his mentee. Working with his team has made me not only a better professional but a better person. I am absolutely sure that under his guidance I am moving in the right direction to pursue my dreams.

I would also like to specially thank Professor El-Korchi, I will always remember him fondly as he was the first person in the WPI community I met, that meeting being among the most fortunate things that have happened to me since arriving here in Worcester, MA. His priceless help and support in difficult times have encouraged me to keep giving my best. He is an excellent leader and host, and he always had a smile and heartening words when I needed it. I will be eternally grateful for everything he has done for me these past few years. Because of people like all of these, I can attest that angels exist on earth.

I would also like to thank my committee members Professor Paul Mathisen, and Professor Jeanine Plummer, for their acceptance in being part of my PhD committee, and whom I have had the great opportunity to work with.

Special thanks as well to Yechan Won and Alexis Simpson, my extra hands in the laboratory, for their help and enthusiasm. I wish you all the best to you both in your future endeavors. I would also like to thank Don Pellegrino, Russell Lang and Andrew Butler; they were really supportive and essential contributors to the completion of this work.

I would like to give special thanks to Agata Lajoie and Marylou Horazny. They were always there when I needed. Thank you ladies for your patience, friendship and kind words. I will really miss you both.

Last but not least, I would also give special thanks to my loving wife, Carolina. She is the engine of my life. Without her support this dream would never have become a reality. When we decided to come to this country, we really did not know all the challenges we would have to overcome to reach the point we currently are. With her help I am totally convinced that we can conquer any mountain and I am very fortunate to have her in my life. She has been at my side in the greatest and worst moments, and always has a word of encouragement and finds an alternative to keep us moving forward together. I would also thank my dear Sasha (our doggy). As my wife said, she is “*my perfect balance*”. The first one that greets me in the morning, and the last one I tuck in at night. Our furry child has been with us during the duration of my PhD studies. She has been my faithful companion during those long nights of study and hard work. I would also like to offer special thanks to my parents, Ana and Benjamin, for their belief in me. They have supported my efforts unwaveringly from the very beginning. I am very honored to be their son. They both have cared for me always; this achievement belongs to them too. Without their help and tenacity the fulfillment of my dreams could not have been realized.

This research was supported by the Stantec R&D Fund. The financial support provided by the funding agency is gratefully acknowledged.

TABLE OF CONTENTS

ACKNOWLEDGMENTS.....	III
I. INTRODUCTION	11
II. FUNDAMENTALS OF THE UV/TiO₂ PHOTOCATALYTIC REACTIONS IN AQUEOUS PHASE	14
2.1. Fundamentals of Oxidation.....	14
2.1.1. Advanced Oxidation Processes (AOP).....	14
2.1.2. Heterogeneous Photocatalysis	16
2.1.3. Photocatalysts/Semiconductors	17
2.1.4. UV Light.....	18
2.1.5. Mechanisms of the UV/TiO ₂ Photocatalytic Process	20
2.2. Kinetic Modeling of the UV/TiO ₂ Process	29
2.2.1. Reaction Rate Model	29
2.3. Organic Contaminants in Water.....	32
2.3.1. 1,4 dioxane.....	33
2.3.2. N-nitrosodimethylamine (NDMA).....	34
2.3.3. Tris (2-chloroethyl) phosphate (TCEP).....	35
2.3.4. Gemfibrozil.....	36
2.3.5. 17 β estradiol	37
III. EXPERIMENTAL MATERIAL AND METHODS.....	38
3.1. Chemicals and Reagents	38
3.2. Bench Scale Batch Reactor	38
3.3. Sample Preparation	39
3.4. Adsorption Experiments	39
3.5. Analytical Methods.....	39
3.6. Langmuir Hinshelwood Parameters.....	41
3.6.1. Langmuir Adsorption Constant, K_L (Lmg ⁻¹)	41
3.6.2. Reaction Rate Constant = k_{LH} (mgL ⁻¹ min ⁻¹)	41
3.7. First-order Reaction Rate Constant (min ⁻¹).....	42
3.8. Effectiveness of the System	43
3.8.1. PFR	43
3.8.2. CSTR	43
3.9. Normalization of First-order Kinetic Rates	43
3.9.1. Energy Normalized to Energy Delivered per Volume (k') - kW·h m ⁻³	43
3.9.2. First Order Removal Normalized to TiO ₂ Surface Area of (k'') - min ⁻¹ m ⁻²	44
3.9.3. First Order Removal Constant Normalized to TiO ₂ Surface Area & Energy Delivered (k''') - m ³ (kW·h) ⁻¹ m ⁻²	44
3.10. Adsorption Rates.....	44
3.11. Identification of intermediates	45
IV. RESULTS	46
4.1. Experimental Controls	46
4.2. Assessment of the Degradation Effectiveness of UV/TiO ₂	46
4.2.1. Factors Influencing the Photocatalytic Degradation	46

4.2.2.	Kinetics of UV/TiO ₂ Photodegradation of contaminants	49
4.2.3.	Kinetic Approaches	50
4.2.3.1.	Langmuir-Hinshelwood Approach	50
4.2.3.2.	Pseudo-First Order Kinetic Modeling Approach	58
4.3.	Additional Parameters to be used as Criterion to Move from Bench Scale Reactor to Pilot Scale System	59
4.3.1.	Normalization of Pseudo-first-order Kinetic Rates	59
4.4.	Extended Time Reactor Experiments	60
4.5.	Adsorption Rate Experiments	60
4.6.	Identification of Intermediates as Result of the Photocatalytic Degradation of Selected Compounds.....	61
4.6.1.	Suggested Pathways of Individual Degradation of Contaminants	63
4.6.2.	Random Interactions Among Partially Degraded Intermediates of the Parent Compounds	65
V.	DISCUSSION OF RESULTS.....	67
5.1.	Assessment of the Effectiveness of UV/TiO ₂	67
5.1.1	Effectiveness of UV/TiO ₂ Oxidation Based on Rate Constants.....	67
5.1.1.1.	1,4 dioxane	68
5.1.1.2.	NDMA	69
5.1.1.3.	TCEP	70
5.1.1.4.	Gemfibrozil.....	71
5.1.1.5.	17β estradiol	72
5.2.	Assessment of Scaling-Up Parameters	73
5.3.	Extended Time Experiments.....	75
5.4.	Adsorption Rate Experiments	76
5.5.	Formation of Oxidation Intermediates.....	76
5.5.1	Intermediates Formation by Random Interactions Among Compounds	79
VI.	CONCLUSIONS AND RECOMMENDATIONS.....	82
VII.	FUTURE WORK	85
VIII.	APPENDICES.....	86
APPENDIX A:	Information on Contaminants and Catalyst	86
APPENDIX B:	Sample Preparation – Analytical Techniques	87
APPENDIX C:	TiO ₂ Properties.....	100
APPENDIX D:	GC Calibration Curves and Detection Limits.....	101
APPENDIX E:	UV/TiO ₂ Oxidation Results at Different pH Levels (TiO ₂ = 0.1 gL ⁻¹).....	102
APPENDIX F:	UV/TiO ₂ Oxidation Results at Different TiO ₂ Concentrations (pH = 5)	103
APPENDIX G:	The Langmuir-Hinshelwood Kinetics Model Trends.....	104
APPENDIX H:	Linearized Langmuir Isotherm	105
APPENDIX I:	Pseudo-First Order Rate Constant Earlier Times – k (min ⁻¹).....	106
APPENDIX J:	Pseudo-First Order Rate Constants Normalized to Energy per Volume -- k' [m ³ (kW·h) ⁻¹]	107
APPENDIX K:	Pseudo-First Order Rate Constants Normalized to TiO ₂ Surface Area -- k'' (min ⁻¹ m ⁻²).....	108
APPENDIX L:	Pseudo-First Order Rate Constants Normalized to Energy & TiO ₂ Surface Area -- k''' (m ³ (kW·h) ⁻¹ m ⁻²)	109
APPENDIX M:	Combined Data Plotted as C/C ₀ versus Time for Each Compound	110
APPENDIX N:	Pseudo-First order Rate Constant for Combined Data (early and extended times).....	111
APPENDIX O:	Pseudo-First Order Rate Constants Normalized to Energy & TiO ₂ Surface Area -- k''' (m ³ (kW·h) ⁻¹ m ⁻²) for Combined Data.....	112
APPENDIX P:	Non-linear Adsorption Rate Data (q _t vs t).....	113
APPENDIX Q:	First Order Adsorption Kinetic Constants	114
APPENDIX R:	Spectral Energy Distribution Lamp series: 7825-30 (Ace Glass, Vineland, NJ, USA).....	115
IX.	BIBLIOGRAPHY	116

LIST OF FIGURES

Figure I-1 Publications pertaining to photocatalysis from the top 12 (overall) publishing nations [10].	11
Figure II-1 Relative disposition of the CB and VB for an insulator, a semiconductor, and a conductor.	17
Figure II-2 Band gap energy values of some photocatalysts.	18
Figure II-3 Range of electromagnetic wave.	19
Figure II-4 Wavelength vs. the rate of photoreaction [30].	19
Figure II-5 Mechanisms of the heterogeneous photocatalysis process.	21
Figure II-6 Typical bench-scale slurry reactor. Adapted from Zhang (2009) [52].	26
Figure II-7 Typical fixed-media reactor (annular type).	26
Figure II-8 Crystal structures of the two forms of titanium dioxide. (A) Rutile unit cell of titanium dioxide. (B) Anatase unit cell [75].	28
Figure II-9 1,4 dioxane structure [96].	33
Figure II-10. Photocatalytic degradation pathway of 1,4 dioxane using UV/TiO ₂ suggested by Maurino and colleagues [102].	34
Figure II-11 NDMA structure [96].	34
Figure II-12. Suggested pathways of NDMA using ozonation by Lv and colleagues [110].	35
Figure II-13 TCEP structure [96].	36
Figure II-14. Suggested pathways of TCEP using UV/H ₂ O ₂ by Ruan and collaborators [120].	36
Figure II-15 Gemfibrozil structure [96].	37
Figure II-16 17β estradiol structure [96].	37
Figure III-1 Photocatalytic reactor scheme.	38
Figure IV-1 Variation of first order degradation rate constants with variation in solution pH, k (min ⁻¹) (TiO ₂ concentration = 0.1 gL ⁻¹ , initial contaminant concentration = ~2 mgL ⁻¹).	47
Figure IV-2 Variation of first order degradation rate constants with variation of TiO ₂ concentration, k (min ⁻¹) (Solution pH = 5.0, initial contaminant concentration = ~2 mgL ⁻¹).	48
Figure IV-3 Degradation of the five contaminants by UV/TiO ₂ oxidation (Solution pH = 5.0, TiO ₂ = 1.5 gL ⁻¹ , initial contaminant concentration = ~2 mgL ⁻¹).	49
Figure IV-4 1,4 dioxane linearized data - Langmuir isotherm.	51
Figure IV-5 NDMA linearized data - Langmuir isotherm.	52
Figure IV-6 TCEP linearized data - Langmuir isotherm.	53
Figure IV-7 Gemfibrozil linearized data - Langmuir isotherm.	54
Figure IV-8 17β estradiol linearized data - Langmuir isotherm.	55
Figure IV-9 L-H model predictions for the UV/TiO ₂ degradation of five selected compounds. (Solution pH = 5.0, TiO ₂ = 1.5 gL ⁻¹ , initial contaminant concentration = ~2 mgL ⁻¹).	58

Figure IV-10 Pseudo-first order rate model predictions for the UV/TiO ₂ degradation of five selected compounds (Solution pH = 5.0, TiO ₂ = 1.5 gL ⁻¹ , initial contaminant concentration = ~2 mgL ⁻¹).....	59
Figure IV-11. Intermediates generated from the partial degradation of individual parent compounds separately.....	62
Figure IV-12. Suggested pathways of the degradation of gemfibrozil.	64
Figure IV-13. Suggested pathway of the degradation of 17β estradiol.....	65
Figure IV-14. Identified intermediates and suggested formation dependence of selected compounds in the simultaneous UV/TiO ₂ oxidation of 1,4 dioxane, 17β estradiol, gemfibrozil, NDMA and TCEP.	66
Figure V-1 CSTR and PFR predictions from collected data using the first order rate model for 5 minutes reaction time.	74
Figure V-2 CSTR and PFR predictions from collected data using the first order rate model for 10 minutes reaction time.	74
Figure V-3 Suggested alkyl shift mechanism to the formation of 2,3-dimethylphenol and 2,6-dimethylphenol.....	77
Figure V-4 Suggested pathway formation of 3-hydroxy-4-methylbenzaldehyde and 2-hydroxy-4-methylbenzyl alcohol.....	78
Figure V-5 Suggested pathway formation of 2,5-dimethyl-1,4-benzonquinone.....	78
Figure V-6 Suggested pathway of 3-methoxybenzaldehyde's formation.	79
Figure V-7 Suggested pathway of acetophenone's formation.	80
Figure V-8 Suggested pathway formation of methylcarbamic acid and 3,5-dimethylphenyl-N-methylcarbamate.....	80
Figure V-9 Suggested pathway formation of N-(4,6-dimethoxypyrimidin-2-yl)-2-methylpropanamide.....	81

LIST OF TABLES

Table II-1 Oxidation potentials of water treatment oxidants [20].	15
Table II-2 Examples of OH [•] reaction pathways [21].	15
Table II-3 List of various known AOPs.	15
Table II-4 Primary processes and time domains in titania-catalyzed mineralization of organic pollutants.	24
Table II-5 Pros and cons of using slurry photoreactors.	26
Table II-6 Pros and cons of using fixed-media photoreactors.	27
Table II-7 Typical support materials used in TiO ₂ photocatalysis in fixed-media reactors	27
Table IV-1 Variation of first order degradation rate constants with variation in solution pH, k (min ⁻¹) (TiO ₂ concentration = 0.1 gL ⁻¹ , initial contaminant concentration = ~2 mgL ⁻¹).	47
Table IV-2 Variation of first order degradation rate constants with variation of TiO ₂ concentration, k (min ⁻¹) (Solution pH = 5.0, initial contaminant concentration = ~2 mgL ⁻¹).	49
Table IV-3 1,4 dioxane adsorption data to obtain K _L parameter.	51
Table IV-4 NDMA adsorption data to obtain K _L parameter.	52
Table IV-5 TCEP adsorption data to obtain K _L parameter.	53
Table IV-6 Gemfibrozil adsorption data to obtain K _L parameter.	54
Table IV-7 17β estradiol adsorption data to obtain K _L parameter.	55
Table IV-8 Values of q _{max} , K _L and k _{LH} for CECs	56
Table IV-9 Solver used to calculate k _{LH}	57
Table IV-10 Values for the L-H kinetic parameters, K _L and k _{LH} , found for the contaminants studied in this work	58
Table IV-11 Normalized pseudo-first order kinetics constants k' , k'' , and k''' . (Conditions: pH 5, 1.5 gL ⁻¹ of TiO ₂).	60
Table IV-12 Final concentrations of contaminants after extended UV/TiO ₂ oxidation reaction times.	60
Table IV-13 Pseudo-first order adsorption rate constants on TiO ₂ surface, using 1.5 gL ⁻¹ of TiO ₂ and initial contaminant concentrations = ~ 3 mgL ⁻¹	61
Table V-1 Comparison between first order kinetics and the product of k_{LH} × K_L	67
Table V-2 Results of 1,4 dioxane - Treatability studies.	69
Table V-3 Results of NDMA - Treatability studies.	70
Table V-4 Results of TCEP - Treatability studies.	71
Table V-5 Results of Gemfibrozil - Treatability studies.	72
Table V-6 Results of 17β Estradiol - Treatability studies.	73
Table V-7 First order degradation rate constants for UV/TiO ₂ oxidation, and % of difference with early times kinetics at 1.5 gL ⁻¹ of TiO ₂ , pH 5.0, and 100W UV power using the combined data	76

Table of abbreviations

K_L	Langmuir adsorption constant (Lmg^{-1})
k_{LH}	Reaction rate constant ($mgL^{-1}min^{-1}$)
k_s	Surface reaction rate constant
k	First-order reaction rate constant (min^{-1})
k'	First order rate constant normalized to energy per volume [$m^3 \cdot (kw \cdot h)^{-1}$]
k''	First order removal normalized to TiO_2 surface area of ($min^{-1}m^{-2}$)
k'''	First order removal constant normalized to TiO_2 surface area & energy delivered ($m^3 (kw \cdot h)^{-1}m^{-2}$)
SA	Surface area of TiO_2 (m^2). The specific surface area of P-25 Degussa TiO_2 is $59 m^2g^{-1}$
r	First order reaction rate ($mgL^{-1}min^{-1}$)
r_s	Photocatalytic first order rate
C_0	Initial concentration of contaminant (mgL^{-1})
C	Final concentration of contaminant at time t (mgL^{-1})
t	Reaction/exposure time (min)
C^*	Adjusted concentration of contaminant (mgL^{-1}) to determine k_{lh} values
C_e	Equilibrium concentration of contaminant after 24 hrs adsorption (mgL^{-1})
q_e	Mass of contaminant adsorbed/mass of TiO_2 ratio present at equilibrium (mgg^{-1})
q_{max}	Maximum contaminant adsorption onto TiO_2 surface at equilibrium (mgg^{-1})
x	Amount of contaminant (mg) adsorbed at different TiO_2 concentrations at equilibrium
m	Mass of TiO_2 (g)
TiO_2	Titanium dioxide
BR	Batch reactor
CSTR	Continuous stirred tank reactor
PFR	Plug flow reactor
UV	Ultraviolet light
E_d	Energy delivered ($kw \cdot h$)
P	Power of the lamp used for performing the experiments in the UV range (constant and equal to 4.6 W for this work)
v	Volume of a sample (ml)
V	Reactor volume (m^3)
CEC	Contaminant of emerging concern
NDMA	N-nitrosodimethylamine
TCEP	Tris-2-chloroethyl phosphate
E	Energy of photon (in eV) as a function of wavelength λ (m)
h	$6.626 \times 10^{-34} J s$ (Planck's constant)
u	$2.998 \times 10^8 m s^{-1}$ (speed of light)
6.24×10^{-18}	Conversion factor for the energy from Joules to electron volts (eV).

I. INTRODUCTION

According to the United Nations, water scarcity issues are linked to most of the Millennium Development Goals [1]; therefore, water pollution control is increasing in importance throughout the world. Numerous studies show that a significant amount of organic pollutants derived from municipal, agricultural, and industrial wastewater sources are now being detected in our waters. These compounds are most commonly so-called Contaminant of Emerging Concern (CECs) and are related to adverse health-effects and environmental impacts, even at very low concentrations [2-6]. To minimize the impacts caused by their uncontrolled disposal, the development and implementation of advanced technologies is needed because conventional treatment processes like precipitation-coagulation, air stripping, and biological treatment have shown to be relatively ineffective in removing them from contaminated waters as compared to advanced oxidation processes (AOPs) [7, 8].

A growing interest in both academic and industrial communities on AOPs is evident by the increased number of publications in peer-reviewed journals, an increasing number of patents, and international conferences dedicated to environmental applications of AOPs. Over 5,700 articles have been published in journals covered by the Science Citation Index between 2005 and 2011 dealing with processes such as heterogeneous photocatalysis, hydrogen peroxide (H_2O_2), ozonation, photolysis, Fenton's reactions, wet air oxidation, and ultrasound. Approximately 25% of these publications are related to the photocatalytic process [9]. Figure I-1 illustrates the increased activity of publications in the photocatalysis area.

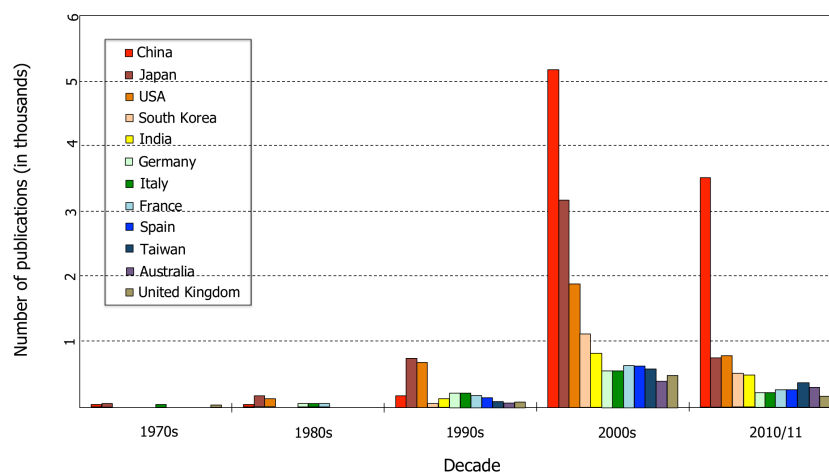


Figure I-1 Publications pertaining to photocatalysis from the top 12 (overall) publishing nations [10].

Heterogeneous photocatalytic oxidation is a promising technique for the degradation of chemicals encountered in our waters. This mechanism involves the acceleration of a

photoreaction in the presence of a solid semiconductor photocatalyst (i.e. TiO_2 , ZnO , ZnS , etc.) [11]. The process of photocatalysis begins with an initiation step or excitation of the photocatalyst by means of an irradiation source (i.e. UV lamp, sunlight) that enhances the production of several highly reactive radical-species (i.e. hydroxyl radicals (OH^\bullet)), which produce redox reactions that contribute to the degradation of organic contaminants.

One of the earliest investigators who focused on the degradation of contaminants in water was Carey (1976) [12]. He reported in his study on the photodechlorination of polychlorobiphenyls (PCBs), that heterogeneous photocatalysis is a potential new method for the treatment of organic pollutants in water. Since then, the evolution of the photocatalytic process for water purification has evolved significantly [16-24].

Among the different photocatalysts available for photocatalysis, the use of titanium dioxide combined with ultraviolet light (UV/ TiO_2) represents a promising technology within the wide range of advanced oxidation processes. This technique has potentially relevant advantages over many of the current AOPs such as high capability to degrade a wide variety of organic contaminants from water, low production of toxic byproducts, availability, and low operational costs [13-15]. The UV/ TiO_2 process may be performed either in a slurry-type reactor (where the TiO_2 particles are suspended in the water to be treated), or in a fixed-media type reactor (where the catalyst particles are onto the surface of a stationary media). A major disadvantage of the slurry technique is that it requires a supplementary solid/liquid separation step such as decantation, filtration or centrifugation to remove the catalyst from the effluent. In spite of immobilized catalysts might be a solution to the separation issue, the main drawback of using this system is its restricted processing capacity due to possible mass transfer limitations [16].

In general terms, detailed kinetics analyses/design of complex photocatalytic reactors for water treatment may be problematic, due to the high degree of difficulty scaling them up to full scale. Simplified models are a good alternative to compare different reaction systems under similar operating conditions and to provide estimated values for scaling-up purposes [17]. The overall aim of this thesis was to investigate the kinetics of the photocatalytic degradation of five compounds that include a nitrosamine (n-nitrosodimethylamine –NDMA–), a flame retardant (tris-2-chloroethyl phosphate –TCEP–), an organic solvent (1,4 dioxane), a hormone (17 β estradiol), and a pharmaceutical (gemfibrozil). This group of contaminants was evaluated by using a bench scale UV/ TiO_2 -slurry reactor. The selection of compounds was based on their occurrence in water sources, their representativeness of individual sub-categories, and their importance as part of the EPA contaminant candidate list 3 (CCL3) [18] and draft regulation of the California Department of Public Health's (CDPH's) [19].

Rate constants with wider applicability for scale-up were also provided. The first-order rate constants were normalized to power delivered in the UV range and TiO_2 surface area. The

parameters obtained from these approaches may help designing pilot units to better understanding of the photocatalytic process and the assessing of its efficacy treating contaminated large water samples. In addition, intermediates produced from the photocatalytic reactions on the TiO₂ surface were identified and pathways of their formation were also suggested, which promote investigation regarding the photocatalytic reaction trends in complex matrices with real samples, and the evaluation of toxicity of intermediates in future studies.

Consistent with the preceding discussion, the following specific aims and hypothesis were defined to guide this research:

Specific aims:

- Assess the ability of the UV/TiO₂ technology to remove selected contaminants from water.
- Evaluate that the adsorption–surface reaction Langmuir–Hinshelwood (L–H) approach effectively describes the kinetics of photodegradation of the selected contaminant as well as its simplification to a first order rate in experiments at low concentration levels of the compounds.
- Determine additional parameters that may assist on the scale up of the bench scale UV/TiO₂ reactor into a pilot scale system to remove contaminants using real water samples.
- Identify and suggest pathways of formation of intermediates generated from the interactions among partial derivatives of the selected compound.

Hypotheses:

- The pH of the water to be treated by UV/TiO₂ significantly influences the effectiveness of the system, because this parameter is related to the adsorption behavior of compounds onto the photocatalyst surface.
- The UV/TiO₂ technology is an AOP that follows either a first order rate law and/or the L–H model at low contaminant concentration levels of pollutants.
- The effectiveness of the UV/TiO₂ technology to degrade contaminants in water strongly depends on the amount of catalyst (surface area).
- Interactions among partially degraded compounds take place on the TiO₂ surface.

II. FUNDAMENTALS OF THE UV/TiO₂ PHOTOCATALYTIC REACTIONS IN AQUEOUS PHASE

A general background and definition of the heterogeneous photocatalytic process including constituents, catalyst properties, mechanisms, and kinetics of degradation will be developed through each section of this chapter based on fundamentals of the reduction and oxidation mechanisms, which belongs to the category of advanced oxidation processes (AOPs) for water treatment.

2.1. Fundamentals of Oxidation

Many chemical species have a natural tendency to either accept or donate electrons based on the fact that a lower energy state (greater stability) is achieved as a consequence of the electron exchange. The reactions that follow such pathways are called oxidation and reduction reactions (redox reactions).

An oxidation half-reaction occurs when a chemical species loses electrons while at the same time the chemical species increases its oxidation number, whereas a reduction half-reaction takes place when a chemical species gain electrons resulting in a decrease in its oxidation number.

Oxidation of reduced inorganic and organic species is commonly utilized in the water treatment field to control taste and odor, hydrogen sulfide, treat for color, iron and manganese removal, and for disinfection processes. Some of the oxidants employed to achieve these purposes are chlorine, oxygen (e.g. aeration processes), H₂O₂, potassium permanganate, chlorine dioxide, iodine, UV light, ozone (O₃), etc. [11].

2.1.1. Advanced Oxidation Processes (AOP)

Advanced oxidation is a process involving hydroxyl radicals (OH[•]) used for the destruction of organic pollutants in water [3]. OH[•] radicals react at fast rates, with rate constants ranging from 10⁸ to 10⁹ M⁻¹s⁻¹ [11]. It is a powerful, non-selective oxidant that is effective for the treatment of many compounds in water due to its high oxidation strength. The hydroxyl radical's oxidation potential (2.80 V) is only surpassed by that of the fluorine molecule (Table II-1).

Table II-1 Oxidation potentials of water treatment oxidants [20].

Species	Symbol	Oxidation potential (Volts)
Fluorine	F ₂	3.00
Hydroxyl free radical	OH [•]	2.80
Ozone	O ₃	2.07
Hydrogen peroxide	H ₂ O ₂	1.76
Permanganate ion	MnO ₄	1.68
Hypochlorous acid	HOCl	1.49
Chlorine	Cl ₂	1.36
Hypobromous acid	HOBr	1.33
Hypoiodous	HIO	0.99
Chlorine dioxide	ClO ₂ (aq)	0.95
Iodine	I ₂	0.54
Oxygen	O ₂	0.40

Once generated, OH[•] can react in water by different pathways listed in Table II-2.

Table II-2 Examples of OH[•] reaction pathways [21].

Mechanism	Example Reaction
Hydrogen abstraction	OH [•] + CHCl ₃ → CCl ₃ + H ₂ O
Addition	OH [•] + C ₆ H ₆ → C ₆ H ₆ - OH
Electron transfer	OH [•] + [Fe(CN) ₆] ⁴⁻ → [Fe(CN) ₆] ³⁻ + OH ⁻
Radical interaction	OH [•] + OH [•] → H ₂ O ₂

Some of the main advantages of using AOPs include the following: (i) they can achieve complete mineralization of organic contaminants, (ii) they can achieve removal of recalcitrant compounds, and (iii) they can be used as a pretreatment step for subsequent biological treatment processes. A list of various AOPs is provided in Table II-3.

Table II-3 List of various known AOPs.

AOP Technologies	
H ₂ O ₂ /UV light	O ₃ /Sonolysis
H ₂ O ₂ /O ₃	Supercritical water oxidation
UV/TiO ₂	O ₃ /TiO ₂
O ₃ /UV	O ₃ /TiO ₂ /H ₂ O ₂
O ₃ /UV/H ₂ O ₂	Nonthermal plasma
O ₃ (8<pH<10)	Electron beam irradiation
(Fe/H ₂ O ₂ or Fe/O ₃)	O ₃ /electron beam irradiation
Sonolysis	Gamma radiation

Some of the commercially available AOP technologies are: (i) ozone (O_3) hydrogen peroxide (H_2O_2) and (ii) UV light and H_2O_2 .

Ozone (O_3) is a strong oxidant that has the capacity to react with organic contaminants and ultimately degrade them. Ozone is able to oxidize organic pollutants directly or indirectly through the formation of OH^\bullet . Nakada et al. [22] showed the removal efficiencies of 24 pharmaceutically active compounds during sand filtration and ozonation including two phenolic antiseptics, thymol and triclosan. Ozonation exhibited good removal efficiencies, producing 91% and 84% removal, respectively. From this study, it was also concluded that compounds with an aromatic structure with electron donors like phenols were specifically susceptible to ozone treatment.

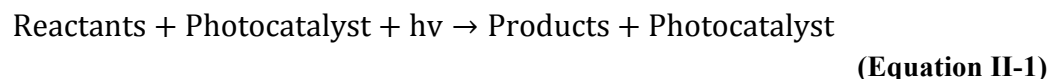
H_2O_2 is another powerful oxidant that can be used to degrade organic contaminants in aqueous solution, and becomes very efficient when combined with other reagents or other energy sources capable of dissociating this oxidant into OH^\bullet radicals.

Radiation may be also employed to enhance the production of OH^\bullet radicals. Some electromagnetic radiation examples are: γ -radiation, electron-beam, ultrasonication and UV radiation. In this category UV/ H_2O_2 and heterogeneous photocatalysis may be included as a combined method using UV radiation.

Kim et al. [23] investigated the removal of 41 pharmaceuticals from wastewater using UV/ H_2O_2 in a $10\text{ m}^3\text{day}^{-1}$ bench-scale experiment. Kim reported 90% removal effectiveness for the majority of the pharmaceuticals investigated using a UV dose of 923 mJcm^{-2} in 5 minutes, which is good, taking into account the recalcitrant nature of this compounds.

2.1.2. Heterogeneous Photocatalysis

A catalyst is defined as a substance that increases the speed of a chemical reaction without being consumed as a reactant. A catalyst reduces the free activation energy of the overall reaction, and is not part of the stoichiometric Equation representing the reaction [24]. Heterogeneous photocatalysis produces an increase in the rate of a chemical reaction brought about by visible, ultraviolet, or infrared radiation absorbed by a photocatalyst. This can be expressed as follows:



UV/ TiO_2 is a heterogeneous photocatalytic AOP technology, which is based on the effect that a semiconductor (TiO_2) has on the degradation of contaminants when activated by UV light. The reaction mechanisms depend on the formation of a redox pair to generate OH^\bullet and other strong oxidants (O_2^\bullet , HOO^\bullet , $HOOH$, HO^\bullet , OH^- , H_2O , h^+_{VB} , and so on). To carry out the photocatalytic

process, there are two important elements to consider: (i) the semiconductor (photocatalyst), and (ii) the light source (UV light in this case).

2.1.3. Photocatalysts/Semiconductors

Semiconductors are materials used in the contemporary age of crystal electronics; their electrical properties are intermediate between those of metals (e.g. gold) and insulators (e.g. silicon oxide). This is due to a special configuration of the energy levels of electrons in semiconductors [25]. In other words, semiconductors can be also defined as a material which energy gap for electronic excitations lies between zero and around 4 electron volts (eV). Materials with zero band-gap are metals or semimetals, while those with an energy level gap (where no electronic states exist), larger than 4 eV are more frequently known as insulators [26].

On figure II-1 each of the constituents of the electronic bands in solids are identified. It is important to explain the meaning of each part that constitutes a semiconductor. In general terms IUPAC [27] defines the valence band (VB) as “the highest energy continuum of energy levels in a solid that is fully occupied by electrons at 0 K. VB is lower in energy than the conduction band and is generally completely full in semiconductors”. When heated, electrons from the VB jump out into the conduction band (CB) across the band gap making the material electrically conductive generating holes and electrons in each band respectively.

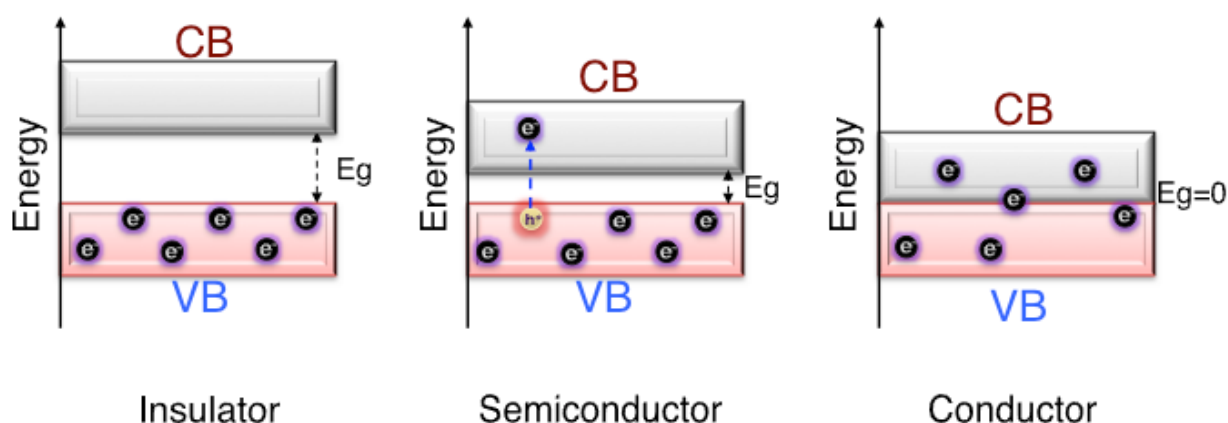


Figure II-1 Relative disposition of the CB and VB for an insulator, a semiconductor, and a conductor.

Different semiconductors have been successfully used to remove organic contaminants from water via advanced oxidation; some of them are: TiO_2 , ZnO , ZrO_2 , CdS , MnOS_2 , Fe_2O_3 , and WO_3 [28]. TiO_2 has been one of the most widely used photocatalysts for environmental applications, especially for the treatment of organic contaminants in water due to its biological

and chemically inertness, economically feasibility, resistance to chemical corrosion and photo corrosion, and its ability to treat a wide range of organic contaminants [29].

When irradiated at appropriate conditions, electrons from the valence band (VB) jump to the conduction band (CB) across the band gap making TiO_2 as well as other semiconductors electrically conductive. The band gap energy (E_g) defines the minimum photon energy absorbed by the photocatalyst. Figure II-2 illustrates the band gaps and the band levels (V vs. standard hydrogen electrode (SHE) at pH 7) of some semiconductive materials. The lower edge of the conduction band (red color) and upper edge of the valence band (blue color) are presented along with the band gap in electron volts. The wider a band gap is, the more energy (short wavelength) is needed to activate the transfer of electrons between bands. In terms of feasibility, TiO_2 forms need less energy than ZnS to activate their photocatalytic behavior. However, in spite of CdS requires less energy than the TiO_2 forms, its nanoparticles could be potentially toxic, making TiO_2 the most widely photocatalyst used in environmental applications [29].

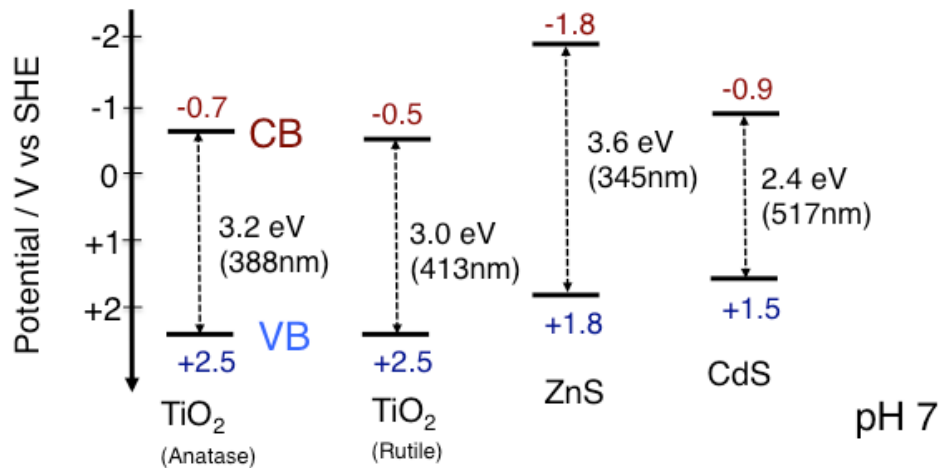


Figure II-2 Band gap energy values of some photocatalysts.

2.1.4. UV Light

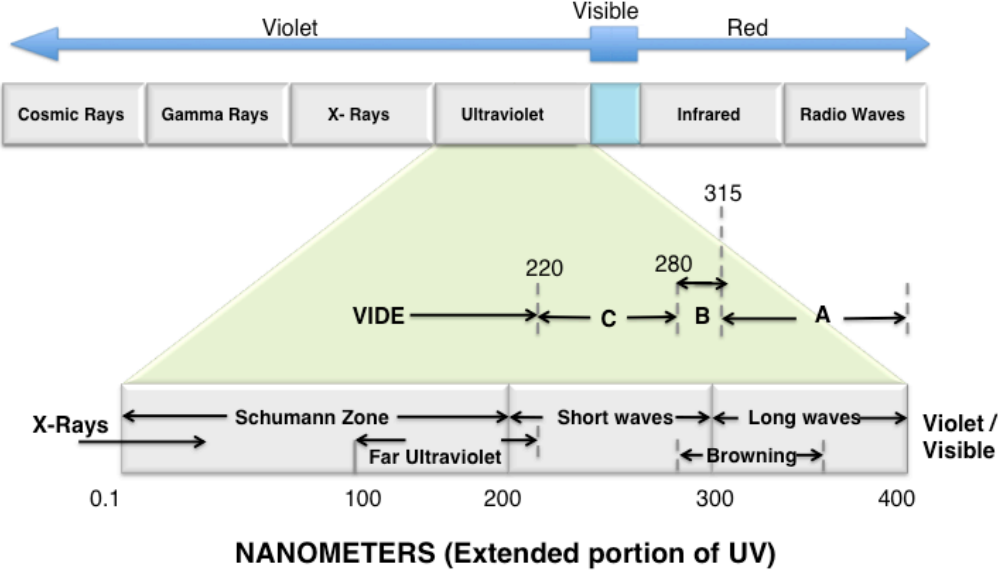
UV light is an electromagnetic radiation with a wavelength that falls between the range of gamma rays and visible light (100 nm to 400 nm), and contains energies from 3 eV to 124 eV respectively (Figure II-3). The energy of a photon (in eV) as a function of wavelength λ (m) as given by:

$$E = \frac{h\nu}{\lambda} \times 6.24 \times 10^{-18}$$

(Equation II-2)

Where, $h = 6.626 \times 10^{-34}$ J s (Planck's constant), $\nu = 2.998 \times 10^8$ m s⁻¹ (speed of light), 6.24×10^{-18} = conversion factor for the energy from Joules to electron volts (eV).

For heterogeneous photocatalysis applied to water treatment, characteristics that affect the overall effectiveness of the process include: wavelength, quantum yield, photon flux rate, and UV irradiance.



NANOMETERS (Extended portion of UV)
Figure II-3 Range of electromagnetic wave.

- Incident UV Wavelength (λ):** UV/TiO₂ photocatalysis requires $\lambda \leq 400$ nm, i.e. near-UV wavelengths (UV-A) for effective treatment. Figure II-4 shows the variations of the reaction rate (r) as a function of incident wavelength, with a threshold corresponding to its band-gap energy. In addition, it must be checked that the reactants do not absorb the light to conserve the exclusive photoactivation of the photocatalyst by heterogeneous photocatalytic regime (no homogeneous or photochemistry in the adsorbed phase). Only 3–5% of solar irradiation is in the UV spectrum. To successfully accomplish photoactivation using sunlight, the TiO₂ surface is often treated by doping or coating mechanisms to widen the range of absorbable wavelength [30].

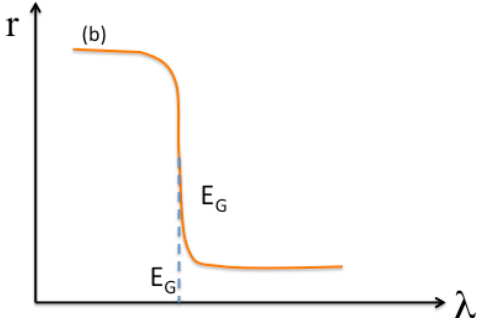


Figure II-4 Wavelength vs. the rate of photoreaction [30].

- Quantum yield: Photocatalytic processes involve the initial absorption of photons by the substrate to produce highly reactive electronically excited states [31]. In terms of effectiveness, one of the most frequently utilized parameters to describe photochemical activity is quantum yield [32], which is defined as the number of radicals produced on the photocatalyst surface during the primary reaction processes per photon absorbed by the photocatalyst [33].

- Irradiance/light intensity: Known as the radiant power of the wavelength incident on a small surface, involving the relationship between the point under consideration and the area of the element. The common units to express this characteristic are Wm^{-2} [27]. Ollis et al. [34] and Hoffmann et al. [35] assessed the effect of the irradiance on the photocatalytic degradation rate and quantum effectiveness, and concluded that:
 - Low irradiance: This case becomes irradiance dependent and the reaction rate obeys a first order decay rate, while the photon flux as well as the quantum yield remains constant.

 - Intermediate irradiance: The reaction rate is directly related to the square root of the irradiance. In this case, the rate transition from intermediate to low intensity depends on the fixed catalytic configuration and mass transferred.

 - High irradiance: This case ends in a growth in volumetric reaction rate until the mass transfer limit is achieved. At this condition, the reaction rate increases volumetrically below the mass transfer limit, and once it is achieved the reaction rate becomes independent of the irradiance, therefore the reaction rate order is zero.

2.1.5. Mechanisms of the UV/TiO₂ Photocatalytic Process

Photocatalysis is a process that involves different steps and a large number of reactions in series and in parallel. Figure II-5 depicts a general overview of the mechanisms involved in the photocatalytic activity of TiO₂ as an AOP process, from the UV light irradiation to the generation of OH[•] radicals and other strong oxidant agents that facilitate the degradation of contaminants in water. The primary mechanisms identified in the UV/TiO₂ process are (1) charge carrier generation, (2) charge transport, (3) charge trapping, (4) charge recombination, and (5) overall TiO₂ surface mechanisms that occur among the other steps.

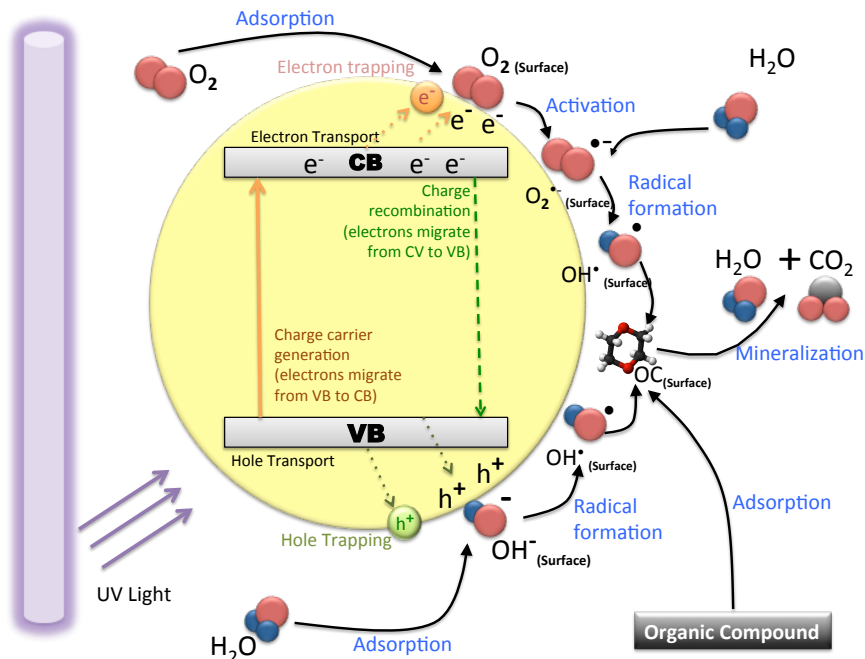
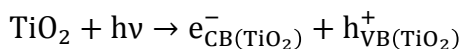


Figure II-5 Mechanisms of the heterogeneous photocatalysis process.

- **Charge Carrier Generation:** TiO_2 molecule photoconductivity is initiated when exposed to a source of light (photons) with an energy level higher than their band-gap energy level ($h\nu \geq E_g$). In general, a light with a wavelength shorter than 387.5 nm gives the amount of energy needed to exceed the band-gap of pure anatase TiO_2 and excite an electron to move from the VB to the CB [36].

This transfer involves the formation of an electronic vacancy or positive hole (h^+_{VB}) at the VB, and presence of an electron (e^-_{CB}) at the CB. This can be expressed as follows:



(Equation II-3)

An important point to keep in mind during this step is the instability of the photogenerated electron-hole pairs, with a high possibility of recombination of the photogenerated electron-hole pairs that occurs in a very short time and dissipate energy as heat [37].

- **Charge transport:** The photocatalytic activity of TiO_2 produces charge migration from the lattice of the TiO_2 structure (where charge carrier generation is originated) to the bulk surface (where the interactions with other compounds will be achieved). Charge separation and thermalization mechanisms are critical components in charge transport.

The dielectric constant is a key parameter for the charge separation step. The more excitation energy applied to the TiO₂ semiconductor, the greater electron and hole activation will take place. Therefore, charge thermalization depends on the photons' energy, and is thought to be a first order mechanism that occurs very quickly (on the order of picosecond timescale in the anatase phase [38]).

- Charge trapping: A trap site is recognized as a location in the TiO₂ material where there is greater charge carrier stability; such location is mostly placed at the surface of TiO₂. Other trap site locations may be particle interfaces, grain boundaries or in the bulk lattice. In the aqueous phase, electrons can also be trapped at the surface of TiO₂ by any of the hydroxyl groups previously formed. It has been shown that timescale is inversely related to the presence of electron scavengers such as O₂ on the TiO₂ surface.

Structural parameters of TiO₂ such as the morphologies of the lattice surface and interface are significant limiting factors that influence electron transport, and consequently affect the trapping and de-trapping phenomena. The latter consists of the conversion of a localized electron state to a free electron. Trapping mechanisms might be favorable only if they allow photon activity to generate charge carriers, and permit charge carriers to reach the electron transfer spots. Otherwise it could be disadvantageous for the overall photocatalytic process.

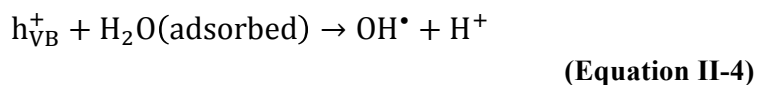
- Charge recombination: This stage corresponds to the end of the charge generation mechanism, and it is considered an adverse outcome in a photocatalytic process because it decreases the probability of keeping a favorable condition for the oxidation of contaminants [39]. In other words, it can reduce the production of hydroxyl radicals.

The degree of crystallinity among the overall structural properties (surface forms, defects and impurities) of TiO₂ plays an important role in the recombination mechanism, which is more likely to be associated with non-irradiative energy release. The common ways to quantify recombination of charge carriers related to non-irradiative actions are through indirect measurements (i.e. photo-acoustic measurements, heat generation measurements, etc.).

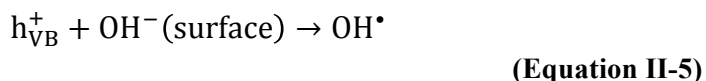
- TiO₂ surface/interfacial mechanisms: There are two essential mechanisms that take place on the surface and interfacial areas of the TiO₂ molecule and allow for the degradation of contaminants. The first one is the generation of active species with high oxidation potential as a consequence of the interaction between the charge carriers with adsorbed oxygen and water molecules. And the other one is the adsorption of pollutants by the semiconductor surface and direct attack by the trapped electrons and holes previously produced. The combination of these two processes makes TiO₂ photocatalysis a powerful

tool to treat organic pollutants in water as well as increase its already large number of applications in other fields.

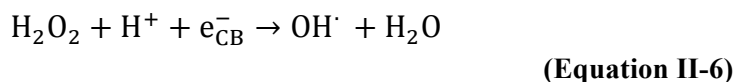
- Generation of active species: One of the key mechanisms carried out during the photocatalysis is the generation of active species such as hydroxyl radicals (OH^\bullet) and superoxide radicals ($\text{O}_2^{\bullet-}$) considered as the most important ones due to their important contribution to the overall effectiveness of the photocatalytic process over other high active species like trapped electrons, hydrogen peroxide (H_2O_2), and single oxygen (O_2) that are also produced but in a minor scale. The holes mediate the oxidation of organic compounds by the formation of hydroxyl radicals, and the electrons mediate reduction and oxidation reactions by the formation of superoxide radicals [40].
 - Hydroxyl radical (OH^\bullet): This high reactive form of the hydroxide ion is one of the most important species generated through the photocatalytic process, and is considered to be the main responsible oxidant in the degradation of organic compounds. It is produced when adsorbed water is oxidized by the electron hole Equation II-4



Another pathway to generate this radical is by the reaction between positive holes and hydroxide ion (Equation II-5)



Studies have shown that in the range of pH between 10.6 and 12.3 the formation of OH^\bullet can occur at a higher standard electrode potential than in the formation of H_2O_2 . Some authors have also concluded that the generation of OH^\bullet in photocatalysis should only obey the pathway portrayed in Equation II-6, instead of those represented by Equation II-4 and Equation II-5. It also has shown in recent studies that the influence of OH^\bullet in photo oxidation is not always predominant [38].



- Superoxide radical ($\text{O}_2^{\bullet-}$): This radical predominately acts as a reductant. In non-alkaline solutions, CB electrons reduce the Ti_4^+ surface, responsible for adsorbing

water, and the molecular oxygen attacks in acidic solutions, while in alkaline solutions, the adsorbed O₂ captures a CB to generate O₂^{•-}.

For anatase thin film, the quantum yield of O₂^{•-} has been reported to be 0.8 in water with a weak irradiation (1 μWcm⁻²) of UV light. Generally speaking, the formation of O₂^{•-} in a photocatalytic process is suggested to follow either Equation II-7 or Equation II-8.



- Adsorption: Since the recombination rate of photogenerated electrons and holes occurs very fast (on the order of picoseconds), the interfacial transfer of electrons is only kinetically competitive when some relevant donor or acceptor is pre-adsorbed prior to the photolysis. Hydroxyl groups or water molecules can act as traps for photogenerated surface holes, forming OH[•] radicals superficially linked, which may act in charge transfer processes with specific functional groups that previously had been adsorbed. The charge transfer between the oxide surface and the adsorbed molecule will produce an alteration within the possible excited states that can be detected. These spectral changes are associated with an offset or widening of the absorption bands.

Table II-4 provides a time estimate for each mechanism in the UV/TiO₂ process. It is important to note that these values may include a large range as they are obtained from different sources.

Table II-4 Primary processes and time domains in titania-catalyzed mineralization of organic pollutants.

Mechanism	Duration
<i>Charge carrier generation</i>	
TiO ₂ + hv → e ⁻ + h ⁺	fs (very fast)
<i>Charge carrier trapping</i>	
h ⁺ + Ti ^{IV} OH → Ti ^{IV} OH ^{•+}	10 ns (fast)
e ⁻ + Ti ^{IV} OH → TiOH ^{III}	100 ps (dynamic equilibrium)
e ⁻ + Ti ^{IV} → Ti ^{III}	10 ns (deep trap)
<i>Charge recombination</i>	
e ⁻ + Ti ^{IV} OH ^{•+} → Ti ^{IV} OH	100 ns (slow)
h ⁺ + Ti ^{III} OH → Ti ^{IV} OH	10 ns (fast)
<i>Interfacial charge transfer</i>	

Mechanism	Duration
$\text{Ti}^{\text{IV}}\text{OH}^{\bullet+} + \text{compound}$ $\rightarrow \text{Ti}^{\text{IV}}\text{OH}$ + oxidized compound	100 ns (slow)
$\text{Ti}^{\text{III}}\text{OH} + \text{O}_2 \rightarrow \text{Ti}^{\text{IV}}\text{OH} + \text{O}_2^{\bullet-}$	ms (very slow)

In terms of quantity and quality, there are numerous parameters that affect the photocatalysis process; and as a consequence, determine the overall performance of the process. Some important parameters are: pH, temperature, type of reactor, photocatalyst (TiO_2) morphology, and light intensity (previously discussed).

- pH: This parameter directly affects the surface charge of the photocatalyst. At low pH values (3–5), the catalyst surface progressively increases its positive charge, becoming more electrostatically attractive to negatively charged compounds, and consequently bringing a favorable condition for the surface adsorption mechanism. In general terms, pH affects the photocatalyst's surface properties and the chemical form of the compound to be degraded. This may be seen in changes in the reaction rates and the tendency for the photocatalyst to aggregate. The more control on the solution pH, the better the treatment effectiveness [41].
- Temperature: The reaction rate of photocatalytic reactions is not appreciably altered when the temperature of the system is modified. The optimum range of temperature varies from 20°C to 80°C [42], where the activation energy in most of the photocatalytic processes is stable. This is the typical range of temperature of reactions photo-chemically initiated by photon adsorption. An increase of temperature above 80°C has been reported to be counterproductive for the overall photocatalytic process [43].
- Type of reactors: Characteristics such as geometry, optical properties, light distribution, type (slurry, batch, plug) will play an important role over the overall performance of the system. All bench-scale photocatalytic reactors are based on two well-identified reactor types: (i) the complete-mixed slurry batch reactor where TiO_2 particles are suspended in the aqueous solution, and (ii) the fixed media reactor where TiO_2 particles are attached onto stationary surfaces within the reactor [44].
- Slurry Reactor: The main characteristic of this type of reactor is that catalyst particles are suspended in water and completely mixed. Most bench scale studies have used slurry-type reactors [45-49]. Figure II-6 illustrates a typical bench-scale slurry reactor configuration. The pros and cons of using a slurry reactor are listed in Table II-5 [34, 50, 51].

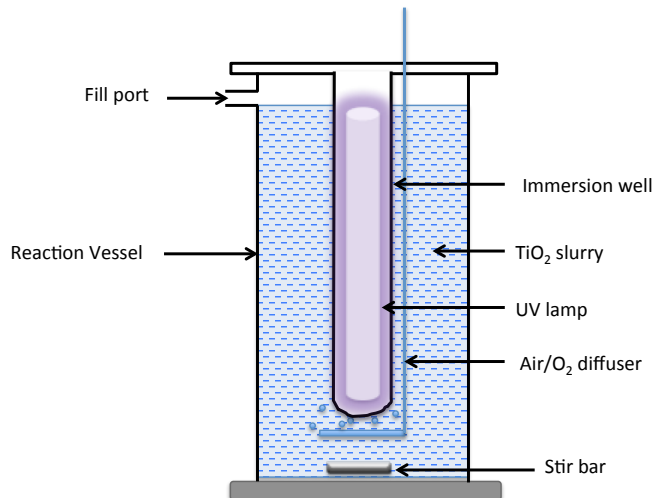


Figure II-6 Typical bench-scale slurry reactor. Adapted from Zhang (2009) [52].

Table II-5 Pros and cons of using slurry photoreactors.

Pros	Cons
High external mass transfer	Requires post treatment separation
Adjustable photocatalytic surface area	Considerable light scattering and attenuation
Uniform catalyst distribution	
Low hydraulic loss through the reactor (for flow-through reactors)	

- Fixed-Media Reactor: As its name indicates, this type of reactor is defined by the immobilization of catalyst on stationary media inside the reactor (Table II-6). Oftentimes, the TiO_2 is coated on support materials within the reactor. Common support materials are listed in Table II-7.

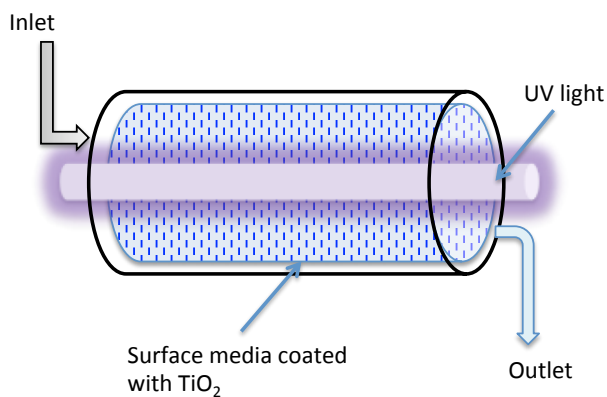


Figure II-7 Typical fixed-media reactor (annular type).

Table II-6 Pros and cons of using fixed-media photoreactors

Pros	Cons
Post treatment separation not required	Limited photocatalyst surface area
Light not attenuated by particles in bulk (does not pass through slurry)	Limited treatment effectiveness due to mass transfer limitations
Allows for continuous flow-through system operation	Cannot quickly switch photocatalysts

Table II-7 Typical support materials used in TiO₂ photocatalysis in fixed-media reactors

TiO ₂ support	Ref
Activated Carbon	[53]
Optical fiber cable	[54, 55]
Fiber glass	[56]
Glass	[57]
Glass beads	[58]
Glass wool	[59]
Membranes	[60]
Quartz sand	[61]
Zeolites	[53]
Silica gel	[16, 62]
Stainless steel	[63, 64]
Ceramic membranes	[65]
Teflon	[66]

- TiO₂ morphology: The overall photocatalytic performance of TiO₂ has been suggested to depend on some specific parameters such as crystallinity, phase, particle size, and surface area [67]. TiO₂ exists in three main different crystalline modifications: the stable rutile, and the metastable both brookite and anatase, which are common in natural and synthetic examples; however, anatase exhibits the highest overall photocatalytic activity [68].

Titanium dioxide materials consist of crystalline and amorphous phases [69]. The crystalline phase of TiO₂ is one of the most important factors influencing its photocatalytic performance. Anatase and rutile TiO₂, both with tetragonal structure, are commonly used in photocatalytic reactions. Anatase TiO₂ is conventionally believed to be more efficient photocatalyst than rutile TiO₂ due to its higher Fermi level, lower capacity to adsorb oxygen and higher degree of hydroxylation [70]. However, some authors has reported that both anatase and rutile have almost the same photocatalyst activity [71], as well as others lean to support that rutile exhibits a higher one [72].

Typically, anatase TiO₂ exists as primary nanoparticles in the 6 nm to 104 nm size range [73]. Surface area impacts the charge transport mechanism and consequently the overall

photocatalytic effectiveness of UV/TiO₂ process [74]. This is attributed to the interfacial characteristics, as well as the photon absorption on the particle due to stable surface sites for electron trapping. Size might also influence the light absorptivity and scattering on the TiO₂ surface also [38].

Figure II-8 illustrates the unit cell structures of rutile and anatase TiO₂ crystals. These two crystalline structures are comprised of chains of TiO₆ octahedra, where each Ti⁴⁺ ion is enclosed by an octahedron of six O₂ ions. These structures vary in the degree of distortion of each octahedron and by the assembly arrangement of the octahedral chains. In rutile, the octahedron exhibits a slight orthorhombic distortion; in anatase, the octahedron is considerably more distorted so that its symmetry is lesser than orthorhombic.

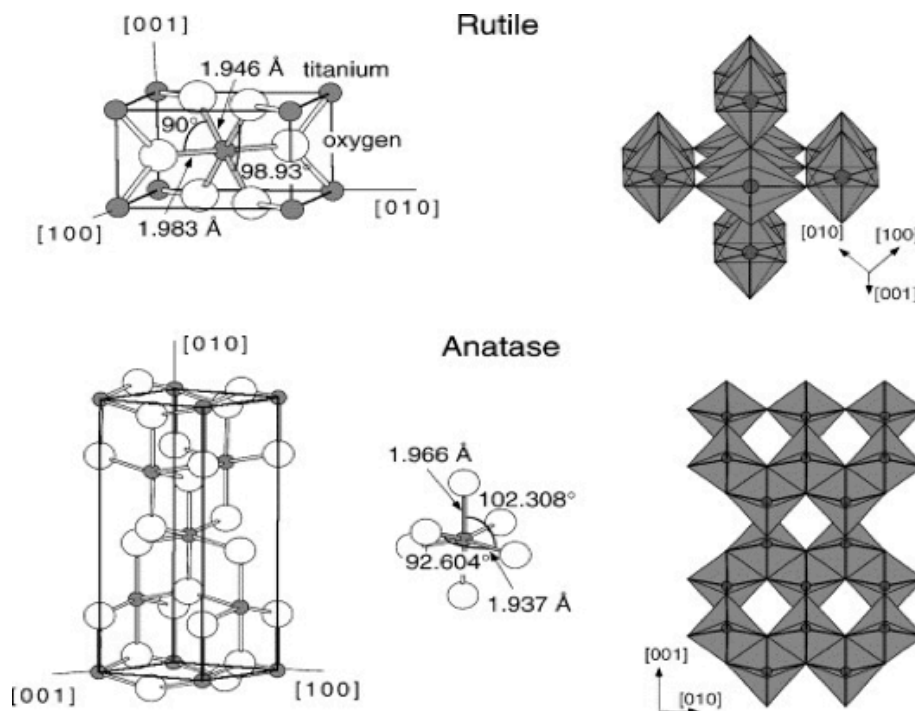


Figure II-8 Crystal structures of the two forms of titanium dioxide. (A) Rutile unit cell of titanium dioxide. (B) Anatase unit cell [75].

The greater photocatalytic effectiveness of Degussa P25 over other forms of TiO₂ photocatalyst is due to (1) a high degree of light absorption effectiveness is attributed to the synergistic combination of anatase-rutile, (2) a longer lifespan of carrier electrons attributed to the stable properties of rutile [76].

2.2. Kinetic Modeling of the UV/TiO₂ Process

An approach to kinetic modeling using chemical reaction rates can be used to: (1) evaluate data obtained from batch and pilot scale reactors, and (2) estimate performance of the UV/TiO₂ process taking place in reactors. There are three general mathematical constructs that have been used for modeling the UV/TiO₂ photocatalytic system:

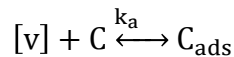
- Reaction rate model: This model describes the reaction carried out in the system using kinetic parameters and empirical and semi-empirical data found in the literature for UV/TiO₂ water treatment modeling.
- Radiation transport model: This model is capable of predicting the local volumetric rate of energy absorption (LVREA) from elements such as catalyst concentration, optical properties of the catalyst model light source, reactor geometry and other parameters.
- Material transport model: This model uses the standard radiation transport model, which is coupled with additional information such as reactor geometry. The substrate concentrations are specified to generate output variables such as the remaining contaminant concentration in a solution.

The reaction rate model has the greatest utility for modeling the UV/TiO₂ treatment process and is described below. It is a useful approach as it can model the treatment effectiveness and is mathematically tractable.

2.2.1. Reaction Rate Model

The photocatalytic process is mainly given by the adsorption of a substrate (C) (e.g. organic contaminant) on the catalyst surface (e.g. TiO₂). The rate of the photocatalytic process depends on the amount of C adsorbed onto the catalyst surface and is represented by the adsorption-desorption and surface reaction mechanisms as follows:

- Adsorption



(Equation II-9)

Where [v] is a vacant site in the surface of a catalyst, and the rate of adsorption (r_a) is given by:

$$r_a = k_a [v]C$$

(Equation II-10)

- Desorption



Where [o] is an occupied site in the surface of a catalyst released, and the rate of desorption (r_d) is given by:

$$r_d = k_d[o]C \quad \text{(Equation II-12)}$$

When Equations II-9 and II-11 reach the equilibrium condition, r_a and r_d are equal. The total sites onto the photocatalyst surface is $[v]+[o]$. Therefore, combining Equations II-9 and II-11 and dividing them by $[v] + [o]$ yields:

$$\frac{k_a[v]C}{[v] + [o]} = \frac{k_d[o]C}{[v] + [o]} \quad \text{(Equation II-13)}$$

Substituting the relationship between $[o]/[v] + [o]$ equals to θ , and $[v]/[v] + [o]$ equals to $(1 - \theta)$ the simplified equation is:

$$k_a C(1 - \theta) = k_d \theta C \quad \text{(Equation II-14)}$$

Where θ is defined as the fractional site covered by the substrate and depends on the substrate concentration in the reactive environment. Rearranging Equation II-14, and substituting the adsorption constant, also known as Langmuir constant $K_{LH}=k_a/k_d$ yields:

$$\theta = \frac{K_{LH}C}{1 + K_{LH}C} \quad \text{(Equation II-15)}$$

- Surface reaction

There are four scenarios in which the OH^\bullet radical may attack a compound in a photocatalytic reaction: (i) when both the contaminant and the OH^\bullet radical are bounded to the photocatalyst surface, (ii) when the OH^\bullet radical is bounded to the photocatalyst surface and the contaminant is in the bulk media, (iii) when the contaminant is bounded to the photocatalyst surface and the OH^\bullet radical is in the bulk media and (iv) when both reactants are in the bulk media.

Assuming that the rate of oxidation is the limiting reaction-mechanism that takes place on the occupied sites of the photocatalyst surface by both reactants (scenario i), the reaction may be expressed as:



Where P corresponds to an intermediate compound generated from the degradation of C by the hydroxyl radical at a specific site. The second order rate (r_s) expression, in which k_s is the surface reaction rate constant can be written as:

$$r_s = -k_s[\text{OH}^{\bullet}][\text{C}] \quad \text{(Equation II-17)}$$

The Langmuir–Hinshelwood (L–H) kinetic model has been widely accepted [28, 29, 58, 77-80] to describe the photocatalytic kinetics, in which the rate of oxidation at maximum coverage of sites on the photocatalyst surface is related to the substrate concentration, and may be expressed as:

$$r = k_s \theta \quad \text{(Equation II-18)}$$

Substituting Equation I-18 into Equation II-15 yields:

$$r = k_s \frac{K_{\text{LH}}C}{1 + K_{\text{LH}}C} \quad \text{(Equation II-19)}$$

For low substrate concentrations ($<10^{-3}\text{M}$ [81]) $K_{\text{LH}}C \ll 1$, therefore the L–H Equation may be simplified to a pseudo-first-order kinetic law (Equation I-20) with respect to Equation II-19 is equal to:

$$r = k_s K_{\text{LH}}C \quad \text{(Equation II-20)}$$

Where:

$$k_{\text{first-order}} = k_s K_{\text{LH}} \quad \text{(Equation II-21)}$$

Substituting Equation II-21 into Equation II-20

$$r = k_{\text{first-order}}C \quad \text{(Equation II-22)}$$

While at high substrate concentrations ($>5 \times 10^{-3} \text{M}$ [81]) $K_{LH}C \gg 1$, the reaction rate is of apparent zero order:

$$r_s = k_s \quad \text{(Equation II-23)}$$

The values of K_{ads} (obtained from the adsorption isotherm) and those of K_{LH} (obtained from the photocatalytic reaction) may differ from each other because the photocatalytic reaction is influenced by several parameters such as reaction mechanisms, formation of intermediates, oxygen concentration, irradiation, total number of adsorption sites, and overall properties of the photocatalyst. Consequently, some assumptions have to be taken into account when using the L-H model to describe the photocatalytic oxidation processes.

Some of the most important considerations taken into account when applying the L-H isotherm model to describe the photocatalytic oxidation process are: (i) one single substrate molecule can only occupy one surface site, (ii) the reaction is assumed to happen between adsorbed species, (iii) the coverage of adsorbed species on the photocatalyst surface is always in equilibrium with the concentration of the species in the fluid phase, therefore the surface reaction is the controlling step of the photocatalytic process, and (iv) the OH^\bullet radical are the predominant oxidizing agent that reacts with the organic compounds.

The study of kinetics models and the interpretation of experimental data are very important for reactor scale-up. Although some authors report that the L-H model could have some issues not fully assimilated [82], the majority of the studies describe the behavior of the UV/TiO₂ process using the L-H model as a useful approach to the heterogeneous reactions involved in the photo-conversion of organic compounds [83-85].

Most published works report kinetic models for fixed media [86] and suspended media [87] systems. These models are exclusively empirical and do not allow any further explanations to the phenomena involved into the system. They generate estimated information about the behavior of process influenced by the different species to be degraded. The majority of published research look at photocatalytic degradation using a single model compound (i.e. 4-chlorophenol, organic dyes, and so on) [40] with the exception of a few studies [40, 78, 88].

2.3. Organic Contaminants in Water

The concern for organic contaminants in water has increased in recent years because a broad range of persistent organic pollutants have been identified in many waters, and are reported to be a danger to humans and aquatic life [89-93]. In this thesis, the UV/TiO₂ degradation of five different contaminants, which include an oxidation byproduct, a flame retardant, an organic solvent, a hormone, and a pharmaceutical, was evaluated through use of a bench scale UV/TiO₂-

slurry reactor. A brief description of each contaminant and treatment methods applied by others for their removal in water are discussed in section 5.1.1.

2.3.1. 1,4 dioxane

1,4 dioxane is classified as cyclic ether that has four carbon and two oxygen atoms resulting in two ether functional groups. Because the oxygen atoms are facing each other to form symmetrical ether bonds, this structure makes the 1,4 dioxane molecule highly stable and relatively resistant to reaction with acids, oxides and oxidizing agents [94]. In addition, 1,4 dioxane is highly soluble in water due to the polarity acquired by the molecule when forms a dimer with two intermolecular hydrogen bonds, and consequently, the two remaining oxygen atoms will be accessible for interaction with the molecule of water [95].

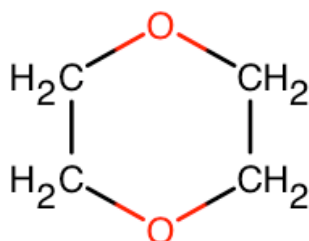


Figure II-9 1,4 dioxane structure [96].

1,4 dioxane is industrially produced from the reaction of ethylene glycol with sulfuric acid heating at 160°C, and also occurs as a reaction byproduct in several industrial processes to produce plastics and soaps. This compound has a wide number of commercial applications being its use as stabilizer for chlorinated solvents and solvent for natural and synthetic resins among the top ones [94]. The U.S. Environmental Protection Agency (USEPA) has classified this compound as a probable human carcinogen [97] among other health hazard effects that require more investigation. According to Fetter [98] 1,4 dioxane is classified as a compound that exhibits a high mobility, which makes its control and treatment very complicated.

This compound has been broadly used in many applications including: electrical, agricultural and biochemical reactants, adhesives, sealants, cosmetics, pharmaceuticals, rubber chemicals, surface coatings, and also as a stabilizer in chlorinated solvents. It has been also found to cause deleterious effects in humans and animals, including cancer, mutagenesis, and teratogenesis.[99]. This compound has low volatility, is resistant to biodegradation in water [100], and has been found to be inefficiently degraded by direct UV photolysis due to weak absorbance of UV light [101]. Figure II-10 shows the photocatalytic degradation pathway of the oxidation of 1,4 dioxane by UV/TiO₂ suggested by Maurino [102]. In addition to the dioxane derivatives shown in figure II-10, another intermediates have been reported by Stefan and Bolton such as: 2-hydroxy-1,4-dioxane, which suggest that the degradation pathway may start with a hydroxylation of the parent compound, and methoxyacetic acid [103].

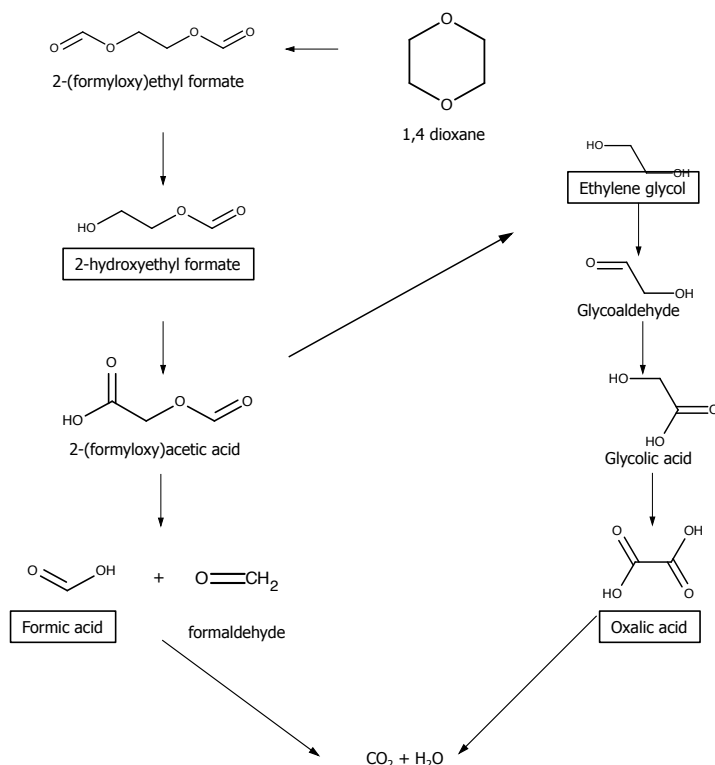


Figure II-10. Photocatalytic degradation pathway of 1,4 dioxane using UV/TiO₂ suggested by Maurino and colleagues [102].

2.3.2. N-nitrosodimethylamine (NDMA)

N-nitrosodimethylamine (NDMA) is a polar and hydrophilic compound that belongs to the nitrosamine group, characterized by the N-N=O structure, which compounds are mainly formed from secondary amines [104]. In drinking water its formation is mainly attributed to a couple of pathways [105] (1) the dichloramine-oxygen pathway during chloramination and (2) free chlorine-nitrate during chlorination in waters with high presence of nitrates.

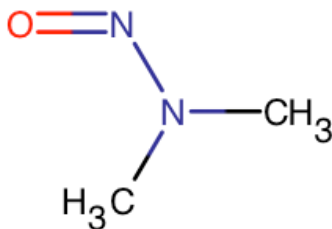


Figure II-11 NDMA structure [96].

The U.S. Environmental Protection Agency (USEPA) has classified this compound as a probable human carcinogen in group B2 [97] and established a cleanup level of 0.7 ngL⁻¹ for NDMA in groundwater [106], there is evidence of the genotoxicity of this compound [107], and it is also

categorized as a recalcitrant organic compound in aqueous phase [108]. In addition, due to its slow rate of degradation in water, NDMA can remain in potable water distribution systems [109]. Suggested pathways and intermediates of the NDMA oxidation by means of ozonation are shown in Figure II-12. Main products of the NDMA degradation are methylamine, ammonia and dimethylamine [110, 111]

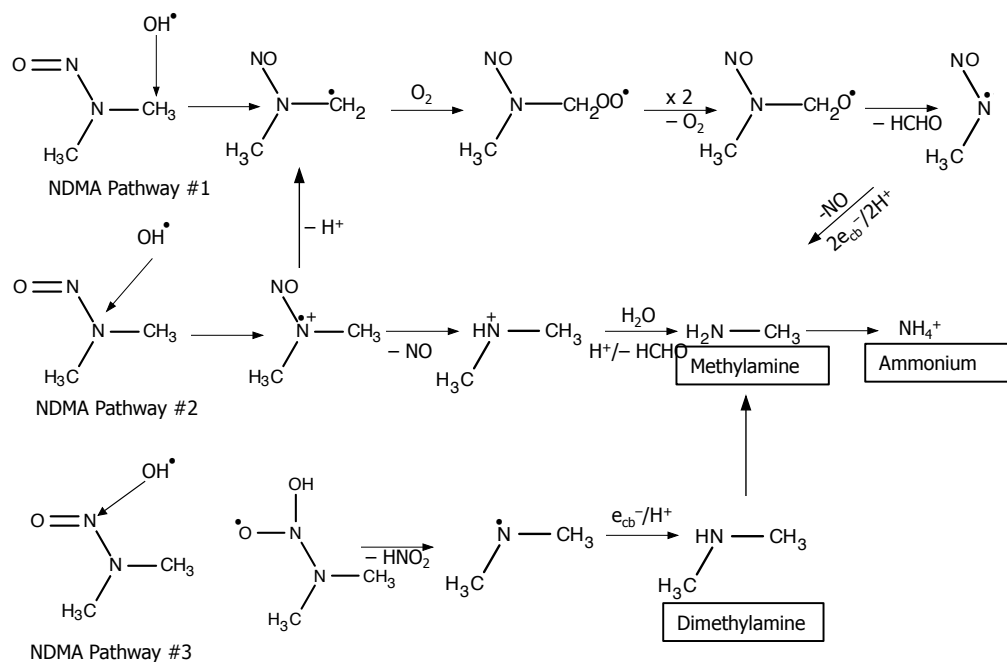


Figure II-12. Suggested pathways of NDMA using ozonation by Lv and colleagues [110].

2.3.3. Tris (2-chloroethyl) phosphate (TCEP)

Tris (2-chloroethyl) phosphate (TCEP) is a halogenated phosphate ester, that is widely used as flame retardant and plasticizer especially used in flexible foams for the automotive, furniture and construction industry. This compound exhibits a recalcitrant nature and has been regularly detected in different water bodies around the world [112-114] because its good solubility in water 7 g L^{-1} [115]. Sigma Aldrich [116] gives a code N to this compound, which means that this compound is hazardous for the environment.

This compound is difficult to remove through conventional treatment methods such as coagulation, sand filtration and chlorination, and represents a health risk as it has been found to be neurotoxic, mutagenic, and carcinogenic [117]. In addition, it has been found to be somewhat resistant to oxidative processes [112], including advanced oxidation, and it has been regularly detected in different water bodies around the world [112-114]. TCEP concentration values have been reported in several water sources. For example, concentrations of TCEP of 23 ng L^{-1} were found in water samples taken from the Danube River at Nussdorf [118]. A maximum

concentration level of 640 ng L^{-1} was found in the influent in the Ruhr/Rhine area, while in other study a level of 7 ngL^{-1} was detected in the Tiber River.

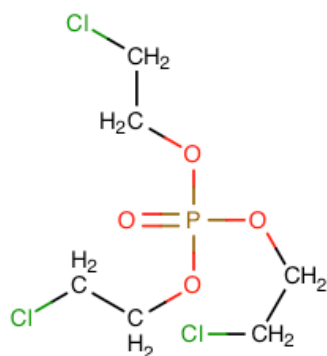


Figure II-13 TCEP structure [96].

Organophosphorous esters such as TCEP can be degraded by nucleophilic substitution reactions at the central phosphorous atom [119]. In the suggested pathway shown on figure II-14, the degradation of TCEP base-catalyzed hydrolysis favors P–O cleavage to end up with phosphoric acid. From the breaking bonds O–R of the TCEP molecule, another moiety is generated (2-chloroethanol), which is finally transformed into glycolic acid and other minor byproducts (not shown) that were described in the degradation pathway of 1,4 dioxane such as formic and acetic acids. This pathway was suggested by Ruan and collaborators [120].

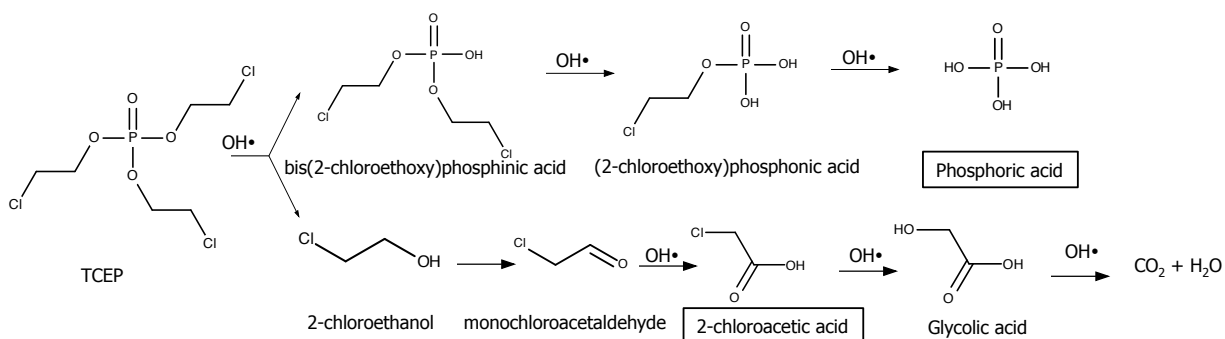


Figure II-14. Suggested pathways of TCEP using UV/H₂O₂ by Ruan and collaborators [120].

2.3.4. Gemfibrozil

Gemfibrozil is a non-biodegradable pharmaceutical mainly used to reduce cholesterol and triglycerides (fatty acids) in human blood. Gemfibrozil solubility in water is 5 mgL^{-1} [121]. This compound is a widely-used pharmaceutical that has been found in the environment in many studies [122, 123]. Studies of its occurrence have reported that it is a highly-persistent compound in water bodies [124]. Daughton [125] reported its presence at ngL^{-1} levels in Brazilian sewage treatment works (STWs) and there is evidence that could potentially affect reproductive systems in aquatic live [126, 127]. It may be treated with variable effectiveness using various treatment technologies such as AOPs.

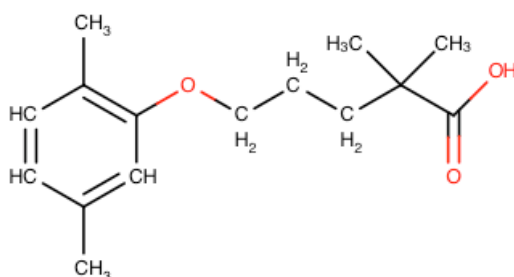


Figure II-15 Gemfibrozil structure [96].

There is a lack of information about detailed degradation pathways of gemfibrozil. Murai et al [128] suggested that degradation of this pharmaceutical is favored by the ethereal oxygen (C-O-C) cleavage, which leads to the formation of the p-xylene moiety. Yukardai and colleagues [128] also support this fact and found that 2,2-dimethyl-5-oxopentanoic acid was also formed as an intermediate of that cleavage by means of UV/TiO₂ photocatalysis..

2.3.5. 17β estradiol

17β estradiol is a hormone that constitutes the most potent form of mammalian estrogenic steroid [129]. There are several reports of environmental occurrence for this compound found in wastewater, drinking water, ground water, and soils [130]. Studies have shown that alterations of this hormone in individuals (females) prone to migraines could cause headaches [131] and can cause negative effects on the endocrine systems of humans and wildlife even at low concentration levels [132]. The exposure to this compound negatively impacts the reproductive function in wildlife [92].

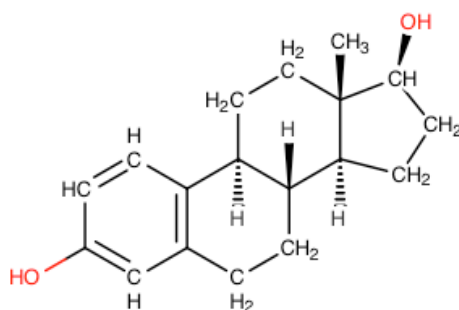


Figure II-16 17β estradiol structure [96].

There is little information about detailed degradation pathways of 17β estradiol. Ohko and colleagues [133] suggested estrogenic species formed in the photocatalytic oxidation of the hormone. Some of their main findings were testosterone species, 2-hydroxyestradiol, estrone, and 17β-dihydroxy-1,4-estradien-one.

III. EXPERIMENTAL MATERIAL AND METHODS

3.1. Chemicals and Reagents

Titanium (IV) oxide nanopowder (Aeroxide P25, $\geq 99.5\%$) was used as a photocatalyst in this work. The following chemicals were used as received: 1,4 dioxane (Sigma-Aldrich, 99.8%), n-nitrosodimethyl-amine (Sigma-Aldrich, 98%), tris (2-chloroethyl) phosphate (Sigma-Aldrich, 97%), gemfibrozil (Sigma-Aldrich, 98%), and 17β estradiol (Sigma-Aldrich, $\geq 98\%$). All reagents used for chromatographic analyses were HPLC grade: methylene chloride (Fisher Scientific, 99.9%) as solid phase extraction eluent, chlorobenzene (Sigma-Aldrich, 99.9%) as internal standard, and purified water was prepared using a Thermo Scientific Barnstead Nanopure Life Science UV/UF system with TOC analyzer, which produced effluent with $\text{TOC} \leq 5 \mu\text{gL}^{-1}$.

3.2. Bench Scale Batch Reactor

Photocatalytic experiments were performed in a 1 L water-jacketed batch photoreactor (Ace Glass, Vineland, NJ, USA), provided with a double-walled quartz immersion well with removable inner cooling tube, and a medium pressure, mercury-vapor lamp of 100 watt with approximately 40-48% of the radiated energy in the ultraviolet portion of the spectrum (Appendix R). A refrigerated bath circulator unit (NESLAB™, RTE-111) was employed to keep the temperature of the water in the reactor constant at $20 \pm 2 \text{ }^\circ\text{C}$ (Figure III-1). During experiments a Fisher Scientific magnetic stirrer was set up to 700 rpm to assure the complete mix of the aqueous samples in the unit, and a constant rate flow of $3 \text{ ft}^3\text{min}^{-1}$ of pure oxygen was supplied.

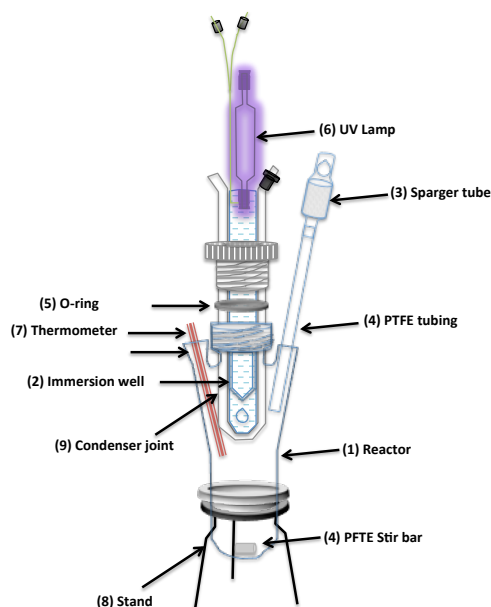


Figure III-1 Photocatalytic reactor scheme.

3.3. Sample Preparation

A solution containing all compounds together, each at $\sim 2 \text{ mgL}^{-1}$, was selected based on the detection limit of the GC instruments and was prepared in a glass carboy each week and mixed with a predetermined mass of TiO_2 to obtain varying catalyst concentrations: 0.5, 1.0, 1.5, 2.0, or 2.5 gL^{-1} . The solution pH for each sample was adjusted to 3.0, 5.0, 7.0 or 9.0. The sample was then transferred to the photoreactor to be subjected to UV for predetermined reaction times (for detailed protocols see Appendix B). As a general note, triplicates tests were performed for each result obtained.

3.4. Adsorption Experiments

Adsorption equilibrium and adsorption rate experiments were performed to determine the adsorption capacities and rates for each contaminant on TiO_2 . To determine the adsorption equilibrium capacities, $\sim 3 \text{ mgL}^{-1}$ solutions were prepared for each of the five compounds selected. The adsorption experiments were conducted in 1 L foil-wrapped bottles at $20 \pm 2 \text{ }^\circ\text{C}$. Adsorption was evaluated with TiO_2 concentrations of 1, 3, 7 and 10 gL^{-1} . The bottles were capped and constantly agitated for 24 h.

The adsorption rate experiments were performed for the same conditions, as for the equilibrium experiments. The samples were collected at 0, 5, 10, 15, 20, 25 and 30 minutes using constant TiO_2 concentration of 1.5 gL^{-1} .

Samples were centrifuged at 4500 rpm for 45 minutes for solid-liquid separation (MARATHON 21000R, Fisher Scientific Inc., Pittsburgh, PA, USA), and then passed through a $0.45 \text{ }\mu\text{m}$ nominal pore size filters (47 mm diameter, GVS Maine, nitrocellulose mixed esters, Fisher Scientific, Pittsburg, PA). The filtered sample was then collected for SPE loading for TCEP, gemfibrozil, and 17β estradiol analysis. Syringe filters with $0.45 \text{ }\mu\text{m}$ pore size (25 mm diameter, mixed cellulose esters (MCE), Fisher Scientific, Pittsburg, PA) were employed to prepare the samples for GC-SPME-FID analysis to detect NDMA and 1,4 dioxane (a detailed protocol is shown in Appendix B).

3.5. Analytical Methods

For detection of 1,4 dioxane and NDMA, a GC-SPME-FID headspace technique was employed using an Agilent 6890N gas chromatograph (Agilent Technologies, Palo Alto, CA, USA), equipped with CTC-PAL autosampler and a flame ionization detector (FID). 10 mL samples

were transferred to 20 mL vials for headspace analysis. The GC column was a Restek RTX-5 capillary column, 30 m x 320 μm x 0.5 μm nominal, with split-less injection (290 °C). A carboxen/polydimethylsiloxane solid-phase micro extraction (SPME) fiber (23-gauge, 85 μm) (Supelco, Inc., Bellefonte, PA) was used. The oven temperature was held at 32 °C for 4 min, ramped to 50 °C at 3 °Cmin⁻¹, and then ramped to 290 °C at 8 °Cmin⁻¹, with a hold time of 3 min at 290 °C for a total run time of 43 min. The FID detector heater was set to 300 °C. The SPME incubation temperature was 80 °C, and extraction time was 1800 s.

For detection of TCEP, gemfibrozil and 17 β estradiol, samples were collected from the photoreactor, then centrifuged and filtered as previously described in section 3.4. Then the samples were then passed through a SUPELCO, Supelclean™ ENVI-18 SPE cartridge (57063, bed wt. 500 mg, volume 3 mL, Supelco, Inc., Bellefonte, PA) at a flow rate of 3 mL min⁻¹, and then extracted into 1.5 mL vials with DCM. GC analysis was carried out using an Agilent 6890 gas chromatograph equipped with Agilent 7863 automatic sampler (Agilent Technologies, Palo Alto, CA, USA) equipped with FID. The sample was injected into a Restek RTX-5 capillary column 30 m x 250 μm x 0.25 μm nominal film thickness after splitless injection (1 μL , 290 °C). The temperature program was as follows: 32 °C for 4 min with a hold time of 4 min, ramped to 50 °C at 3 °Cmin⁻¹, and finally ramped to 290 °C at 8 °Cmin⁻¹ with a hold time of 3 min for a total run time of 43 min. The FID heater was set to 300 °C. The method detection limit (MDL) for each compound were determined using the Environmental Protection Agency (EPA) MDL 40 CFR Part 136. Appendix B, revision 1.11 [134], and the results were as follows: (a) 1,4 dioxane: 45 μgL^{-1} ; (b) NDMA: 51 μgL^{-1} ; (c) TCEP: 29 μgL^{-1} ; (d) gemfibrozil; 80 μgL^{-1} , and (e) 17 β estradiol: 52 μgL^{-1} .

For oxidation byproducts identification, GC-MS analyses were carried out using an Agilent 7890A gas chromatograph, mass spectrometer 5975C VL MSD with Triple Axis Detector (Agilent Technologies, Palo Alto, CA). Separation was carried out in a 19091S-433UI (HP-5MSUI – ultra inert), 325 °C, 30 m x 250 μm x 0.25 μm nominal film thickness column. Helium was the carrier gas at 1.6 mLmin⁻¹. Splitless injection mode (2 μL , 290 °C) was used. The temperature program was set as follows: 32 °C for 4 min with a hold time of 4 min, ramped to 50 °C at 3 °Cmin⁻¹, and finally ramped to 290 °C at 8 °Cmin⁻¹ with a hold time of 3 min for a total run time of 42 min. Electron ion mass spectra was monitored from 30 m/z to 400 m/z, 2.4 minute solvent delay. The ion source and quadrupole temperatures were set at 230 and 150 °C, respectively. The instrument was operated in Electron Impact Ionization (EI) mode.

An additional set of experiments was conducted at reaction conditions found optimal for this process (pH = 5.0, TiO₂ slurry concentration = 1.5 gL⁻¹, and UV lamp nominal power = 100W). Extended reaction times of 18, 22, 24, and 26 minutes, and low concentration levels of the compounds were also measured in order to validate the results obtained from the GC instruments. These samples were analyzed by an external laboratory (Weck Laboratories, Inc.,

CA) using the following analytical methods: EPA 8270M for 1,4 dioxane, EPA 521 for NDMA, EPA 1694M-APCI for TCEP, EPA 1694M-ESI for gemfibrozil, and EPA 1694M-ESI+ for 17 β estradiol; the detection limits were 0.04 μgL^{-1} , 0.28 ngL^{-1} , 0.34 ngL^{-1} , 0.08 ngL^{-1} and 0.31 ngL^{-1} respectively.

3.6. Langmuir Hinshelwood Parameters

3.6.1. Langmuir Adsorption Constant, K_L (Lmg^{-1})

The amount of each compound adsorbed onto TiO_2 surface was calculated by using the following expression:

$$q_e = \frac{(C_0 - C_e)V}{m}$$

(Equation III-1)

where q_e is the equilibrium adsorption capacity of the contaminant adsorbed on unit mass of TiO_2 (mgg^{-1}); C_0 and C_e are the initial and equilibrium concentrations of the desired contaminant to evaluate. K_L was obtained from the equilibrium adsorption data by fitting the data to the linearized Langmuir isotherm. This involves plotting the reciprocal of q_e (equilibrium mass of contaminant adsorbed divided by the mass of TiO_2 adsorbent) versus the reciprocal of the equilibrium concentration (mgL^{-1}) (measured at 24 hr of contact) for each compound. The reciprocal of the trend line y-axis intercept corresponds to the maximum adsorption capacity (q_{max}) of the TiO_2 for that specific contaminant, and the reciprocal of the slope of the trend line is equal to the product of q_{max} and K_L . Therefore the value of K_L was determined from the trend-line intercept and slope (Equation III-2 and Equation III-3).

$$q_{\text{max}} = \frac{1}{y_{\text{intercept}}}$$

(Equation III-2)

$$K_L = \frac{1}{(q_{\text{max}})(\text{slope})}$$

(Equation III-3)

3.6.2. Reaction Rate Constant = k_{LH} ($\text{mgL}^{-1}\text{min}^{-1}$)

For a batch reactor using the L-H kinetic model, the governing equation for concentration can be expressed as:

$$\frac{dC}{dt} = -k_{LH} \frac{K_L C}{1 + K_L C}$$

(Equation III-4)

Rearranging:

$$-\left(\frac{1 + K_L C}{k_{LH} K_L}\right) dC = dt$$

(Equation III-5)

Integrating:

$$-\frac{1}{k_{LH} K_L} \int_C^{C_0} \frac{dC}{C} + \frac{1}{k_{LH}} \int_C^{C_0} dC = \int_t^0 dt$$

(Equation III-6)

Solving for C_0 at $t_0 = 0$ and C at t yields:

$$-\left[\frac{\ln\left(\frac{C}{C_0}\right) + K_L(C - C_0)}{k_{LH} K_L} \right] = t$$

(Equation III-7)

In order to determine a unique value of k_{LH} for each compound were determined by non-linear regression to Equation III-7, the values of the adjusted final concentration (C^*) in Equation III-8, were corrected until reaching the corresponding value of t (min) for its respective initial concentration. Experimental values of C and C^* are relatively similar between them. k_{LH} is calculated as by Excel using the solver application.

$$-\left[\frac{\ln\left(\frac{C^*}{C_0}\right) + K_L(C^* - C_0)}{k_{LH} K_L} \right] = t$$

(Equation III-8)

3.7. First-order Reaction Rate Constant (min^{-1})

The constant k (min^{-1}) is obtained by plotting the natural logarithm of the concentration of each compound measured at different times during the UV/TiO₂ operation versus its related time at specific conditions of pH, TiO₂ concentration and UV irradiation power ($\ln(C)$ vs t).

$$\frac{dC}{dt} = -kC$$

(Equation III-9)

$$C = C_0 e^{-(k)(t)}$$

(Equation III-10)

3.8. Effectiveness of the System

For a first order reaction under steady conditions, simulation of the effectiveness of the photocatalytic unit was carried out in two types of reactors: (i) plug flow reactor PFR and (ii) continuous stirred tank reactor CSTR.

3.8.1. PFR

Also known as a tubular reactor. In this type of system it is assumed that there is no mixing of the medium along the long axis of the reactor. The conversion “ X_{PFR} ” can be written as Equation III-11.

$$X_{PFR} = \left(\frac{C_0 - C}{C_0} \right)$$

(Equation III-11)

3.8.2. CSTR

This unit consists of well-stirred batch-reactor tank from which the partially reacted material passes continuously. The conversion “ X_{CSTR} ” can be written as Equation III-12.

$$X_{CSTR} = 1 - \left[\frac{1}{1 + (kt)} \right]$$

(Equation III-12)

Where t is the equivalent to the hydraulic retention time (HRT).

3.9. Normalization of First-order Kinetic Rates

First-order kinetic constants were normalized to other design parameters such as energy delivered by the UV lamp ($\text{kW}\cdot\text{h}$), volume of the reactor chamber (m^3), and surface area of the photocatalyst (m^2).

3.9.1. Energy Normalized to Energy Delivered per Volume (k') - $\text{kW}\cdot\text{h m}^{-3}$

This parameter is given by Equation III-13

$$C = C_0 e^{-(k')(P^t/V)}$$

(Equation III-13)

Where:

E_d = energy delivered ($\text{kW}\cdot\text{h}$) = $P \times t$,

P = Net power of the lamp in the UV range (constant and equal to 4.6 W),

t = exposure time (min).

For example the energy delivered at t = 5 min will be:

$$E_d = 4.6 \text{ W} \times \frac{1 \text{ kW}}{1000 \text{ W}} \times 5 \text{ min} \times \frac{1 \text{ h}}{60 \text{ min}} = 3.83 \times 10^{-4} \text{ kW} \cdot \text{h}$$

If the volume of the water sample is 0.5 L, the energy delivered per unit of volume (V), E will be:

$$E = \frac{E_d}{V} = \frac{3.83 \times 10^{-4} \text{ kW} \cdot \text{h}}{0.5 \text{ L}} \times \frac{1000 \text{ L}}{1 \text{ m}^3} = 0.767 \frac{\text{ kW} \cdot \text{h}}{\text{m}^3}$$

3.9.2. First Order Removal Normalized to TiO₂ Surface Area of (k'') - min⁻¹m⁻²

This parameter is given by the Equation III-14.

$$C = C_0 e^{-(k'')(t \times SA)}$$

(Equation III-14)

According to the reported TiO₂ particle diameter (listed in Appendix C), and assuming that TiO₂ particles are spherical, the specific surface area of TiO₂ is 59 m²g⁻¹. Therefore, the value of the total surface area depends on the concentration of the TiO₂ in each sample. For example, in a volume of 500 mL the surface area corresponding to a concentration of 0.1 gL⁻¹ of TiO₂ is 2.95 m² (0.5 L × 0.1 $\frac{\text{g}}{\text{L}}$ × 59 $\frac{\text{m}^2}{\text{g}}$).

3.9.3. First Order Removal Constant Normalized to TiO₂ Surface Area & Energy Delivered (k''') - m³ (kW·h)⁻¹m⁻²

This parameter is given by the Equation III-15.

$$C = C_0 e^{-k''' \frac{(P)(t)(SA)}{V}}$$

(Equation III-15)

The k''' values were determined by conducting a regression analysis of k' values for different surface areas of TiO₂. The slope of the resulting line provides the value of k''' given in m³ (kW·h)⁻¹m⁻².

3.10. Adsorption Rates

An analysis of adsorption rates was performed at initial concentrations of 3 mgL⁻¹ for all the compounds over 30 minutes in darkness. Appendix P shows results for each adsorbed

contaminant concentration (q_t) vs. adsorption time (q_t is defined as the mass of contaminant adsorbed divided by the mass of adsorbent, TiO_2 in this case). TiO_2 achieved its maximum adsorption capacity at different times depending on the contaminant selected. The maximum adsorption values obtained from these experiments correspond to the adsorption values given at 24 hours for each compound, which were employed to determine K_L values.

In an adsorption process, the rate of adsorption (dq/dt) is proportional to the difference between the amount adsorbed at time (t), and the adsorption capacity of adsorbent ($q_e - q_t$):

$$\frac{dq}{dt} = k_{\text{ads}}(q_e - q_t)$$

(Equation III-16)

Integrating Equation III-16 from $t = 0$ to $t = t$, and $q_t = 0$ to $q_t = q_t$, yields to:

$$\ln(q_e - q_t) = \ln(q_e) - k_{\text{ads}}t$$

(Equation III-17)

where q_e is the mass of contaminant adsorbed at equilibrium divided by mass of TiO_2 , and q_t is the mass of compound adsorbed at time t divided by mass of TiO_2 , and k_{ads} (min^{-1}) is the first-order adsorption rate constant. The plots of $\ln(q_e - q_t)$ vs. time are shown in appendix Q to obtain k_{ads} .

3.11. Identification of intermediates

Some intermediates of the photocatalytic oxidation of the selected compounds were identified by GC/MS analysis by comparison with standards and by interpretation of identified fragment ions. Byproducts were identified from two sources: (i) direct degradation of each compound individually and (ii) random interactions among partially degraded intermediates of the parent compounds. Experiments to identify byproducts were undertaken by subjecting a prepared sample to UV/ TiO_2 oxidation at two different reaction times, 2 min and 26 min. The operational conditions to perform the experiments were the same as those used for assessing the kinetics of the degradation reactions. The samples consisted of solutions containing the five compounds at an initial concentration of $\sim 2 \text{ mgL}^{-1}$.

IV. RESULTS

This chapter presents findings of the laboratory study to determine the ability of the UV/TiO₂ process for removing five organic contaminants listed as follows: 1,4 dioxane, NDMA, TCEP, gemfibrozil, and 17 β estradiol. Degradation of each contaminant was measured at different reaction times using GC-SPME-FID and SPE-GC-FID analyses under variable conditions of pH, and catalyst concentration to determine optimum operational parameters of the photocatalytic process. The kinetics constants were evaluated from two approaches, the L-H model and the first order rate.

4.1. Experimental Controls

Blank experiments were carried out to confirm there was no presence of any different compound out of the photodegradation process in the samples. pH, temperature and TiO₂ surface area were identified as primary variables that must be maintained at favorable conditions to maximize the extent of degradation. Tests were therefore conducted to identify experimental conditions that meet this requirement. To verify that there was no hydrolysis of the compounds, samples were taken directly from the stock solution ($C_0 = \sim 2 \text{ mgL}^{-1}$) without being subjected to any treatment to be analyzed at different pH values (3, 5, 7, and 9), and no degradation was observed. To check there was no presence of any other compounds different to the parent ones, analyses of the samples at 1.5 gL^{-1} for 24 hours of contact time and pH 5 were also performed. A reduction of the concentration of the selected compounds was observed due to the adsorption on the photocatalyst surface, but no intermediates were detected.

4.2. Assessment of the Degradation Effectiveness of UV/TiO₂

The effectiveness of the UV/TiO₂ process was determined initially by identifying operational parameters that affect the speed of oxidation reaction. Once the parameters were set at the optimal conditions, rate constants were calculated from two different approaches (L-H and first order) to finally get them compared to other advanced oxidation alternatives.

4.2.1. Factors Influencing the Photocatalytic Degradation

The pH of the sample and TiO₂ concentration (surface area) were varied in order to determine the effect on degradation rate and extent. Other parameters, such as initial concentration of the contaminants, UV radiant flux, UV wavelength, and type of photocatalyst, remained constant.

Effect of pH

A series of experiments were conducted with solution pH varied from 3 to 9. The TiO₂ slurry concentration was fixed at a concentration of 0.1 gL⁻¹ while the pH of the samples were adjusted with 0.01 N and 0.1 N solutions of hydrochloric acid (HCl) and sodium hydroxide (NaOH). First order degradation rate constants were found from the concentration versus time data, and are listed in Table IV-1. The greatest degradation rate constants for all compounds studied was found to be at pH 5.0 as shown in Figure IV-1. As it can be seen from table IV-1, the highest degradation rate was found to be at pH 5.

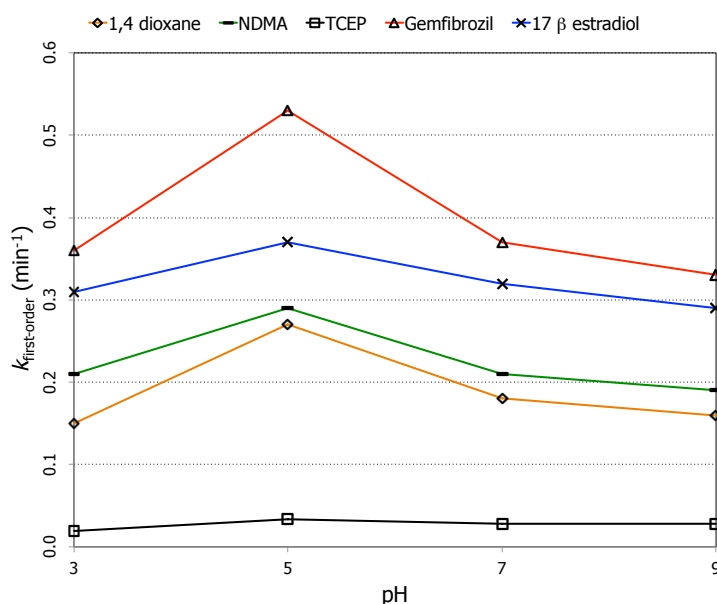


Figure IV-1 Variation of first order degradation rate constants with variation in solution pH, k (min⁻¹) (TiO₂ concentration = 0.1 gL⁻¹, initial contaminant concentration = ~2 mgL⁻¹).

Table IV-1 Variation of first order degradation rate constants with variation in solution pH, k (min⁻¹) (TiO₂ concentration = 0.1 gL⁻¹, initial contaminant concentration = ~2 mgL⁻¹).

pH	3	5	7	9
1,4 dioxane	0.150	0.270	0.180	0.160
NDMA	0.210	0.290	0.210	0.190
TCEP	0.019	0.033	0.028	0.028
Gemfibrozil	0.360	0.530	0.370	0.330
17β estradiol	0.310	0.370	0.320	0.290

Effect of Temperature

Although temperature is not reported to dramatically affect photo-catalytic reactions [42, 43] all experiments were conducted at a controlled temperature of 20±2°C by means of a chilled water-cooling system.

Effect of TiO₂ Slurry Concentration

The effect of different concentrations of TiO₂ on the photocatalytic degradation of the five different contaminants was also observed (See Appendix F). The increase in TiO₂ slurry concentration in water samples results in greater surface area and more active sites available for the oxidation of compounds. However, at some point an increased slurry concentration will decrease the ability of the UV radiation to reach the TiO₂ surface because a portion of the UV light is attenuated [135] and/or scattered [136] by the TiO₂ particles. Therefore, a range from 0.1 to 2.5 gL⁻¹ of TiO₂ concentrations was evaluated to determine the impact on degradation kinetics. First order degradation rate constants were found from the concentration versus time data, and are as shown in Figure IV-2 and Table IV-2.

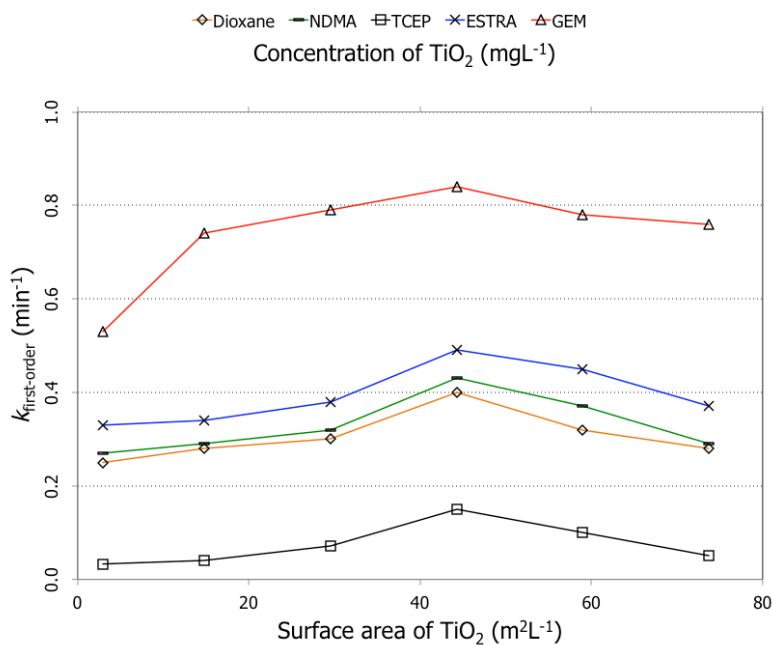


Figure IV-2 Variation of first order degradation rate constants with variation of TiO₂ concentration, k (min⁻¹) (Solution pH = 5.0, initial contaminant concentration = ~2 mgL⁻¹).

Table IV-2 Variation of first order degradation rate constants with variation of TiO₂ concentration, k (min⁻¹) (Solution pH = 5.0, initial contaminant concentration = ~2 mgL⁻¹).

TiO ₂ (gL ⁻¹)	0.1	0.5	1.0	1.5	2.0	2.5
TiO ₂ SA (m ²)	2.95	14.75	29.50	44.25	59.00	73.75
1,4 Dioxane	0.270	0.280	0.300	0.400	0.320	0.280
NDMA	0.290	0.290	0.320	0.430	0.370	0.290
TCEP	0.033	0.040	0.070	0.150	0.100	0.050
Gemfibrozil	0.530	0.740	0.790	0.840	0.780	0.760
17β estradiol	0.370	0.340	0.380	0.490	0.450	0.370

Note that the degradation rate constants were greatest at TiO₂ concentration of 1.5 gL⁻¹ (corresponding to approximately 44.25 m² of TiO₂ surface area). An average 36 % increase in the removal rate constants for 1,4 dioxane, NDMA, gemfibrozil and 17β estradiol was obtained compared with results found using 0.1 gL⁻¹ TiO₂ concentration (2.95 m² surface area). Under the same conditions, TCEP's reaction rate increased 78 %.

4.2.2. Kinetics of UV/TiO₂ Photodegradation of contaminants

The kinetics of degradation of the five selected compounds were evaluated for pH 5.0 and 1.5 gL⁻¹ of TiO₂; the C/C₀ results are shown in Figure IV-3. The final concentration of all the compounds decreased to below method detection limits after 10 minutes of reaction time, except for TCEP, which remained above the detection limit after 15 minutes of reaction time.

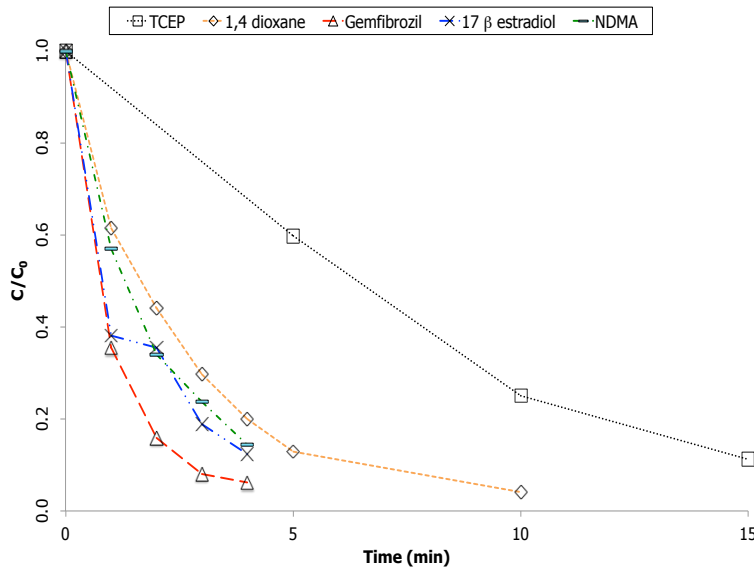


Figure IV-3 Degradation of the five contaminants by UV/TiO₂ oxidation (Solution pH = 5.0, TiO₂ = 1.5 gL⁻¹, initial contaminant concentration = ~2 mgL⁻¹).

4.2.3. Kinetic Approaches

Modeling of the kinetics of degradation of the contaminants in the UV/TiO₂ batch reactor was approached using the Langmuir-Hinshelwood (L-H) and the pseudo-first order models. The modeling results were assessed to determine the goodness of fit of each approach to the experimental data.

4.2.3.1. Langmuir-Hinshelwood Approach.

The L-H kinetic model has been widely utilized to describe the kinetics of the photocatalytic process [28, 29, 58, 77-80]. The rate of oxidation with maximum coverage of sites on the photocatalyst surface is controlled by the reaction rate of the adsorbed molecules and is given by Equation IV-1.

$$\frac{dC}{dt} = k_{LH} \frac{K_L C}{1 + K_L C}$$

(Equation IV-1)

Where, K_L = Langmuir adsorption constant (Lmg^{-1}) and k_{LH} = Langmuir-Hinshelwood reaction rate constant ($mgL^{-1}min^{-1}$) (See Appendix G and Appendix H). The parameters of the L-H Equation were determined by determining the values of these constants.

- Equilibrium experiments

In order to determine the K_L parameter several experiments were performed at dark conditions for each compound separately. Figures in Table IV-3 to Table IV-7 illustrate the parameters needed to plot equilibrium adsorption data in linearized Langmuir isotherm forms (Figure IV-4 to Figure IV-8). From the tables, x_n is the amount of compound (mg) that remains in the sample after adsorption using different amounts TiO₂ for 24 hours. For $m=0$ g of TiO₂, the amount of compound (x_0) in the sample is simply equal to the initial concentration of the sample (C_0) multiply by the total volume (V) of the sample treated. Therefore, the difference (x_0-x_n) corresponds to the adsorbed mass of compound by the photocatalyst at specific concentration values of TiO₂. The ratio of (x_0-x_n)/ m represents the equilibrium adsorption capacity of a specific concentration of TiO₂, and by means of plotting $1/q_e$ vs. $1/C_e$ the value of K_L is obtained.

Accordingly, table IV-3 and Figure IV-4 show adsorption data to obtain K_L and the plotting of the equilibrium adsorption data in linearized Langmuir isotherm form for 1,4 dioxane.

Table IV-3 1,4 dioxane adsorption data to obtain K_L parameter.

TiO ₂ (gL ⁻¹)	V (mL)	TiO ₂ [m] (g)	C _e (mgL ⁻¹)	1/C _e (Lmg ⁻¹)	x _n (mg)	x ₀ - x _n (mg)	q _e = (x ₀ - x _n)/m	1/q _e
0.0	510	0.0000	3.04		1.55040	0		
2.0	510	1.0200	2.65	0.3774	1.35150	0.19890	0.20	5.13
4.0	510	2.0400	2.33	0.4292	1.18830	0.36210	0.18	5.63
7.0	510	3.5700	2.01	0.4975	1.02510	0.52530	0.15	6.80
10.0	510	5.1000	1.68	0.5952	0.85680	0.69360	0.14	7.35

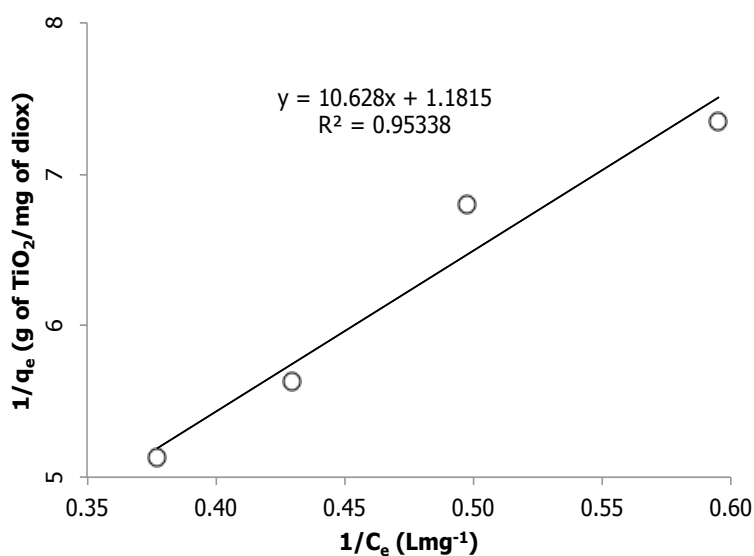


Figure IV-4 1,4 dioxane linearized data - Langmuir isotherm.

As shown in the figure above,

$$q_{\max} = \frac{1}{y_{\text{intercept}}} = \frac{1}{1.1815} = 0.85 \text{ mg of 1,4 dioxane per gram of TiO}_2$$

Therefore, for 1,4 dioxane:

$$K_L = \frac{1}{(q_{\max})(\text{slope})} = \frac{1}{(0.85 \text{ mgg}^{-1})(10.628 \text{ gL}^{-1})} = 0.111 \text{ Lmg}^{-1}$$

Table IV-4 and Figure IV-5 show adsorption data to obtain K_L and the plotting of the equilibrium adsorption data in linearized Langmuir isotherm form for NDMA,

Table IV-4 NDMA adsorption data to obtain K_L parameter.

TiO ₂ (gL ⁻¹)	V (mL)	TiO ₂ [m] (g)	C _e (mgL ⁻¹)	1/C _e (Lmg ⁻¹)	x _n (mg)	x ₀ -x _n (mg)	q _e =x/m	1/q _e
0.0	510	0.0000	3.04		1.55040			
2.0	510	1.0200	2.51	0.3984	1.28010	0.27030	0.2650	4.55
4.0	510	2.0400	2.24	0.4464	1.14240	0.40800	0.2000	4.83
7.0	510	3.5700	1.95	0.5128	0.99450	0.55590	0.1557	5.32
10.0	510	5.1000	1.82	0.5495	0.92820	0.62220	0.1220	5.90

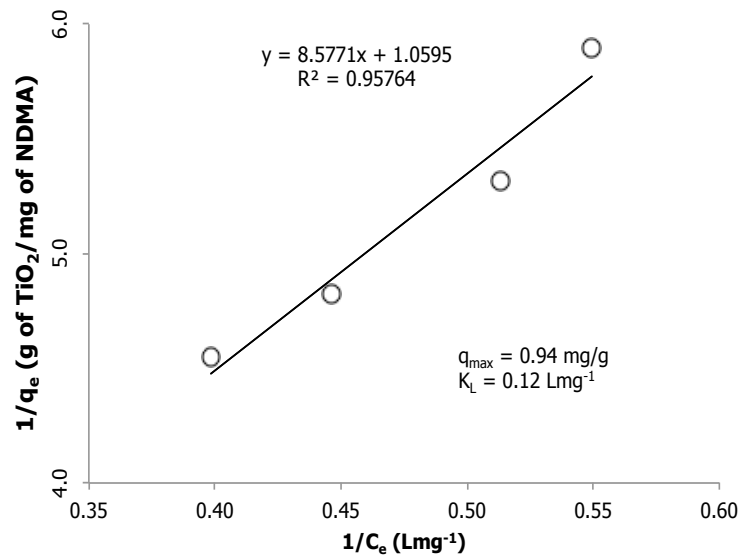


Figure IV-5 NDMA linearized data - Langmuir isotherm.

As shown in the figure above:

$$q_{\max} = \frac{1}{y_{\text{intercept}}} = \frac{1}{1.0595} = 0.94 \text{ mg of NDMA per gram of TiO}_2$$

Therefore, for NDMA:

$$K_L = \frac{1}{(q_{\max})(\text{slope})} = \frac{1}{(0.94 \text{ mgg}^{-1})(8.5771 \text{ gL}^{-1})} = 0.123 \text{ Lmg}^{-1}$$

Table IV-5 and Figure IV-6 show adsorption data to obtain K_L and the plotting of the equilibrium adsorption data in linearized Langmuir isotherm form for TCEP,

Table IV-5 TCEP adsorption data to obtain K_L parameter

TiO ₂ (gL ⁻¹)	V (mL)	TiO ₂ [m] (g)	C _e (mgL ⁻¹)	1/C _e (Lmg ⁻¹)	x _n (mg)	x ₀ -x _n (mg)	q _e =x/m	1/q _e
0.0	510	0	3.05		1.55550			
2.0	510	1.02	2.90	0.3448	1.47900	0.07650	0.0750	13.3
4.0	510	2.04	2.76	0.3623	1.40760	0.14790	0.0725	13.7
7.0	510	3.57	2.57	0.3891	1.31070	0.24480	0.0685	14.5
10.0	510	5.1	2.41	0.4149	1.22910	0.32640	0.0640	15.6

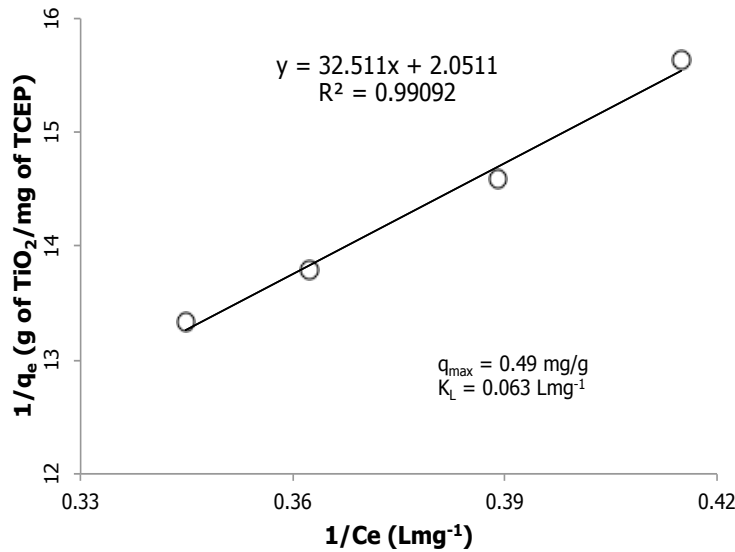


Figure IV-6 TCEP linearized data - Langmuir isotherm.

As shown in the figure above:

$$q_{\max} = \frac{1}{y_{\text{intercept}}} = \frac{1}{2.0511} = 0.49 \text{ mg of TCEP per gram of TiO}_2$$

Therefore for TCEP:

$$K_L = \frac{1}{(q_{\max})(\text{slope})} = \frac{1}{(0.49 \text{ mgg}^{-1})(32.511 \text{ gL}^{-1})} = 0.063 \text{ Lmg}^{-1}$$

Table IV-6 and Figure IV-7 show adsorption data to obtain K_L and the plotting of the equilibrium adsorption data in linearized Langmuir isotherm form for gemfibrozil,

Table IV-6 Gemfibrozil adsorption data to obtain K_L parameter

TiO ₂ (gL ⁻¹)	V (mL)	TiO ₂ [m] (g)	C _e (mgL ⁻¹)	1/C _e (Lmg ⁻¹)	x _n (mg)	x ₀ -x _n (mg)	q _e =x/m	1/q _e
0.0	510	0	3.10		1.58100			
2.0	510	1.02	2.19	0.4566	1.11690	0.46410	0.4550	2.20
4.0	510	2.04	1.70	0.5882	0.86700	0.71400	0.3500	2.86
7.0	510	3.57	1.11	0.9009	0.56610	1.01490	0.2843	3.52
10.0	510	5.1	0.91	1.0989	0.46410	1.11690	0.2190	4.57

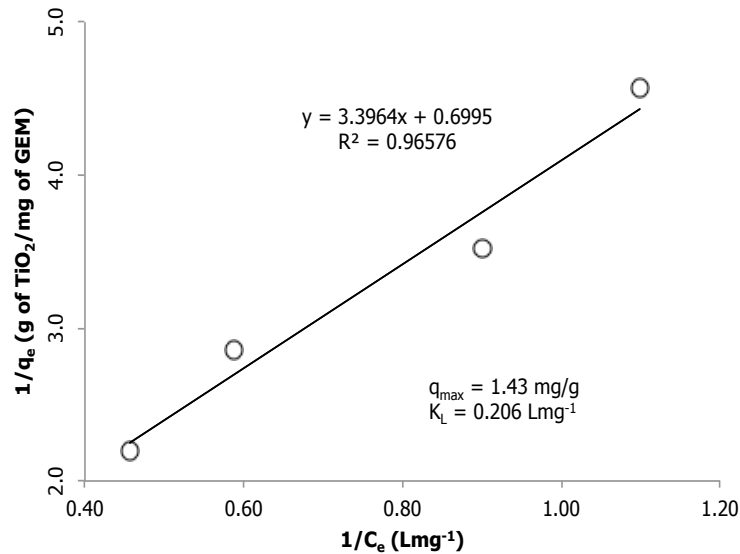


Figure IV-7 Gemfibrozil linearized data - Langmuir isotherm.

As shown in the figure above:

$$q_{\max} = \frac{1}{y_{\text{intercept}}} = \frac{1}{0.6995} = 1.43 \text{ mg of 1,4 dioxane per gram of TiO}_2$$

Therefore, for gemfibrozil:

$$K_L = \frac{1}{(q_{\max})(\text{slope})} = \frac{1}{(1.43 \text{ mgg}^{-1})(3.3964 \text{ gL}^{-1})} = 0.206 \text{ Lmg}^{-1}$$

And finally table IV-7 and Figure IV-8 show adsorption data to obtain K_L and the plotting of the equilibrium adsorption data in linearized Langmuir isotherm form for for 17 β estradiol,

Table IV-7 17 β estradiol adsorption data to obtain K_L parameter.

TiO ₂ (gL ⁻¹)	V (mL)	TiO ₂ [m] (g)	C _e (mgL ⁻¹)	1/C _e (Lmg ⁻¹)	x _n (mg)	x ₀ -x _n (mg)	q _e =x/m	1/q _e
0.0	510	0	2.90		1.47900			
2.0	510	1.02	2.20	0.4545	1.12200	0.35700	0.3500	2.86
4.0	510	2.04	1.80	0.5556	0.91800	0.56100	0.2750	3.64
7.0	510	3.57	1.40	0.7143	0.71400	0.76500	0.2143	4.67
10.0	510	5.1	1.05	0.9524	0.53550	0.94350	0.1850	5.41

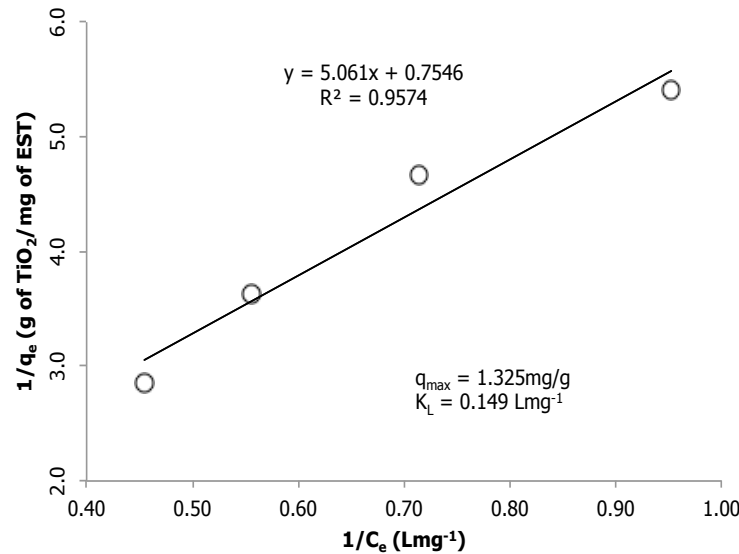


Figure IV-8 17 β estradiol linearized data - Langmuir isotherm.

As shown in the figure above:

$$q_{\max} = \frac{1}{y_{\text{intercept}}} = \frac{1}{0.7546} = 1.325 \text{ mg of } 17\beta \text{ estradiol per gram of TiO}_2$$

Therefore, for 17 β estradiol:

$$K_L = \frac{1}{(q_{\max})(\text{slope})} = \frac{1}{(1.325 \text{ mgg}^{-1})(5.061 \text{ gL}^{-1})} = 0.149 \text{ Lmg}^{-1}$$

The two appendices G and H show the extent of equilibrium adsorption of the five contaminants on the TiO₂ surfaces in the UV/TiO₂ reactor. The results are represented as fraction of

contaminant remaining in aqueous solution after 24 hours contact time. These data were obtained for adsorption only – the UV lamp was not activated, therefore contaminant mass did not decrease via chemical oxidation. A summary of the data obtained is shown in table IV-8.

Table IV-8 Values of q_{\max} , K_L and k_{LH} for CECs

Contaminant	q_{\max} (mg g^{-1})	K_L (L mg^{-1})
1,4 dioxane	0.850	0.111
NDMA	0.940	0.124
TCEP	0.490	0.063
Gemfibrozil	1.430	0.206
17 β estradiol	1.325	0.149

- Finding the Surface Adsorption Rate

Figures in table IV-9 shows the solution of the L-H equation as a function of time (column 6) that is calculated from known values of C_0 and K_L , while varying values of k_{LH} until calculated values of column 6 converged to the t values in column 3. Values of C^* are simultaneously observed (column 4) for each row to adjust to the same k_{LH} value. Values in columns 1, 2 and 3 were obtained from the experiments, corresponding to initial concentration, and final concentration at the given times.

Table IV-9 Solver used to calculate k_{LH}

1,4 dioxane					
1	2	3	4	5	6
C_0 (mgL ⁻¹)	C (mgL ⁻¹)	t (min)	C* (mgL ⁻¹)	k_{LH} (mgL ⁻¹ min ⁻¹)	$-\left[\frac{\ln\left(\frac{C^*}{C_0}\right) + K_L(C^* - C_0)}{k_{LH}K_L}\right] = t$
1.95	1.20	1	1.318460712	4.152	0.999999383
1.95	0.86	2	0.873185738	4.152	2.000000344
1.95	0.58	3	0.569274083	4.152	2.999999570
1.95	0.25	5	0.234723778	4.152	4.999999450
NDMA					
2.86	1.63	1	1.934078554	4.093	0.999999975
2.86	0.97	2	1.266799382	4.093	1.999999803
2.86	0.68	3	0.808586897	4.093	2.999999132
2.86	0.41	4	0.506270377	4.093	3.999999808
2.86	0.35	5	0.312753447	4.093	4.999999943
TCEP					
1.96	1.17	5	1.003061822	2.315	5.000000073
1.96	0.49	10	0.498877754	2.315	10.000000275
1.96	0.22	15	0.244243555	2.315	14.999999678
Gemfibrozil					
1.13	0.4	5	0.505911331	4.526	0.999999716
1.13	0.18	10	0.211626822	4.526	2.000000717
1.13	0.09	15	0.085511738	4.526	3.000000406
17β estradiol					
1.86	0.71	1	1.15172207	3.923	1.000000069
1.86	0.66	2	0.687652385	3.923	2.000000477
1.86	0.35	3	0.399918978	3.923	2.999999991
1.86	0.23	5	0.228579877	3.923	3.999999957

- Column 1, 2 and 3 = values obtained from the experiments, corresponding to initial concentration, and final concentration at a given times.
- The solution of the L-H Equation as a function of time (column 6) is calculated from known values of C_0 and K_L , while varying values of k_{LH} until calculated values of column 6 converged to the t values in column 3.
- Values of C^* are simultaneously observed (column 4) for each row to adjust to the same k_{LH} value

Next, the degradation trends were plotted with the data obtained from the experiments as shown on Figure IV-9, by substituting the respective values of k_{LH} and K_L in the L–H equation (Equation III-1) for each compound

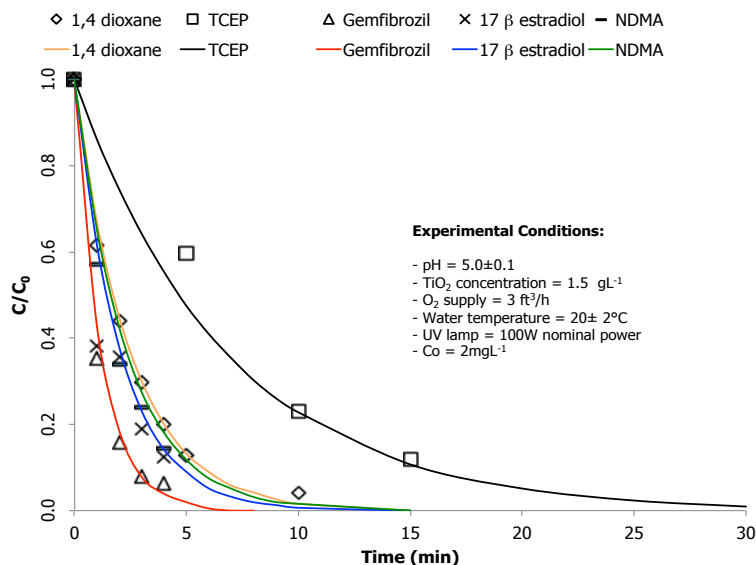


Figure IV-9 L-H model predictions for the UV/TiO₂ degradation of five selected compounds. (Solution pH = 5.0, TiO₂ = 1.5 gL⁻¹, initial contaminant concentration = ~2 mgL⁻¹).

A summary of L-H constants obtained for each contaminant is given in Table IV-10.

Table IV-10 Values for the L-H kinetic parameters, K_L and k_{LH}, found for the contaminants studied in this work

Contaminant	k _{LH} (mgL ⁻¹ min ⁻¹)	K _L (L mg ⁻¹)
1,4 dioxane	4.152	0.111
NDMA	4.093	0.124
TCEP	2.315	0.063
Gemfibrozil	4.526	0.206
17β estradiol	3.923	0.149

4.2.3.2. Pseudo-First Order Kinetic Modeling Approach

Figure IV-10 shows the data for the UV/TiO₂ degradation of contaminants with the first order reaction rate equation fit (Equation II-9) (refer to Appendix I). Regression curves for each contaminant are provided on figure IV-10 for the first order approach. Good linear correlations of the experimental data to the pseudo-first order rate equation were obtained for each contaminant: 0.95 for 1,4 dioxane; 0.99 for NDMA; 0.98 for TCEP; 0.99 for gemfibrozil, and 0.95 for 17β estradiol.

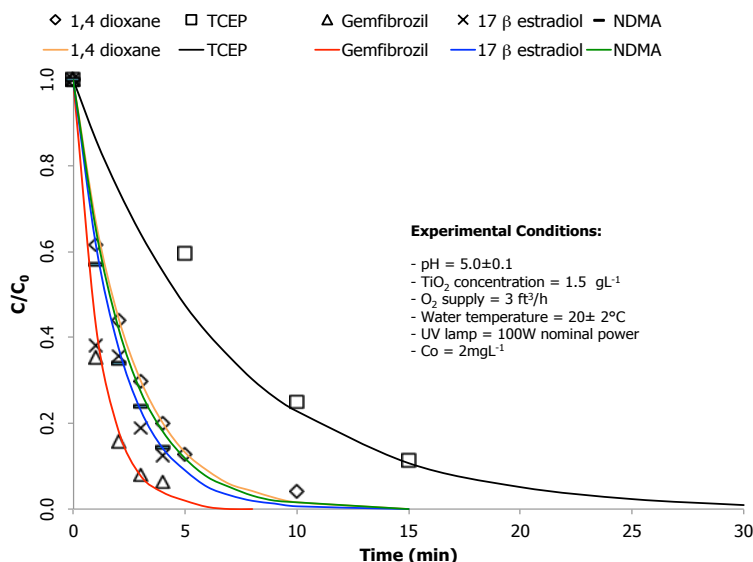


Figure IV-10 Pseudo-first order rate model predictions for the UV/TiO₂ degradation of five selected compounds (Solution pH = 5.0, TiO₂ = 1.5 gL⁻¹, initial contaminant concentration = ~2 mgL⁻¹).

4.3. Additional Parameters to be used as Criterion to Move from Bench Scale Reactor to Pilot Scale System

The purpose of normalizing first order rate constants units to volume, power, and surface area of the catalyst is to provide information about retention time, UV power, and catalyst dose to be used in the design of large-scale units.

4.3.1. Normalization of Pseudo-first-order Kinetic Rates

Table IV-11 shows a summary of the rate constants normalized to different operational parameters. For the calculation of these constants (k' , k'' and k'''), equations III-13, III-14 and III-15 from the previous chapter were employed. k' indicates the volume of sample treated per energy delivered by the power of light source emitted in the UV range; k'' shows a first-order degradation approach in terms of surface area of the photocatalyst; and k''' represents the relationship of volume treated by energy delivered in the UV range and surface area of the photocatalyst, which is a partial combination of the first two constants.

Table IV-11 Normalized pseudo-first order kinetics constants k' , k'' , and k''' . (Conditions: pH 5, 1.5 gL⁻¹ of TiO₂).

Contaminant	k' ($m^3(kW\cdot h)^{-1}$)	k'' ($min^{-1}m^{-2}$)	k''' ($[m^3(kW\cdot h)^{-1}m^{-2}]$)
1,4 dioxane	2.69	0.0024	0.0161
NDMA	3.00	0.0033	0.0209
TCEP	0.92	0.0028	0.0182
Gemfibrozil	5.73	0.0063	0.0402
17 β estradiol	3.57	0.0038	0.0255

4.4. Extended Time Reactor Experiments

An additional set of experiments were conducted at conditions found optimal for this process (pH = 5.0, TiO₂ slurry concentration = 1.5 gL⁻¹, and UV lamp nominal power = 100W) but with extended reaction times of 18, 22, 24, and 26 minutes. These extended reaction time samples were shipped to an external laboratory (Weck Laboratories, Inc., CA) for low concentration analyses. The concentrations obtained for each compound at the extended reaction times are shown in Table IV-12.

Table IV-12 Final concentrations of contaminants after extended UV/TiO₂ oxidation reaction times.

Contaminant/ Time (min)	1,4 dioxane (μgL^{-1})	NDMA (ngL^{-1})	TCEP (μgL^{-1})	Gemfibrozil (ngL^{-1})	17 β estradiol (ngL^{-1})
18	6.80	83	170	1.50	12.5
22	4.60	38	160	1.20	10.5
24	1.95	40	155	0.96	9.60
26	1.45	12.5	67	0.49	8.55

The first order degradation rate constants were determined using the combined data; the data previously presented plus the new data obtained from these extended time experiments. The predicted concentrations using these first-order rate constants are shown in Appendix N. The Langmuir-Hinshelwood and first order rate constants were also found from the combined data, and the predicted concentrations are also shown in Appendix M for each compound. Note that there is very little difference in the predictions using the first-order rate model and the Langmuir-Hinshelwood model.

4.5. Adsorption Rate Experiments

The compounds reached equilibrium concentrations at different times: NDMA and gemfibrozil at 15 minutes, 1,4 dioxane and 17 β estradiol at 20 minutes, and TCEP at 25 minutes. These data

were fit to a first order rate model [137] to calculate first order adsorption rate constants k_{ads} (min^{-1}). The first order adsorption rate constants are shown in Table IV-13.

Table IV-13 Pseudo-first order adsorption rate constants on TiO_2 surface, using 1.5 gL^{-1} of TiO_2 and initial contaminant concentrations = $\sim 3 \text{ mgL}^{-1}$.

Contaminant	k_{ads} (min^{-1})
1,4 dioxane	0.096
NDMA	0.120
TCEP	0.075
Gemfibrozil	0.136
17 β estradiol	0.127

4.6. Identification of Intermediates as Result of the Photocatalytic Degradation of Selected Compounds

Experiments to identify intermediates were undertaken by subjecting a prepared sample to UV/ TiO_2 oxidation at two different reaction times, 2 min and 26 min. The operational conditions to perform the experiments were the same as those used for assessing the kinetics of the degradation reactions. The samples analyzed consisted of solutions initially containing the five compounds at 2 mgL^{-1} separately and then all five together.

At 2 minutes, specific compounds were identified using GC/MS. The 2 minutes reaction time leads to the formation of fourteen identified intermediates. These intermediate compounds were not detected in control experiments. The compounds were identified by interpretation of identified fragment ions and by comparison with standards. Conversely, at 26 minutes no byproducts were detected, indicating that any byproducts formed were fully destroyed by the oxidation process.

The compounds identified as intermediates of the degradation process were hypothesized to come from two sources: (i) direct degradation of each individual compound and (ii) random interactions among partially degraded intermediates of the parent compounds. A wide variety of byproducts are expected from oxidative degradation of organics in real water samples because of the presence of a number of chemical species that are potentially prone to react. Intermediates generated from individual oxidation of parent compounds were identified and listed in table IV-14 and showed in figure IV-11.

Table IV-4 List of intermediates generated from the partial degradation of individual parent compounds separately.

Contaminant (parent compound)	Oxidation byproducts
1,4 dioxane	- 2-hydroxyethyl formate - Ethylene glycol - Formic acid
NDMA	- Dimethylamine - Methylamine - Ammonium
TCEP	- Phosphoric acid - 2-chloroacetic acid
Gemfibrozil	- 2,5-dimethylphenol - 2-hydroxy-4-methylbenzaldehyde - 4-methylsalicylate - 4-methyl-2-oxopent-4-enoate - Acetaldehyde - Pyruvic acid
17 β estradiol	- 4-hydroxyestradiol - Estrone - Testosterone species - 6-methyloctan-2-one

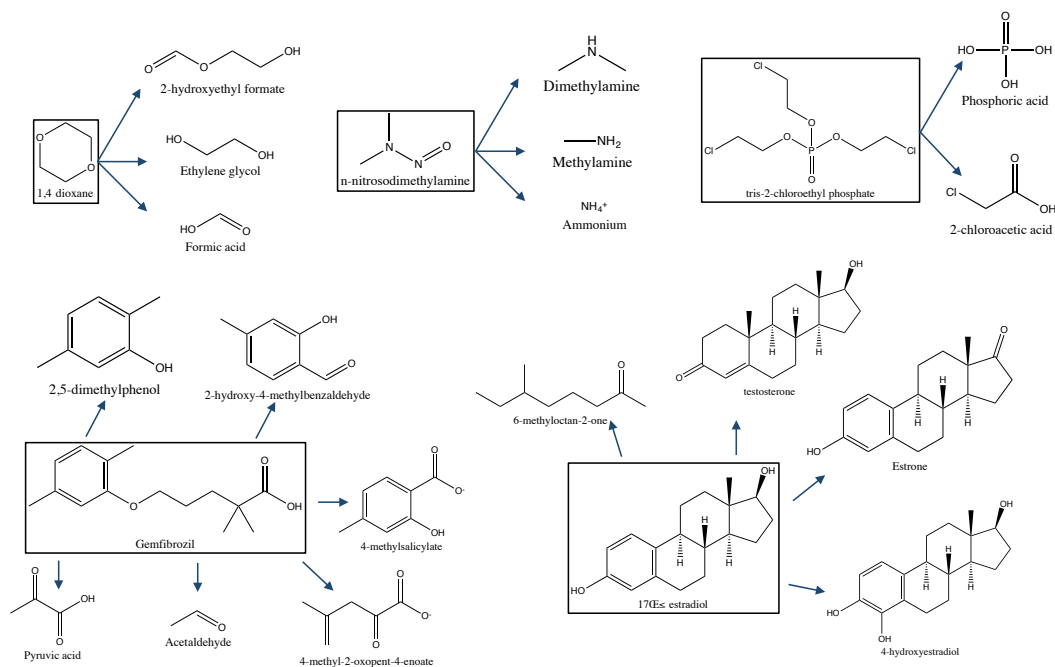


Figure IV-11. Intermediates generated from the partial degradation of individual parent compounds separately.

4.6.1. Suggested Pathways of Individual Degradation of Contaminants

Intermediates as part of the sole degradation pathway of their respective parent compounds such as 1,4 dioxane, NDMA and TCEP have been amply described elsewhere and previously suggested by others [103, 110, 133]. Intermediates formed from random interactions among partial degradation compounds or other fragments, will be discussed in this work. Because gemfibrozil's and 17 β estradiol's intermediates are lesser known than the other compounds' byproducts as reported in the literature, and the majority of random interactions among compounds derivatives comes from the gemfibrozil structure, this study also contributes with the generation of gemfibrozil's intermediates as an important step in the explanation of derivatives from this parent compound. Byproducts detected in this work are shown within boxes.

Gemfibrozil's molecule has two main forms: one composed by a carboxyl group (protonated form) (A), and the other by an acetate ion (deprotonated form) (A'). At pH 5, the form (A') (79.30%) prevails over the (A) (20.70%) [138]. As shown on figure IV-12, the suggested pathway initiates with the attack of the hydroxyl radical at the oxygen of the aromatic-aliphatic ether linkage, which exhibits the highest electronegativity of the molecule (11.41) [138], separating the molecule into two different moieties: 2,5-dimethylphenol (B) and 2,2-dimethyl-5-oxopentanoate (N) [139]. Then, the two molecules initiate their own degradation pathways independently. Two degradation paths are proposed for the phenolic compound.

In the first one, hydroxylation is available on position 6 [140] transforming the phenol into 3,6-dimethylcatechol (C). The hydroxyl radical attack breaks the 5–6 bond transforming the molecule to 3-methyl-2-oxopent-4-enoate (D) [141], then is converted into 4-hydroxy-2-oxopentanoate (E) by hydrolysis of the C3–C4 bond [142] to finally get degraded to acetaldehyde (F) and pyruvic acid (G).

In the second pathway of the 2,5-dimethylphenol (B), the presence of oxygen favors the hydroxylation of this molecule either in the methyl groups at positions 1 or 4 to form 4-(hydroxymethyl)benzene-1,3-diol (H) [143], which is transformed into 2-hydroxy-4-methylbenzaldehyde (I) [144]. The aldehyde is then transformed into 4-methylsalicylate by hydration (J) [145], and this into 4-methylcatechol (K) [146] by transformation of the acetyl into –OH group. Following the same transformation route of the previous catechol derivative to 2-oxopent-4-enoate derivative [141], 4-methyl-2-oxopent-4-enoate (L) is formed to finally degrade to pyruvic acid (G) and acetone (M).

On the other hand, the suggested pathway for gemfibrozil's other moiety starts at (N). The degradation of the hydrogen of the first carbon is substituted by an –OH group, which at pH 5 switches to acetate ion [147], followed by thiolytic cleavage [148] of the acetate ion and other

substitutions and oxidation steps towards the formation of 2-carboxy-2,2-dimethylacetate (P) [149], and finally by the previous described steps be transformed into isobutyric acid (Q) and formic acid (R).

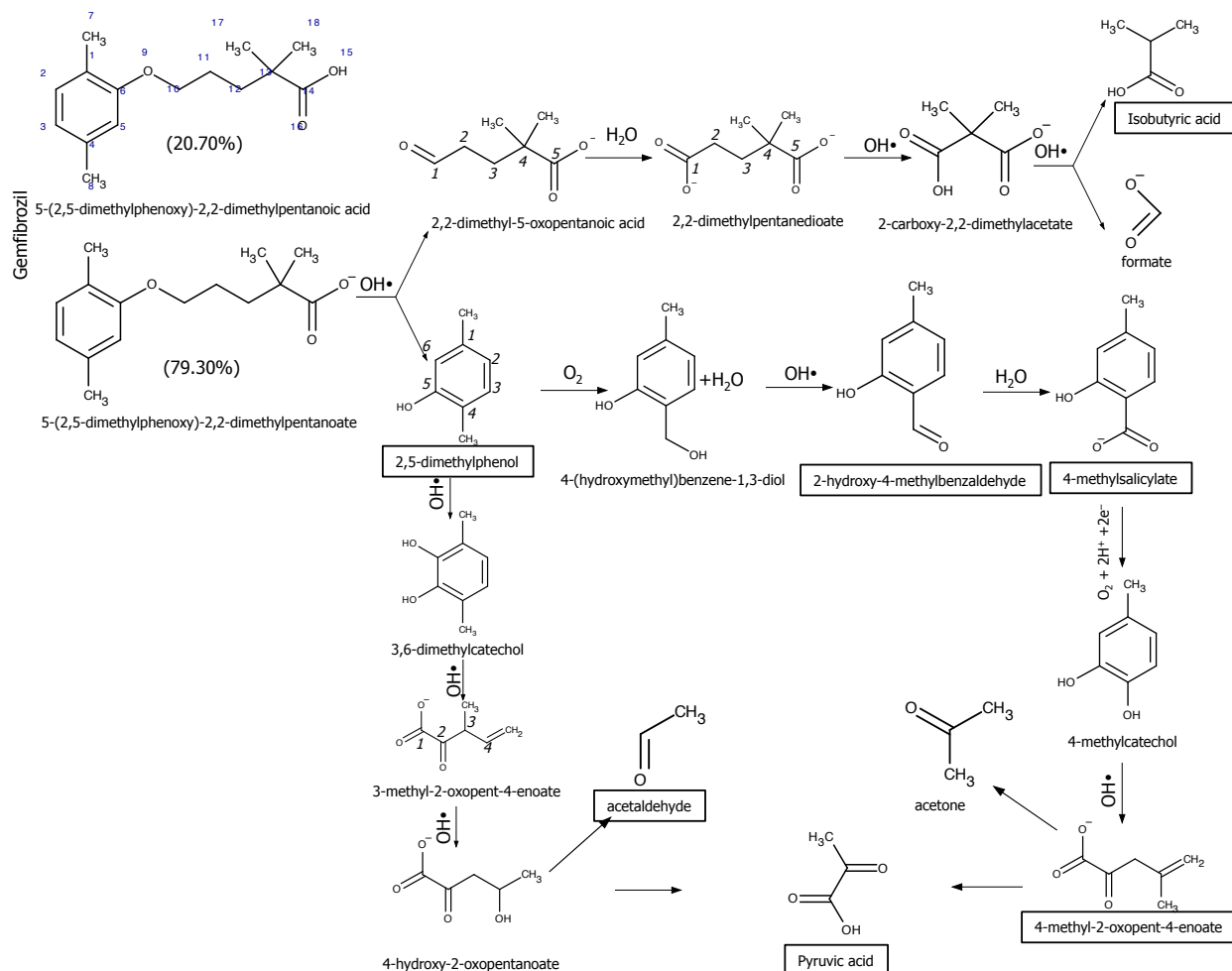


Figure IV-12. Suggested pathways of the degradation of gemfibrozil.

For the 17β estradiol, the identified pathway shown on Figure IV-13 starts with the hydroxylation of the benzene ring right next to the position of the existing OH- group forming a catechol moiety that transforms the 17β estradiol (A) into 4-hydroxyestradiol (B) [150], which was identified in this study. Next step is the breakage of the benzene ring at the bond confined by the two -OH groups (C), followed by a rearrangements of the carbon bonds of the 2-oxidoprop-2-enoate moiety [151] to form 2-oxopropanoate moiety (D) [152]. Then, similar steps described for 3,6-dimethylcatechol's degradation were applied to suggest degradation at step (E) for the 17β estradiol's, in addition the -OH group of the cyclopentane molecule was converted to double C=O bond.

In step (F) the acetate group is also separated from the cyclohexanone moiety [153]. Then at the ketone group position, the cyclopentane is converted to a cyclic ester (G) [154]. The ester group

of the previous step is after transformed into an alcohol plus a carboxylate breaking the oxan-2-one moiety, and transforming the remaining cyclohexane moiety into a hemiacetal (H), then in step (I) the acetate group is separated. In step (J) the cyclohexane moiety is broken at the –OH group position to get transformed into an acetyl group single bonded to a 2-oxopropanoate moiety, which is then transformed into 2-oxepanone (K) following the same degradation pathway to step (G), to then break the cycloheptanol moiety and produces a long chain molecule (L) that is fragmented until 6-methyloctanone (M) to finally get degraded into minor byproducts such as pyruvic acid and acetone.

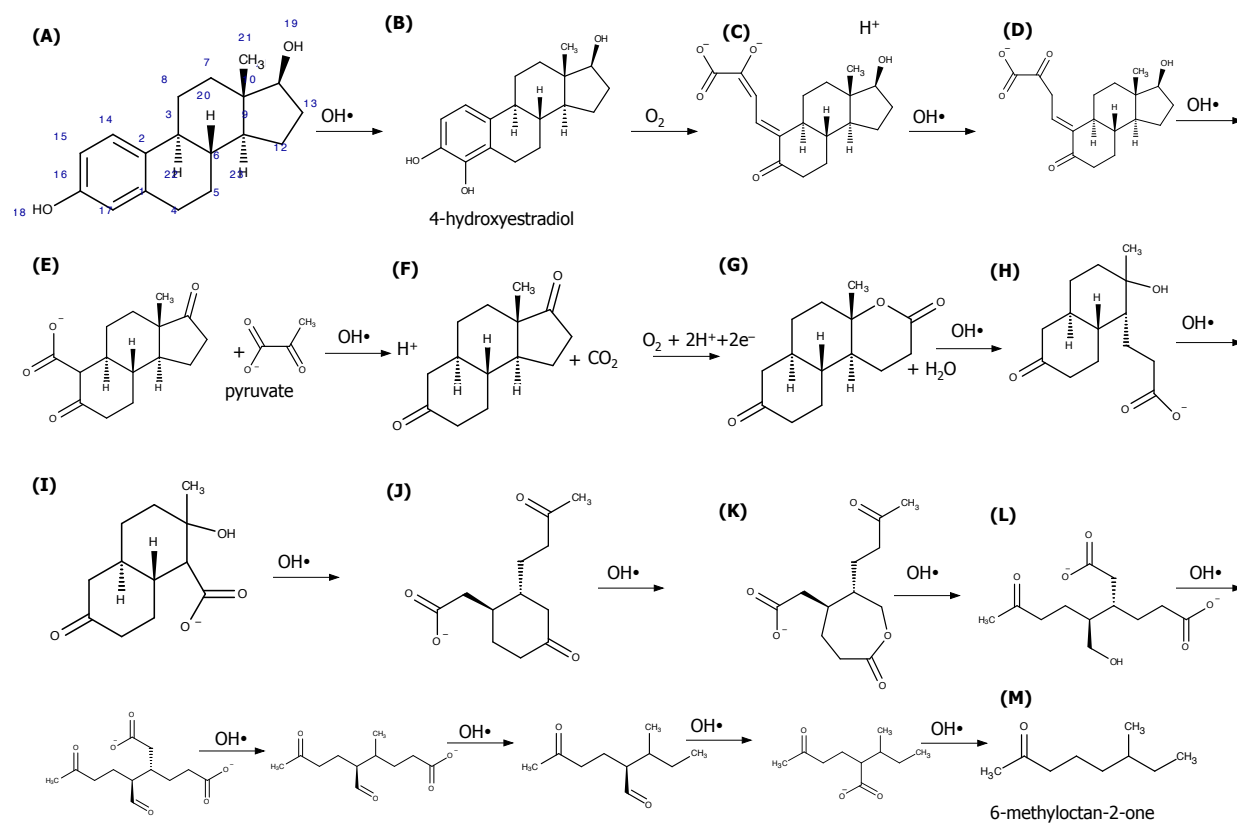


Figure IV-13. Suggested pathway of the degradation of 17β estradiol.

4.6.2. Random Interactions Among Partially Degraded Intermediates of the Parent Compounds

The majority of the intermediates found originated from gemfibrozil's 1,4 xylene moiety: acetophenone, 2,5-dimethylcyclohexane-1,4-dione, 2,3-dimethylphenol, 1-phenylethan-1-one, limonene, 2,6-dimethylphenol, 2-hydroxy-5-methylbenzaldehyde, and 3-methoxy-benzaldehyde. It is suggested that interactions between the intermediates from the degradation of NDMA and gemfibrozil might have produced 3,5-dimethylphenyl N-methylcarbamate and N-(4,6-dimethoxypyrimidin-2-yl)-2-methylpropanamide. Also, reactions between the byproducts from NDMA and 17β estradiol degradation suggested the generation of 1-methylpyrrolidin-2-one and 2-methyl-4,5-dihydro-1H-imidazole respectively. In addition to (5Z)-4-methyl-5-(2-

oxopropylidene)-2,5-dihydrofuran-2-one, there were other intermediates identified including: testosterone, estrone and 2-hydroxyestradiol (not shown in Figure IV-14). The presence of these intermediates is consistent with Zhao's findings [155], where it was shown that the attack of reactive species mostly started at 17 β estradiol's aromatic ring moiety, leading to the formation of similar estrogenic intermediates by modifying the structure of the parent compound at early stages of the heterogeneous photo-fenton reaction. (2-chloroethoxy)ethene was identified may have been produced from the interaction of intermediate compounds from 1,4 dioxane and TCEP partial degradations. Conversely, at 26 minutes no byproducts were detected, indicating that any byproducts formed were fully destroyed by the oxidation process.

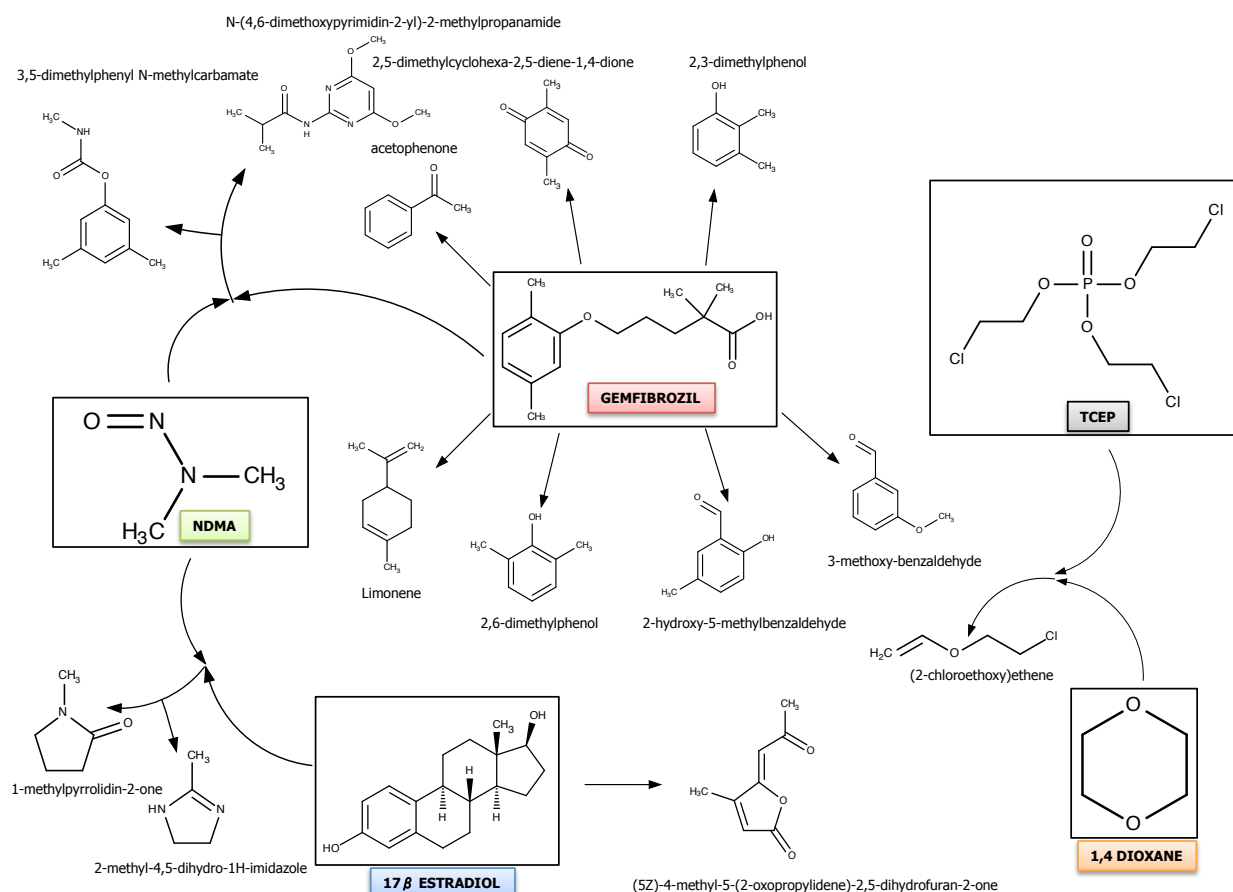


Figure IV-14. Identified intermediates and suggested formation dependence of selected compounds in the simultaneous UV/TiO₂ oxidation of 1,4 dioxane, 17 β estradiol, gemfibrozil, NDMA and TCEP.

V. DISCUSSION OF RESULTS

As presented in the previous section, all five contaminants of interest were successfully reduced in concentration at different chemical reaction rates. The discussion below will first focus on how well the photocatalytic results fit into either the L-H model or the first order approach, then a comparison of first-order rate constants for each contaminant obtained in this work with rate constants and treatment performance assessments presented by others. This will be followed by a discussion on the applicability of reaction rate constants presented in this study for design scale-up. The concluding portions of this section will address contaminant to TiO₂ adsorption measurements and byproduct formation.

5.1. Assessment of the Effectiveness of UV/TiO₂

According to the results previously shown in the last chapter, minor differences were found on the trends of degradation rates of the selected contaminants by the two studied approaches (L-H and first order). A comparison of the results obtained from the two models studied is shown in Table V-1. As noticed, there was a small difference (column 6) between using either the L-H or the first order model. Consequently, in terms of simplicity, first order model describes very well the photocatalytic degradation process of the selected compounds.

Table V-1 Comparison between first order kinetics and the product of $k_{LH} \times K_L$.

1	2	3	4	5	6
Contaminant	k (min ⁻¹)	K_L (Lmg ⁻¹)	k_{LH} (mgL ⁻¹ min ⁻¹)	$(k_{LH} \times K_L)$ (min ⁻¹)	% Difference
1,4 dioxane	0.404	0.111	4.152	0.461	-14.11%
NDMA	0.429	0.124	4.093	0.508	-18.41%
TCEP	0.149	0.063	2.315	0.146	+2.01%
Gemfibrozil	0.839	0.206	4.526	0.932	-11.08%
17β estradiol	0.489	0.149	3.912	0.583	-19.22%

Column 2 = First Order reaction constant value found through regression analysis of ln C vs t

Column 3 = Langmuir adsorption constant found as described in Appendix H

Column 4 = Langmuir-Hinshelwood reaction rate constant found as described in Appendix I

5.1.1 Effectiveness of UV/TiO₂ Oxidation Based on Rate Constants

As shown in Figure IV-3, it is apparent that a relatively even competition for active sites on the TiO₂ surface between gemfibrozil and 17β estradiol is observed at early stages of the process (up to 1 min). However, the presence of a deprotonated carboxyl group in gemfibrozil's structure is

expected to enhance its adsorption strength on the photocatalyst surface [156]. This trend is observed in Figure IV-3 for reaction times greater than 1 min. As the solution pH is greater than gemfibrozil's pKa (4.42 [60]), gemfibrozil is expected to have a greater affinity for the positively charged TiO₂ surface ($P_{ZC} = 6.25$) [157], and may be oxidized by direct interaction with photogenerated holes of the photocatalyst surface [158]. Conversely, 17 β estradiol's pKa (10.33) [136-138] indicates a protonated state of the molecule at the same pH condition, giving the hormone lower affinity for the TiO₂ surface than the gemfibrozil.

The relatively rapid degradation of gemfibrozil and 17 β estradiol when compared with the other compounds may be also explained by comparing their solubilities. It has been found that compounds with lower solubilities have greater adsorption rates to catalyst surfaces [159]. Gemfibrozil and 17 β estradiol have low aqueous solubilities; 10.9 mgL⁻¹ [160] and 5 mgL⁻¹ [161] respectively. However, the other compounds have greater solubilities: 1,4 dioxane is 213 gL⁻¹ [94], NDMA is 4 gL⁻¹ [162], and TCEP is 7 gL⁻¹ [163]. The compounds with lower aqueous solubilities are expected to have greater affinity for the TiO₂ surface, and are more readily oxidized.

Moreover, 1,4 dioxane does not contain functional groups capable of dissociation [94, 164], and its relative stable nature [94] can affect its propensity for oxidation when competing with NDMA for TiO₂ active sites. The NDMA's pKa of 3.52 [138] provides for a negative charge at pH 5.0, and the N-NO bond is capable of acting as a donor of an NO [165] to the positive holes on the TiO₂ surface, while the four C-O bonds in the 1,4 dioxane act as hydrogen bond acceptors available for dipolar attractions [94]. Finally, TCEP does not have ionizable functional groups, however the high pKa (14.86) [136-138] of its leaving group 2-chloroethanol [166] and higher dipole moment (1.79 D) as compared to 1,4 dioxane (0.04 D) [138] makes this molecule more difficult to remove at the conditions evaluated. This agrees with these results, which showed TCEP with the slowest degradation rate of the contaminants evaluated in this work. It is important to point out that the kinetic rates and degradation effectiveness reported in the literature are based on different operational conditions of each work, which makes comparisons among them being difficult, however some relevant information based on the removal of the selected contaminants of this study from others is detailed as follows.

5.1.1.1. 1,4 dioxane

As mentioned in previous chapters, conventional water and wastewater treatment processes including precipitation-coagulation, air stripping, and conventional biological treatment have shown to be relatively ineffective in removing 1,4-dioxane in water due to its recalcitrant behavior and high solubility [167, 168]. Studies regarding direct UV photolysis or ozonation (alone) have reported to produce low removal efficiencies of 1,4 dioxane [168, 169]. Other AOPs such as H₂O₂/O₃, UV/H₂O₂, and UV/TiO₂ have been reported to attain significant removal

of this compound [103, 170, 171]. Table V-2 summarizes results of treatability studies from this research and referenced studies.

Table V-2 Results of 1,4 dioxane - Treatability studies.

Technology	Initial conc.	Operation time (min)	% removal	Reaction rate constant
Batch O ₃ [172]	1 mgL ⁻¹			0.03 (min ⁻¹)
Batch O ₃ /H ₂ O ₂ [172]	1 mgL ⁻¹			2.2 (min ⁻¹)
O ₃ /H ₂ O ₂ [173]	14 µgL ⁻¹	9	86.0%	--
Batch UV/TiO ₂ (1500W) [102]	35 mgL ⁻¹	10	94.5%	0.29 (min ⁻¹)
Batch UV /H ₂ O ₂ with ferrioxalate [174]	450 mgL ⁻¹	30	99.8%	--
Batch UV/H ₂ O ₂ (1 kW) [103]	88 mgL ⁻¹	5	90.0%	0.52 (min ⁻¹)
Batch UV photolysis (1 kW) [103]	88 mgL ⁻¹	5	2.0%	0.0038 (min ⁻¹)
Batch UV/TiO ₂ (this work)	2 mgL ⁻¹	25	97.8%	0.4 min ⁻¹

The first order reaction rate constant for the removal of 1,4-dioxane found in this research at pH 5, with TiO₂ concentration of 1.5 gL⁻¹, was 0.4 min⁻¹. This value is very close to the rate constant reported by Maurino et al. [102] (0.29 min⁻¹) for UV/TiO₂, and comparable to the value reported by Stefan and Bolton [103] (0.52 min⁻¹) for UV/H₂O₂, and it is two orders of magnitude greater than the rate constant found by Stefan and Bolton [103] for UV photolysis of 1,4-dioxane.

Now, regarding effectiveness of the photocatalytic process evaluated in this work, by using the 0.4 min⁻¹ rate constant found in this research, a removal percentage in a batch reactor was predicted of 86.5% for a 5 min reaction time, and 98.2% for a 10 min reaction time. The predicted removal percentage using a CSTR was of 66.7% for a 5 min residence time, and of 80.0% for a 10 min residence time.

5.1.1.2.NDMA

NDMA is a stable compound in aqueous solution and exhibits resistance to treatment by air stripping and adsorption technologies as well as by biodegradation [175, 176]. However, it is reported to be susceptible to chemical oxidation [177] and UV photolysis [178-181]. Moreover, most of the AOPs reported to degrade NDMA make use of oxidants such as ClO₂ and O₃ [182] and H₂O₂/O₃ [111], while other studies have reported a combination of reverse osmosis and UV treatment [183] as effective methods of degradation. The treatment effectiveness of various chemical oxidation technologies reported in the literature is shown in Table V-3.

Table V-3 Results of NDMA - Treatability studies.

Technology	Initial conc.	Operation time (min)	% removal	Reaction rate constant
Batch UV/TiO ₂ (16W) [184]	30 mgL ⁻¹	100	99.0%	--
CSTR ClO ₂ [182]	0.46 µgL ⁻¹	5	63.0%	--
CSTR O ₃ [182]	0.46 µgL ⁻¹	5	90.0%	--
Semi-batch Rayox® UV photolysis (1 kW medium pressure) [185]	74 mgL ⁻¹	70	99.9%	0.32 min ⁻¹
Batch UV photolysis (pulsed UV irradiation 5 kW) [186]	2.8 µgL ⁻¹	1.5	97.9%	12.2 min ⁻¹
Batch UV/TiO ₂ (this work)	2 mgL ⁻¹	23	97.5%	0.42 min ⁻¹

The reaction rate constant for the removal of NDMA with UV/TiO₂ found in this work (at pH 5, TiO₂ = 1.5 gL⁻¹) was 0.42 min⁻¹ as listed in Table IV-3. This is similar to the rate constant found by Stefan and Bolton [185] (0.32 min⁻¹) for UV photolysis of NDMA in water using a 1 kW lamp. Using the rate constant determined in this work, the predicted removal percentage using a batch reactor was found to be 88% for a 5 min reaction time, and 98.6% for a 10 min reaction time. The predicted removal percentage using a CSTR was found to be 68% for a 5 min reaction time, and 81% for a 10 min reaction time.

5.1.1.3.TCEP

TCEP has been found to be somewhat resistant to oxidative processes [20], including advanced oxidation [186, 187], and has been found to be recalcitrant and persistent in the environment. It has been regularly detected in different water bodies around the world [112-114]. Processes such as ozone oxidation have been found by others to be relatively ineffective for treating TCEP in water [188, 189]. Snyder and colleagues [189] reported low TCEP removal rates in bench scale experiments using O₃/H₂O₂ and O₃. Benotti and collaborators [190] reported better removal rates using UV/TiO₂ plus H₂O₂, and UV photolysis. Recent research from WPI has found that other AOPs are able to degrade TCEP in water, albeit at lower reaction rates than typically encountered for most other contaminants in water [187, 191]. Findings regarding TCEP treatability by AOPs reported in the literature are shown in Table V-4.

Table V-4 Results of TCEP - Treatability studies.

Technology	Initial conc.	Operation time (min)	% removal	Reaction rate constant
CSTR O ₃ /H ₂ O ₂ [189]	0.34 µgL ⁻¹	24	9.0%	--
PFR UV/H ₂ O ₂ (2.3kW) [190]	3.1 µgL ⁻¹	--	--	0.35 m ³ (kW·h) ⁻¹ , 0.42 min ⁻¹
PFR (2.3kW) Photocatalytic reactor membrane [190]	1.3 µgL ⁻¹	--	--	0.063 m ³ (kW·h) ⁻¹ , 0.085 min ⁻¹
Batch Cl ₂ [192]	100 ngL ⁻¹	1440	10.0%	--
PFR RO-UV [193]	284 ngL ⁻¹	60	91.9%	--
Batch O ₃ /H ₂ O ₂ [187]	2 mgL ⁻¹			0.0477 min ⁻¹
Batch H ₂ O ₂ /Fe ²⁺ [191]	2 mgL ⁻¹			0.0052 min ⁻¹
Batch UV/TiO ₂ (100 W) (this work)	2 mgL ⁻¹	30	98.6%	0.15 min ⁻¹

For this compound, the first order reaction rate constant for the removal of TCEP with the UV/TiO₂ process in the batch reactor found in this work (pH 5, TiO₂ = 1.5 gL⁻¹) was 0.15 min⁻¹ as shown in Table V-4. This is somewhat faster (higher first-order rate constant) than the constant reported by Nguyen [191] and Votruba [187], where they found rate constants of 0.0477 min⁻¹ and 0.0052 min⁻¹, respectively. It is suspected that the UV/TiO₂ system employed in this work produced hydroxyl radicals at a higher rate than in the systems used by both Nguyen and Votruba. The reaction rate constants for the oxidation of TCEP using the UV/TiO₂ process is lower than the rate constants for the other contaminants evaluated in this work. This is consistent with other treatability results reported by others, [190] and [193].

Using the rate constant found in this research, the predicted removal percentage using a mixed batch reactor is 53% for a 5 min reaction time, and 78% for a 10 min reaction time. The predicted removal percentage using a CSTR is 43% for a 5 min reaction time, and 60% for a 10 min reaction time.

5.1.1.4. Gemfibrozil

Gemfibrozil is a widely-used pharmaceutical that has been found in the environment in many studies [122, 123] and has been degraded with effectiveness using AOPs [194]. It may be treated with variable effectiveness using various treatment technologies as shown in Table V-5. Adsorption to granular activated carbon has been reported to be relatively ineffective (8% removal as reported by Snyder [195], and removal in a membrane bioreactor was found to be 46% [195]. However, the use of O₃ was also reported achieving a removal of 99% [189], and Molinari [196] found 98.5% destruction with UV/TiO₂.

Table V-5 Results of Gemfibrozil - Treatability studies.

Technology	Initial conc.	Operation time (min)	% removal	Reaction rate constant
CSTR O ₃ [189]	0.36 µgL ⁻¹	24	99.0%	--
PFR (2.3kW) Photocatalytic reactor membrane [190]	0.17 µgL ⁻¹	--	--	0.80 m ³ (kW·h) ⁻¹ , 0.89 min ⁻¹
CSTR UV/TiO ₂ (125W) [196]	10 mgL ⁻¹	30	98.5%	--
Batch Cl ₂ [192]	100 ngL ⁻¹	1440	98.0%	--
PFR RO-UV [195]	2.74 µgL ⁻¹	120	99.9%	
Batch UV/TiO ₂ (100 W) (this work)	2 mgL ⁻¹	12	96.0%	0.84 min ⁻¹

The first order reaction rate constant found in this study for the removal of gemfibrozil with the UV/TiO₂ process in the batch reactor (pH 5, TiO₂ = 1.5 gL⁻¹) was 0.84 min⁻¹. This is similar to Kim and colleagues who found 1.12 min⁻¹ [197], and values found in Molinari's work [196], 2.15 min⁻¹. Using the first order rate constant obtained in this work, the predicted removal percent using a batch reactor was found to be 98.5% for a 5 min reaction time, and 99.98% for a 10 min reaction time. The predicted removal percentage using a CSTR is 81% for a 5 min reaction time, and 89.4% for a 10 min reaction time.

5.1.1.5. 17β estradiol

Finally, the hormone 17β estradiol is a contaminant commonly found in domestic wastewater [91, 132] due to limited treatment in conventional wastewater treatment plants. It has been found in natural waters due to anthropogenic activity [130, 196]. It is amenable to various treatment processes including chemical oxidation (e.g. ozonation) and adsorption. For 17β estradiol treatment, Snyder and colleagues found a removal effectiveness higher than 99% using ozonation [189]. Coleman and Bistan also achieved high removal efficiencies using UV/TiO₂. Nevertheless, Coleman [198] showed a 98% of removal for this compound in 3.5 h by photocatalysis using TiO₂, and in a different study developed by Bistan [132] using UV/TiO₂, a 100% removal of the hormone was achieved after 30 minutes.

Table V-6 Results of 17 β Estradiol - Treatability studies.

Technology	Initial conc.	Operation time (min)	% removal	Reaction rate constant
CSTR O ₃ [189]	0.35 μgL^{-1}	24	99.0%	--
PFR (2.3kW) Photocatalytic reactor membrane [190]	18 ngL^{-1}	--	--	12 $\text{m}^3 (\text{kW}\cdot\text{h})^{-1}$, 2.01 min^{-1}
CSTR UV/TiO ₂ (150W) [132]	0.3 mgL^{-1}	240	99.9%	--
Batch Cl ₂ (3.8 mgL^{-1}) [192]	100 ngL^{-1}	1440	98.0%	--
Batch UV/TiO ₂ (this work)	2 mg/L	21	97.4%	0.49 min^{-1}

In this study, the first order reaction rate constant for the removal of 17 β estradiol by UV/TiO₂ process (pH 5, TiO₂ = 1.5 gL^{-1}) was found to be 0.49 min^{-1} . This is similar to the rate constant found in Snyder's work using ozonation [189]. Using the first order rate constant obtained in this work, the predicted removal percent using a batch reactor is calculated to be 91.4% for a 5 min reaction time, and 99.2% for a 10 min reaction time. On the other hand, the predicted removal percentage using a CSTR is 71% for a 5 min reaction time, and 83% for a 10 min reaction time.

5.2. Assessment of Scaling-Up Parameters

Using the first-order rate constants obtained from data collected in this work, predictions for treatment in CSTR and PFR reactors were made and are shown in Figure V-1 for 5 minutes reaction time, and Figure V-2 for 10 minutes reaction time.

As expected, a PFR (which is the same as a batch reactor in terms of percent removal capabilities) will out-perform a CSTR based on mass-balance equations while assuming an ideal hydraulic condition. Also, as expected, the degree of removal is shown to be related to time of reaction – which is the primary variable used in the simplified first-order model (based on contaminant present – C, and process time – t).

The first-order kinetic model is the most common model applied to treatment systems. It has been found to follow the data obtained in this work, yet can only be applied when conditions are identical (i.e., same TiO₂ concentration and UV power/reactor volume).

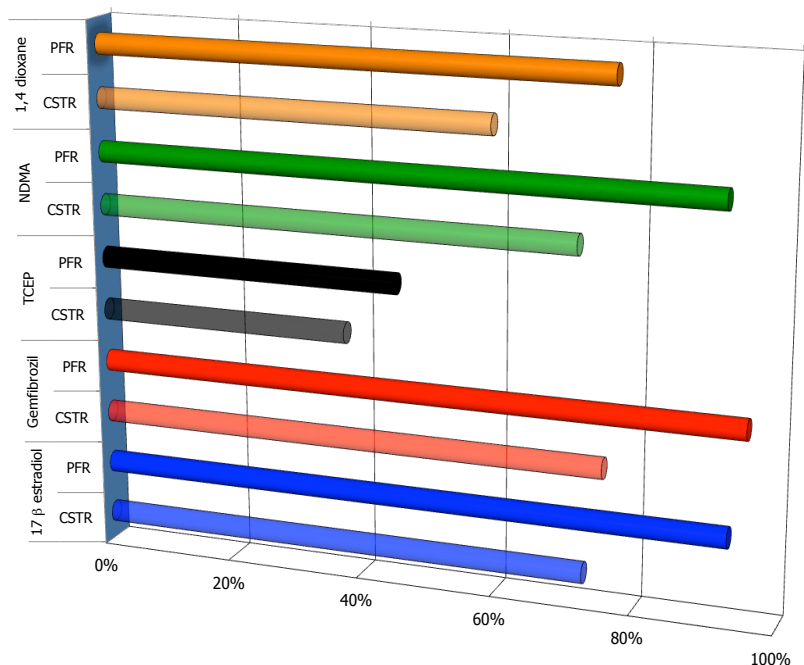


Figure V-1 CSTR and PFR predictions from collected data using the first order rate model for 5 minutes reaction time.

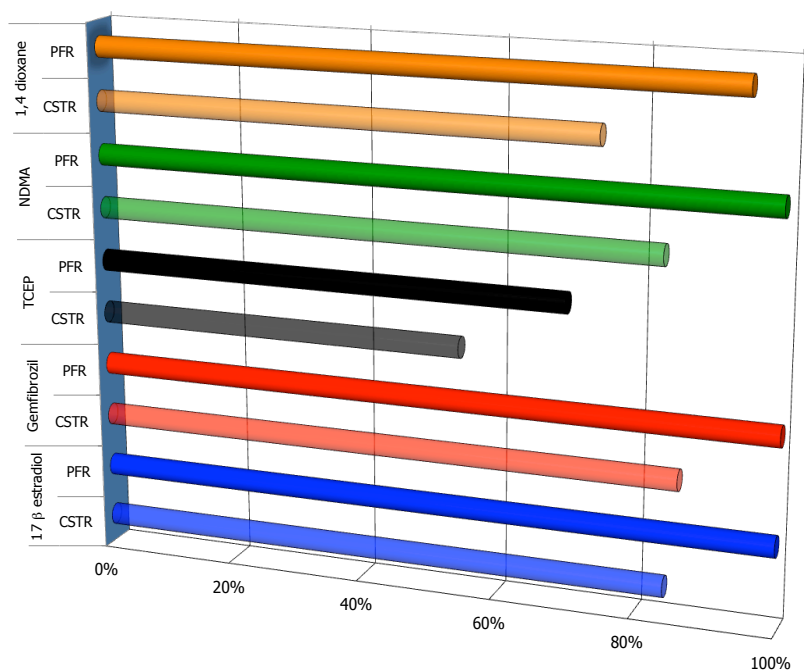


Figure V-2 CSTR and PFR predictions from collected data using the first order rate model for 10 minutes reaction time.

To provide rate constants with wider applicability for scale-up, the first-order rate constants were normalized to UV power delivered divided by the reactor volume, then normalized to the TiO_2

surface area, and finally normalized to UV power/reactor volume and TiO₂ surface area together. This approach allows scale-up to systems utilizing alternate UV power, and alternate TiO₂ concentrations (surface area is proportional to TiO₂ concentration). These rate constants, k' , k'' , and k''' , were listed in Table IV-10.

The first-order rate constants normalized to UV power/reactor volume are: 2.63 m³(kW·h)⁻¹ for 1,4 dioxane, 2.79 m³(kW·h)⁻¹ for NDMA, 0.97 m³(kW·h)⁻¹ for TCEP, 5.47 m³(kW·h)⁻¹ for gemfibrozil, and 3.19 m³(kW·h)⁻¹ for 17β estradiol. These rate constants are comparable to those reported by Benotti *et al.* [190] for a similar UV/TiO₂ system. Multiplying these rate constants by the UV power delivered divided by the reactor volume; they can be used in first-order rate equations to predict performance for scaled-up reactors.

The first order rate constants normalized to TiO₂ surface area, k'' , are: 0.0024 min⁻¹m⁻² for 1,4-dioxane, 0.0033 min⁻¹m⁻² for NDMA, 0.0028 min⁻¹·m⁻² for TCEP, 0.0063 min⁻¹·m⁻² for gemfibrozil, and 0.0038 min⁻¹·m⁻² for 17β estradiol. The use of this rate constant allows for prediction of reactor performance for varying concentrations of TiO₂ concentrations up to and including 1.5 gL⁻¹, above which light attenuation limits treatment effectiveness.

Normalizing the first-order rate constant to both power/reactor volume and TiO₂ surface area allows the greatest utility for predicting treatment performance with scale-up under variable UV power, reactor volume, and TiO₂ concentration. The first-order rate constants normalized to power/volume and TiO₂ surface area, k''' , were found to be: 0.0161 m³·(kW·h)⁻¹·m⁻² for 1,4-dioxane, 0.0209 m³·(kW·h)⁻¹·m⁻² for NDMA, 0.0182 m³·(kW·h)⁻¹·m⁻² for TCEP, 0.0402 m³·(kW·h)⁻¹·m⁻² for gemfibrozil, and 0.0255 m³·(kW·h)⁻¹·m⁻² for 17β estradiol.

5.3.Extended Time Experiments

As previously mentioned, extended time experiments were carried out to validate the GC analytical methods developed for the purpose of this study, and verify that degradations trends were sustained over time even at the ngL⁻¹ range. First order rate constants calculated from the combined data set show ready degradation of all five contaminants. The results from the combined data set are comparable to the previous results over a limited (shorter) reaction time. It should be expected that there would be some difference in reaction rate constants when data is analyzed over a greater time range. The changes in reaction rate constants over the larger time range for the combined data set are minimal.

Figures in Table V-7 summarize first order reaction rate constants (min⁻¹) and first order rate constants normalized to volume and energy delivered (m³(kW·h)⁻¹) using the combined, updated data. These results show that the general trend for the kinetics found in the initial experiments in our laboratory at early times (from 0 to 10 min) did not significantly vary along the

photocatalytic process even at late times (from 18 to 26 min). The percentages of difference of the data obtained at early vs. extended times are also listed in table V-7.

Table V-7 First order degradation rate constants for UV/TiO₂ oxidation, and % of difference with early times kinetics at 1.5 gL⁻¹ of TiO₂, pH 5.0, and 100W UV power using the combined data

Contaminant	<i>k</i> (min ⁻¹)	<i>k'</i> (m ³ (kW·h) ⁻¹)	% Difference w/early times
17β estradiol	0.53	3.46	- 8%
NDMA	0.50	3.24	- 16 %
TCEP	0.12	0.80	+ 20 %
Gemfibrozil	0.61	4.00	+ 27 %
1,4 dioxane	0.29	1.89	+ 28%

5.4. Adsorption Rate Experiments

Adsorption of the selected contaminants to titanium dioxide follows a first order rate model (Appendix Q). As can be observed from these results, gemfibrozil has the greatest adsorption kinetic constant (0.136 min⁻¹), which confirms that its affinity to the TiO₂ surface enhances its degradation in the photocatalytic process as has been shown in this work, while for TCEP the constant obtained was the lowest one (0.074 min⁻¹). The results found in this work for the degradation rate of contaminants subjected to UV/TiO₂ oxidation, support the hypothesis that photocatalysis is a surface dependent mechanism. The compounds reached equilibrium concentrations at different times: NDMA and gemfibrozil at 15 minutes, 1,4 dioxane and 17β estradiol at 20 minutes, and TCEP at 25 minutes.

The variation in the values of adsorption constants for each contaminant may be explained by analyzing the relationship between the pH of water and the contaminant pKa values. The experiments were performed at pH of 5, which is below the TiO₂ point of zero charge (6.25). At pH 5 adsorbent surface of the TiO₂ is positively charged attracting negatively charged molecules. Contaminants such as gemfibrozil (pKa=4.39), 17β estradiol (pKa=3.75), and NDMA (pKa=3.52) with pKa values lower than the pH of the water, are deprotonated and negatively charged; therefore will be prone to get attracted to the TiO₂ surface. Conversely, TCEP and 1,4 dioxane both do not have ionic species on their structures, therefore be subject to increase coulombic repulsion to the TiO₂ surface.

5.5. Formation of Oxidation Intermediates

According to GC/MS results, it was noticed that most of the intermediates detected were composed by 2,5-dimethylphenol (p-xyleneol), a gemfibrozil's moiety. This behavior suggests

that individual gemfibrozil's pathway might have started with a heterolytic cleavage at the ether oxygen position dividing the molecule into two main moieties: p-xylenol (detected in this work) and 2,2-dimethyl-5-oxopentanoate (at pH 5), which is consistent with Yurdakal and collaborators' work [199]. Four derivatives that are suggested to come directly from p-xylenol structure were well identified: 2,3-dimethylphenol, 2,6-dimethylphenol, 2-hydroxy-5-methylbenzaldehyde, and 2,5-dimethylcyclohexa-2,5-diene-1,4-dione.

Transformation of the p-xylenol molecule to m-xylenol and o-xylenol isomers is suggested. This pathway can undergo by alkyl shift mechanism based on electrophilic aromatic substitution due to the hydroxyl radical attack [200, 201] (Figure V-3). Photocatalytic isomerization of organic compounds has been previously study by Kodama and Yagi [202], as well as xylene's isomerization over Friedel-Crafts catalysts [203].

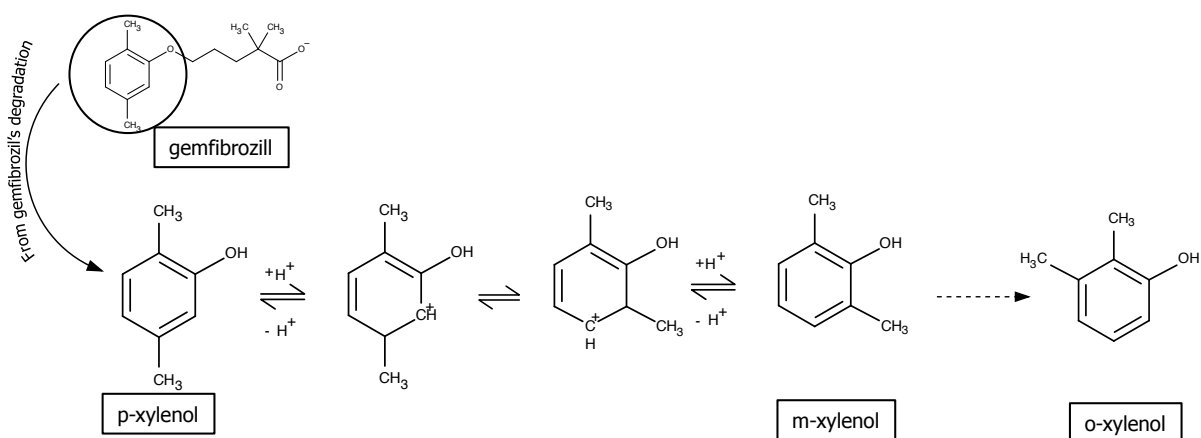


Figure V-3 Suggested alkyl shift mechanism to the formation of 2,3-dimethylphenol and 2,6-dimethylphenol

Suggested mechanism of formation of 3-hydroxy-4-methylbenzaldehyde and 5-hydroxymethyl-2-methylphenol is favored by the attack of hydroxyl radicals that can abstract the hydrogen from any of the two methyl-groups of the p-xylenol to convert into a methyl radical and water. Then, the reaction of the radical formed with oxygen produces a peroxy radical form that combined to the same molecule leads to produce a tetraoxide group bonding the two molecules. Finally the molecule is break down into 3-hydroxy-4-methylbenzaldehyde and 2-hydroxy-4-methylbenzyl alcohol as shown on figure V-4. Similar facts were suggested by Ryas and colleagues [204].

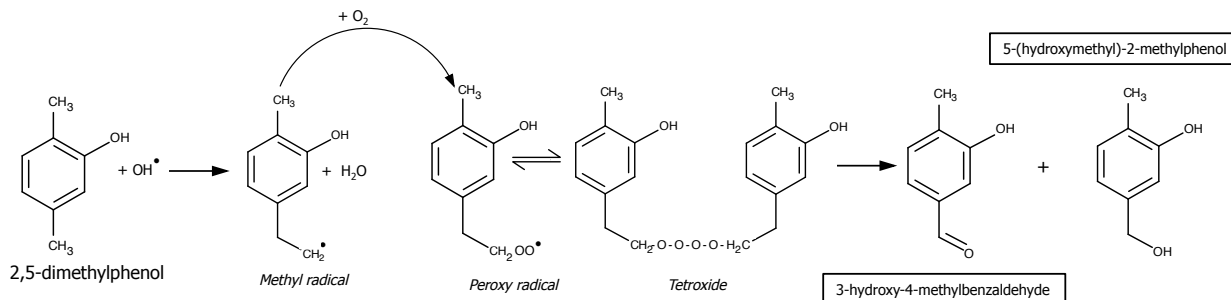


Figure V-4 Suggested pathway formation of 3-hydroxy-4-methylbenzaldehyde and 2-hydroxy-4-methylbenzyl alcohol

The suggested formation of 2,5-dimethyl-1,4-benzoquinone corresponds to a well know process of oxidation of phenols to benzoquinones. The process starts with the hydroxylation at the C4 of the benzene ring of the p-xylene moiety as shown on figure V-5. Then, a continuous protonation-deprotonation mechanism is suggested until the formation of the benzoquinone structure occurs as detected in the analysis. Similar results were obtained by Terzian and Serpone [205] and Huang and Qiang [206].

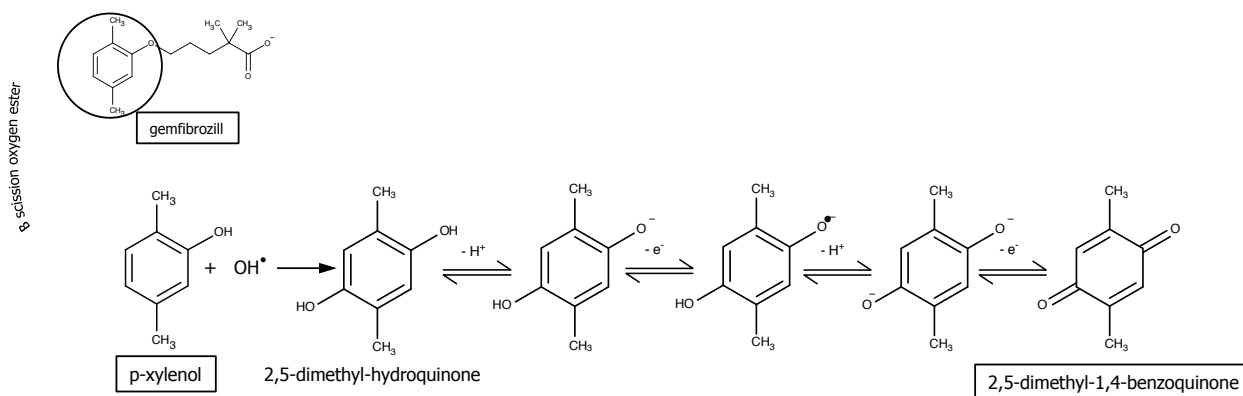


Figure V-5 Suggested pathway formation of 2,5-dimethyl-1,4-benzoquinone

Finally, another intermediate of the gemfibrozil's molecule is the 3-methoxybenzaldehyde (Figure V-6), which is suggested to be formed from partial hydroalkylation of the 1,4-xylene to form 3-methylphenol and methane. Then, hydroxylation of the methyl group in the para position by the hydroxyl radical 3-(hydroxymethyl)phenol and subsequent oxidation of the -OH group come up with an aldehyde derivative. The final stage in the formation of 3-methoxybenzaldehyde is the alkylation with a methyl group by nucleophilic substitution of phenol at the alcohol group in the benzene ring.

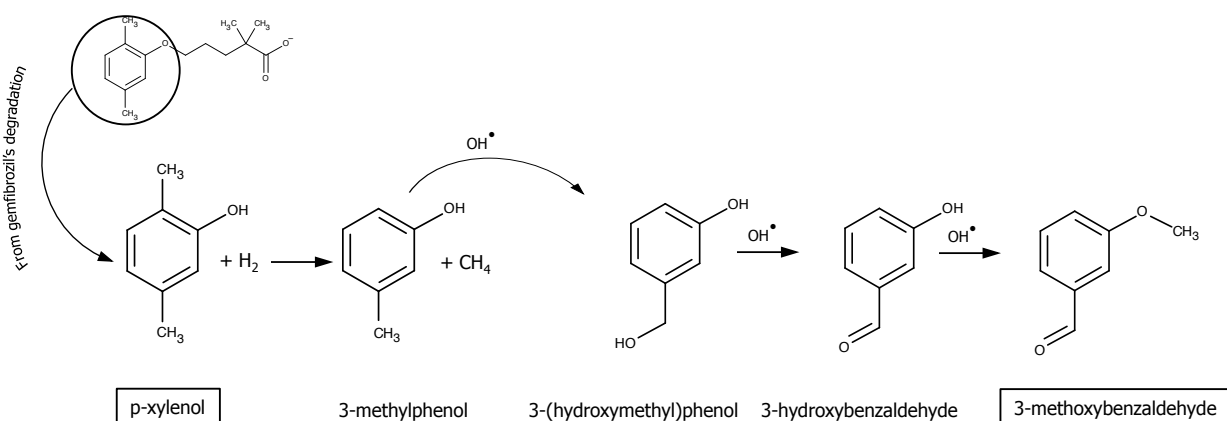


Figure V-6 Suggested pathway of 3-methoxybenzaldehyde's formation.

5.5.1 Intermediates Formation by Random Interactions Among Compounds

Several intermediates from the random reaction among different products were also identified. Different mechanisms were suggested to come up with the synthesis of these compounds that took place at the catalyst surface by the influence of favorable conditions on their formations. A wide variety of different derivatives were identified: carbamates, imidazoles, pyrrolidines, propanamides, acetophenone, furans, long chain hydrocarbons, and so on. Possible pathways of formation for some of these compounds are suggested.

Figure V-7 suggests a heterolytic scission of the gemfibrozil to form the p-xyleneol molecule, which may be attacked by an electron of the conduction band of the TiO₂ at the -OH group [207], and then a thermal hydrodealkylation of the 1,4-xylene might have lead to the formation of benzene. Judging by what was found by GC/MS, parallel to this reaction the also detected chloroacetic acid [208], a possible byproduct of the chlorination (produced by TCEP) and acetic acid (a 1,4-dioxane's minor intermediate), could have reacted with benzene to produce acetophenone following the Friedel-Crafts (F-C) acylation mechanism, a similar mechanism studied by Afzal Pasha and colleagues [209].

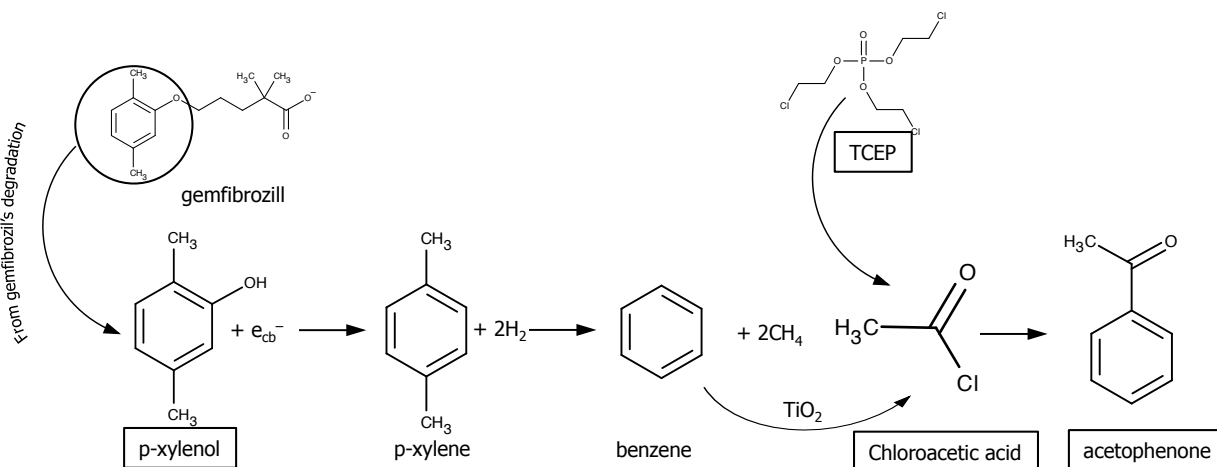


Figure V-7 Suggested pathway of acetophenone's formation.

On the other hand, as carbamic acids are compounds derived from the attachment of an acid group to an amine [210], the formation of methylcarbamic acid is suggested via hydrochloric hydrolysis of the R-N=O structure of the NDMA [211]. Then, a suggested o-acylation of the 2,6 dimethylphenol and the unstable methylcarbamic acid takes place to form 3,5-dimethylphenyl-N-methylcarbamate as illustrate on figure V-8.

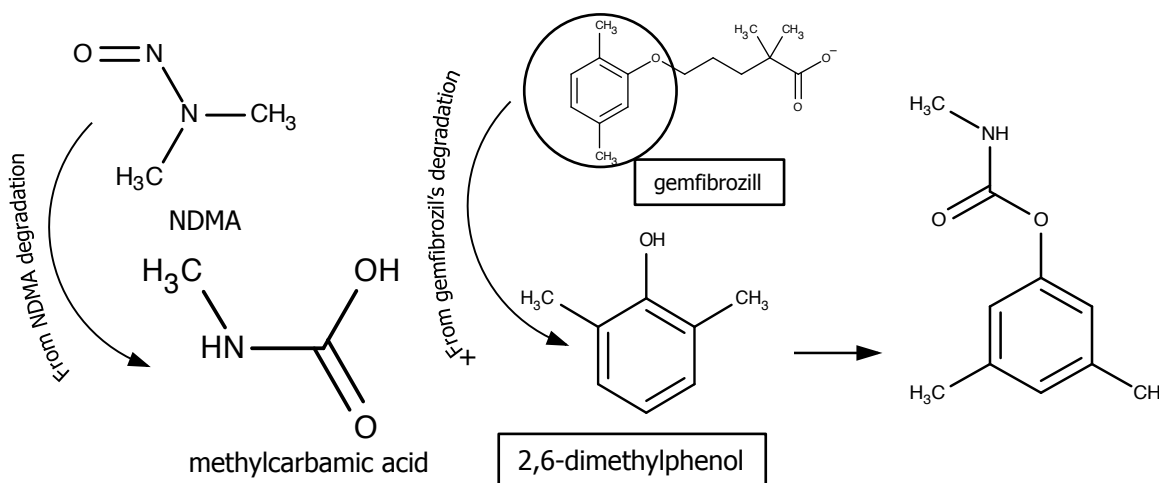


Figure V-8 Suggested pathway formation of methylcarbamic acid and 3,5-dimethylphenyl-N-methylcarbamate.

Finally, compounds like N-(4,6-dimethoxypyrimidin-2-yl)-2-methylpropanamide were also detected. The suggested pathway for this pyrimidine derivative involves several intermediates as dimethyl malonate (a malonic acid derivative [103]), guanidine (nitrosamide) and isobutyric acid (a suggested product of gemfibrozil's pentanoate moiety) that also comes from 1,4 dioxane, NDMA and gemfibrozil respectively. This pathway starts with a protonation of one of the carbonyl oxygen of the ester derivative by the double bonded amino group of the unstable

guanamide, and then a proton transfer from the amino group takes place to link the two molecules. Consequently, the ring closure of the carbinolamine forms a diol structure followed by two successive eliminations and proton transfers to end with 2-amino-4,6-dimethoxypyrimidine [212], which finally interacts with the carboxylic acid to form the pyrimidine derivative.

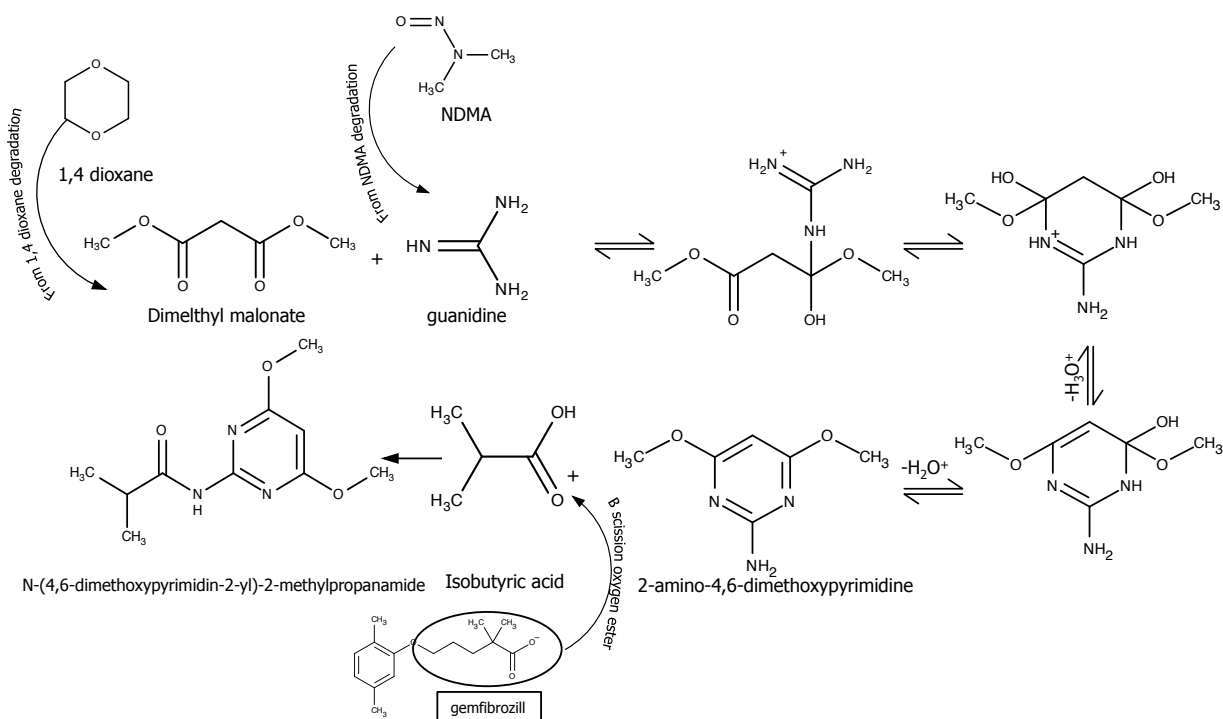


Figure V-9 Suggested pathway formation of N-(4,6-dimethoxypyrimidin-2-yl)-2-methylpropanamide.

As explained above, several oxidation byproducts were identified in this work, but not enough to construct a more detailed degradation pathway for all the compounds of the studied matrix. However, the formation pathways suggested, although with some similarities, are reported for the first time contributing to findings published by others and expanding the knowledge in the water treatment field by AOP technologies.

VI. CONCLUSIONS AND RECOMMENDATIONS

This dissertation assessed the effectiveness of using the slurry UV/TiO₂ process in the simultaneous degradation of five different compounds (1,4 dioxane, NDMA, TCEP, gemfibrozil, and 17 β estradiol) from water. Also, experiments to identify intermediates of the UV/TiO₂ oxidation of these five contaminants were conducted. At 26 min reaction time, no byproducts were found indicating successful mineralization. However, at 2 min reaction time, many byproducts were identified, many of which had not been previously reported in the literature.

On the basis of the results obtained in this work, TiO₂ photocatalysis (using Degussa P25) has shown to be a good alternative for photocatalytic degradation of contaminants. The results show that both the first order rate and the L-H models described the degradation of the five compounds well. In addition, rate data for the adsorption of the five contaminants to TiO₂ was obtained. The adsorption rate data showed significant time (up to 25 minutes for TCEP) required to reach adsorption equilibrium under these conditions. Accordingly, major outcomes of this dissertation are:

1. The effects of pH and TiO₂ surface area on the UV/TiO₂ process were systematically evaluated, and the most favorable conditions were found to be at solution pH of 5.0 and slurry TiO₂ concentration of 1.5 gL⁻¹.
2. According to the results obtained, it could be concluded that the general trend of the kinetics found in the initial experiments at early times (from 0 to 10 min in the μgL^{-1} range) using GC-SPME-FID and SPE-GC-FID analytical techniques did not significantly vary along the photocatalytic process even at late times (from 18 to 26 min in the ngL^{-1} range). The extended-time analyses were conducted in an external laboratory using EPA detection methods, which would validate the data previously obtained in the high concentration range.
3. Both the L-H and pseudo-first order modeling approaches provided a good fit to the degradation experimental data. While some minor variations were observed, both models were successfully applied to the UV/TiO₂ oxidation data. Therefore, to simplify calculations and for a scale up analysis the first order rate is recommended to describe the photocatalytic process.
4. After 5 minutes of UV/TiO₂ process reactions, significant degradation of the contaminants was observed: 77% for 1,4 dioxane, 92% for NDMA, 95% for gemfibrozil and 93% for 17 β estradiol. Degradation of 45% for TCEP was also observed. Compounds with lower aqueous solubilities (gemfibrozil and 17 β estradiol) were more rapidly degraded in comparison with those more soluble in water. However, gemfibrozil's

degradation intermediates were prone to react with other compounds (such as NDMA's intermediates) to produce other categories of byproducts like pyrimidine intermediates and a secondary amine. TCEP exhibited the slowest degradation rate of all the compounds in this matrix mostly due to its chemical nature and the operational conditions of the experiments.

5. TCEP and dioxane exhibited a low degradation rate in comparison with the other compounds of the matrix due to the lack of ionizable groups. Conversely, the presence of carboxyl and hydroxyl groups in the gemfibrozil and 17 β estradiol structures respectively, their low solubilities, and pKa values below the P_{ZC} of the TiO₂, favored their fast degradation rates.
6. The results indicated that gemfibrozil had the greatest affinity for the TiO₂ surface, with 70% of the gemfibrozil adsorbed (with 10 gL⁻¹ TiO₂). Conversely, TCEP had the least affinity for the TiO₂ surface with only 20% removed from aqueous solution due to adsorption. This fact may lead to the conclusion that the level of affinity that a compound has to the photocatalyst surface directly affects its speed of degradation. The Langmuir adsorption constants, K_L , which are a measure of adsorption capacity, follow this trend as well. TCEP has the lowest value K_L , 0.063 Lmg⁻¹, and gemfibrozil the highest, 0.206 Lmg⁻¹. The other three contaminants were found to have intermediate values: 0.111 Lmg⁻¹ for 1,4-dioxane, 0.124 Lmg⁻¹ for NDMA, and 0.149 Lmg⁻¹ for 17 β estradiol.
7. The normalized values of the first order rate constants to energy per volume as well as the normalized values of photocatalyst surface area obtained in this study are useful tools to the pre-design of higher scale prototypes by modeling desired removal efficiencies to obtain design parameters such as volume, energy requirements, and amount of photocatalyst.
8. Compounds treated by UV/TiO₂ photocatalysis find a suitable environment for random interactions among them making difficult the prediction of the intermediates and making important to control reaction times to ensure total mineralization of treated compounds, as otherwise partial degradations might occur and generate unexpected and even more toxic intermediates.
9. Gemfibrozil's intermediates were much prone to react with other pollutants such as NDMA's derivatives to produce other categories of byproducts like pyrimidine derivatives and a secondary amine. TCEP exhibited the slowest degradation rate of all the compounds of the matrix mostly due to its chemical nature and the operational conditions of the experiments. In addition, the variation in the gemfibrozil's p-xylene moiety suggests that there could be more than one possible pathway for the degradation of this

compound and therefore, the formation of other byproducts might come up with along the photocatalytic oxidation.

VII. FUTURE WORK

The results obtained and conclusions drawn from this dissertation have established that TiO₂ photocatalysis has shown to be a good alternative for photocatalytic degradation of contaminants. The recommended next step would be the evaluation of a pilot unit of this system, using real water samples. Also, as the UV/TiO₂ process is a surface-based process, the effect of mass transfer, from dissolved to the adsorbed state, on the process should be further investigated with a more complex matrix.

In addition, further studies may include the analysis and determination of possible degradation pathways of these intermediates. This will contribute to the understanding of the UV/TiO₂ photocatalytic degradation process applied to real water samples. In addition, the evaluation of a scaled up UV/TiO₂ system, using real water samples would be the next step to determine the feasibility of the photocatalytic process as an alternative for the degradation of emerging contaminants in water.

VIII. APPENDICES

APPENDIX A: Information on Contaminants and Catalyst

Table A1: Information on Contaminants.

Compound	1,4 Dioxane	NDMA	TCEP	Gemfibrozil	17 β estradiol
CAS No. [121]	123-91-1	62-75-9	115-96-8	25812-30-0	50-28-2
Formula [121]	C ₄ H ₈ O ₂	C ₂ H ₆ N ₂ O	C ₆ H ₁₂ Cl ₃ O ₄ P	C ₁₅ H ₂₂ O ₃	C ₁₈ H ₂₄ O ₂
MW (g mol ⁻¹) [121]	88.11	74.08	285.49	250.33	272.38
Pure phase [121]	Liquid	Liquid	Liquid	Powder	Powder
PKa [213]	--	3.52	--	4.39	3.75
Log Kow	-0.27 [214]	-0.57 [215]	1.44 [213]	4.77 [213]	4.01 [213]
Pure phase Density (gL ⁻¹)[121]	1.030	1.005	1.390	1.000	1.200
Melting point (°C) [121]	12	<25	-55	129	180
Boiling point (°C) [121]	101	153	192	362	395
Water solubility[121]	1 kgL ⁻¹ (20°C)	1 kgL ⁻¹ (24°C)	7.82 gL ⁻¹ (25°C)	5 mgL ⁻¹ (25°C)	50 mgL ⁻¹ (25°C)

APPENDIX B: Sample Preparation – Analytical Techniques

B.1. Experimental Procedure

Reactor Operation and sample preparation

- In a glass carboy (20L capacity), 2L of purified water were added, and then the respective amounts of the compounds listed in table B1 (stock solution A) was also added, and stirred for 60 minutes. Then 2L of purified water were added and the solution was stirred for 240 more minutes. Finally 6L of purified water were added to complete 10L volume and the mixture was stirred for 24h period (this solution was used with no longer a week from its preparation each time, and was kept stirring at room temperature during that period).

Table B1. Preparation of sample stock solution (A).

Compound	Amount
TCEP (μL)	14.5
Gemfibrozil (mg)	20.0
17 β estradiol (mg)	20.0
Total volume of purified water (L) =	10.0
Stock Conc. per contaminant (mgL^{-1}) =	2.0

- 100 mL of the stock solution (A) prepared in step 1 was added to 250 mL beaker, then 20 and 19.5 μL of NDMA and 1,4 dioxane respectively are added according to table 2 (stock solution B), and stirred for 45 min.

Table B2. Preparation of sample stock solution (B).

Compound	Amount
NDMA (μL)	20.0
Dioxane (μL)	19.5
Volume of purified water to add (mL) =	100
Stock Conc. per contaminant (mgL^{-1}) =	200.0

- From the prepared stock solution in step 1, 504.9 mL of sample stock solution A were taken and poured into a 600mL beaker and spiked with 5.1 mL of the preparation given in step 2. Therefore, all the five compounds were at 2 mgL^{-1} .

8. The desired slurry concentration of TiO₂ to be added was selected from table B3.

Table B3. Desired TiO₂ concentrations.

TiO ₂ slurry concentration (gL ⁻¹)	0.10	0.50	1.00	1.50	2.00	2.50
Amount of TiO ₂ to add (mg)	51	255	510	765	1020	1275

9. 510 mL of stock solution was measured prepared in step 3, the respective amount of TiO₂ was added, and the mixture transferred to the reactor.
10. The stir bar was adjusted to 700 rpm; the oxygen supply valve adjusted to a rate of 3 ft³h⁻¹, and the UV lamp turned on for the desired exposure time (1, 2, 3, 4, 5, 10, 15, 30, 45 min).
11. The UV lamp was turned off once the desired reaction time was reached. Note: Every time a sample is tested, the reactor was properly cleaned and dried (see cleaning section).
12. The total volume of 510 mL was transferred from the reactor to a 500 mL beaker, 10 mL of sample was pipetted from the beaker using a 25 mm syringe filter to a 10 mL vial for GC-SPME analysis, and the remain 500 mL was centrifuged using a Marathon 21000R centrifuge for 60 minutes, then filtered with a glass vacuum filtration unit using 47 mm cellulose membrane filter circles of 42 μm pore size to separate the TiO₂ nanoparticles from the water sample. The 500 mL filtered sample was collected in a 1000 mL filter flask and then transferred into a 500 mL beaker ready for SPE loading procedure.
13. 50 μL of internal standard, which consists of a solution of 0.05M chlorobenzene in MeCl were added to the 1.5 mL vials filled out with the eluent collected from the SPE procedure to then be analyzed by using GC-FID technique (see GC-FID analysis).
14. The 10 mL vials for GC-SPME-FID analysis were spiked with 50 μL of internal standard, which consisted of a solution of 0.09M chlorobenzene in water. After this step the samples were analyzed by using GC-FID technique (see GC-SPME-FID analysis).
15. Steps 1 to 8 were repeated every time a sample was prepared to analyze samples at different times.

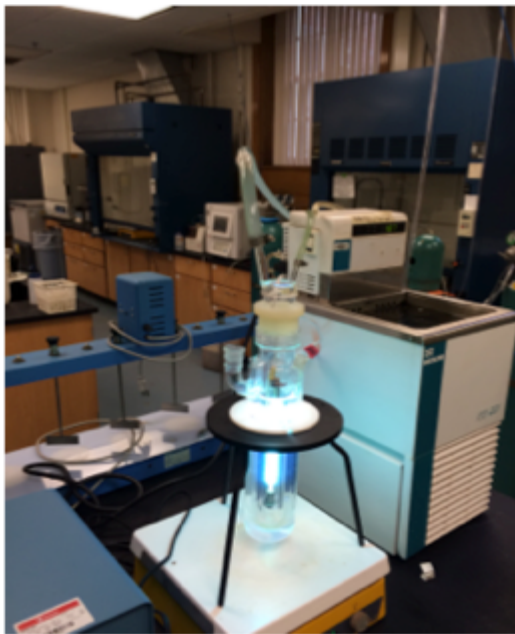


Figure B1. Reactor assembly.

B.2. Solid Phase Extraction (SPE) and Filters

SPE cartridge: 57063 SUPELCO, Supelclean™ ENVI-18 SPE Tube, Bed wt. 500 mg, volume 3 mL, pkg of 54 ea (Supelco, Inc., Bellefonte, PA). The bed capacity can be estimated to be ~5% of the bed weight. So for 500 mg the bed capacity is 25mg [216].



Figure B2. SPE cartridges.

Filters

For the adsorption constants experiments of NDMA and 1,4 Dioxane, 0.45 μm nominal pore syringe filters (25 mm diameter, GVS Maine, nitrocellulose mixed esters, Fisher Scientific, Pittsburg, PA) were employed. For the adsorption constants experiments and before the SPE procedure of TCEP, gemfibrozil and 17 β estradiol, 0.45 μm nominal pore filters (45 mm diameter, GVS Maine, nitrocellulose mixed esters, Fisher Scientific, Pittsburg, PA) were employed.

B.3. SPE Procedure

a) Sample pretreatment:

- **Condition/Equilibration:** For conditioning, the cartridge was filled with approximately 3 mL methylene chloride, the vacuum turned on, and the solvent pulled through, aspirating completely. This step was repeated one more time using the same initial volume of solvent.
- For equilibration, the cartridge was filled with approximately 3 mL of purified water, the vacuum turned on, and the water pulled through, this step was repeated without allowing the cartridge to go dry in between washes or at the end.

b) Sample Load: A transfer tube from the sample bottle to a cartridge was attached and then the vacuum turned on. The vacuum was adjusted so that the approximate flow rate was 10 mL/min. After the entire 500 mL sample (from step 1) had passed through the SPE cartridge, the reservoir and draw air through the cartridge was detached for 10 minutes at full vacuum. Then the vacuum was turned off and released. Immediately the cartridge elution took place.

c) Elution: The extraction manifold top was lifted and a rack with a collection tube inserted into the extraction tank to collect the extract as it is eluted from the cartridges. The cartridge was filled with methylene chloride (3 mL) and pulled into the cartridge at low vacuum to soak the sorbent. The vacuum was turned off and the system vented. The sorbent was allowed to soak in methylene chloride for approximately 1 minute. A low vacuum was applied and the methylene chloride pulled through the cartridge in a drop-wise fashion into the collection tube. The eluate was evaporated to complete dryness under a gentle nitrogen stream at room temperature using a RapidVap Labconco Evaporator (Kansas City, MO), then reconstituted to a final volume of 1.5 mL in DCM and finally stored in 1.5 mL glass vials in a refrigerator for analysis. Finally, the eluate volume was transferred into a 1.5 mL vial to be analyzed using GC-FID instrument.

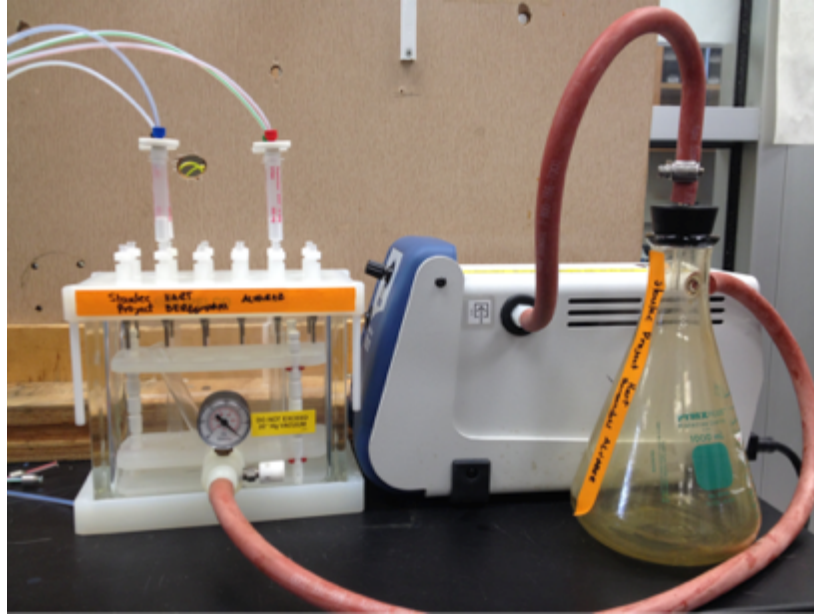


Figure B3. SPE assembly.

B.4. SPME procedure

- Measure 4 g of NaCl and poured into each 10 mL vial.
- Add 10 mL of the sample to analyze
- Add 50 μL of IS in water prior to GC analysis.

B.5. GC-FID Analysis

Instrument #1 GC-SPME-FID (1,4 Dioxane and NDMA)

GC analyses were carried out using an Agilent 6890 gas chromatograph equipped with Agilent 7863 automatic sampler and controlled by a computer running Agilent Chemstation software (Agilent Technologies, Palo Alto, CA, USA), equipped with flame ionization detector. (GC-FID).

- Configuration details:
 - **Injector**
Volume = 1.0 to 2.0 μL
 - **Inlet**
Mode: Splitless
Gas: N_2
Heater: 290 $^{\circ}\text{C}$
Pressure: 8.91 psi
Total Flow: 45.6 mLmin^{-1}

Purge flow to split vent 38.9 mLmin⁻¹ at 0.40 min

○ **Column:**

Mode: constant pressure

Model No. Restek RTX-5Sil MS – Capillary 30.0m x 320 µm x 0.5 µm nominal
350C max temp

Flow 2.2 mLmin⁻¹

Vel : 35 cm/sec

○ **Oven configuration:**

Oven ramp	°C/min	Next °C	Hold min	Run Time
Initial		32	4.00	4.00
Ramp 1	3.00	50	0.00	10.00
Ramp 2	8.00	290	3.00	43.00

○ **FID Detector:**

Heater: 300 °C

H₂ flow: 40.0 mLmin⁻¹

Air flow: 450 mLmin⁻¹

Makeup N₂: 45 mLmin⁻¹

○ **Signals:**

Signal 1: 50Hz -- 0.004 min

Signal 2: 20 Hz -- 0.01 min

Instrument #2 SPE-GC-FID (TCEP, gemfibrozil and 17 beta estradiol)

GC analyses were carried out using an Agilent 6890 gas chromatograph equipped with Agilent 7863 automatic sampler and controlled by a computer running Agilent Chemstation software (Agilent Technologies, Palo Alto, CA, USA), equipped with flame ionization detector. (GC-FID).

• Configuration details:

○ **Injector**

Volume = 1.0 to 2.0 µL

○ **Inlet**

Mode: Splitless

Gas: N₂

Heater: 290 °C

Pressure: 15 psi

Total Flow: 4.7 mLmin⁻¹

Purge flow to split vent 1.0 mLmin⁻¹ at 0.00 min

Gas saver: 20 mLmin⁻¹ at 2min

○ **Column:**

Mode: constant flow

Model No. Restek RTX®-5 – Capillary 30.0m x 250 µm x 0.25 µm nominal 350C
max temp

Pressure 15 psi

Flow 1.6 mLmin⁻¹

Vel : 36 cmsec⁻¹

○ **Oven configuration:**

Oven ramp	°C/min	Next °C	Hold min	Run Time
Initial		32	4.00	4.00
Ramp 1	3.00	50	0.00	10.00
Ramp 2	8.00	290	3.00	43.00

○ **FID Detector:**

Heater: 300 °C

H₂ flow: 40.0 mLmin⁻¹

Air flow: 450 mLmin⁻¹

Makeup N₂: 25 mLmin⁻¹

○ **Signals:**

Signal 1: 20Hz -- 0.01 min

Signal 2: 50 Hz -- 0.004 min

Instrument #3 SPE-GC-MS

GC analyses were carried out using an Agilent 5975C gas chromatograph/mass selective detector model controlled by a computer running Agilent Chemstation software (Agilent Technologies, Palo Alto, CA, USA), equipped with mass spectrometer. (GC-MS).



Figure B.4. Syringe 10 µL Agilent.

- Configuration details:
 - **Injector**
Volume = 1.0 μL
 - **Inlet**
Mode: Splitless
Gas: He
Heater: 290 $^{\circ}\text{C}$
Pressure: 15 psi
Total Flow: 4.7 mLmin^{-1}
Purge flow to split vent 1.0 mLmin^{-1} at 0.00 min
Gas saver: 20 mLmin^{-1} @ 2min
 - **Column:**
Mode: constant flow
HP-5MS capillary column (95% dimethyl-siloxane – 5% diphenyl) 30 m x 250 μm x 0.25 μm nominal film thickness Pressure 15 psi
Flow 1.6 mLmin^{-1}
Vel : 36 cmsec^{-1}
 - **Oven configuration:**

Oven ramp	$^{\circ}\text{C}/\text{min}$	Next $^{\circ}\text{C}$	Hold min	Run Time
Initial		32	4.00	4.00
Ramp 1	3.00	50	0.00	10.00
Ramp 2	8.00	290	3.00	43.00

 - **MS** Electron ion mass spectra was monitored from 50 m/z to 400 m/z. The ion source and quadrupole temperatures were set at 230 and 106 $^{\circ}\text{C}$ respectively. The instrument worked in positive chemical ionization (PCI) mode.

B.6. Calibration curve

- Solvent MeCl (for SPE GC-FID and GC-MS)
- a. A MeCl solution of the compounds listed in table B4 was prepared as follows:
- b.

Table B4. Solution – calibration curve.

Compound	Amount
TCEP	18 μL
Gemfibrozil	25 mg
17 beta estradiol	25 mg

V of solvent (MeCl) =	16.0 mL
V solution =	16 mL
Stock Concentration =	1,563 mgL⁻¹
Vial volume (1.5 mL) x 3 =	4.5 mL

- c. The series dilution method was implemented to prepare three samples of 1.5 mL each at the concentrations given in table B5.

Table B5. Series dilution method (MeCl as solvent).

Sample No.	1	2	3	4	5	6
Des. Conc. (mgL ⁻¹) =	500	100	50	10	5	1
V of previous solution to add (mL) =	4	2	5	3	5	3
V of MeCl (mL) =	8.5	8	5	12	5	12
Final V (mL) =	12.5	10	10	15	10	15
Volume to be tested (1.5mL) x 3=	8	5.5	5.5	10.5	5.5	10.5
Available vol next dilution (mL) =	OK	OK	OK	OK	OK	OK

- d. Each vial was spiked with 50 µL of the selected internal standard in MeCl to then be analyzed by using GC-FID technique (see GC-FID analysis instrument #2). The concentrations in MeCl measured on the GC-FID instrument #2 have an equivalent concentration in water according to table B6.

Table B6. Conversion of concentrations from MeCl to water

Concentration (MeCl)	Concentration (water)
1,563 mgL ⁻¹	9,378 µgL ⁻¹
500 mgL ⁻¹	3000 µgL ⁻¹
100 mgL ⁻¹	600 µgL ⁻¹
50 mgL ⁻¹	300 µgL ⁻¹
10 mgL ⁻¹	60 µgL ⁻¹
5 mgL ⁻¹	30 µgL ⁻¹
1 mgL ⁻¹	6 µgL ⁻¹

- Solvent H₂O (for GC-SPME-FID)

- a. A H₂O solution of the compounds listed in table B7 was prepared as follows:



Figure B.5 GC-SPME-FID instrument

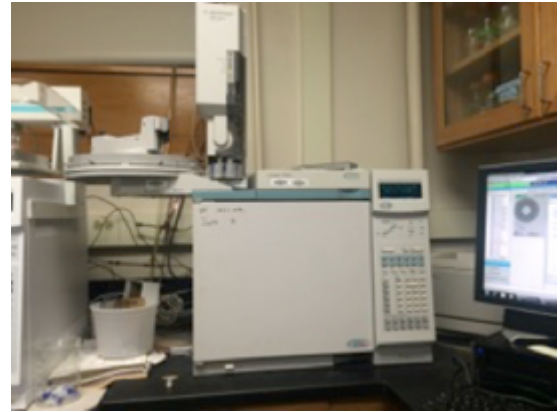


Figure B6. GC-FID instrument

Table B7. Solution – calibration curve.

Compound	Amount
NDMA	20.0 μL
Dioxane	19.5 μL
V of H₂O =	1000 mL
V solution =	1000 mL
Stock Concentration =	20 mgL⁻¹
Vial volume (10 mL) x 3 =	30 mL

- b. The series dilution method was implemented to prepare three samples of 10 mL each at the concentrations given in table B7.

Table B7. Series dilution method (H₂O as solvent).

Sample No.	1	2	3	4	5	6
Des. Conc. (mgL ⁻¹) =	10	5	1	0.5	0.25	0.1
V of previous solution to add (mL) =	250	250	100	250	250	200
V of H ₂ O (mL) =	250	250	400	250	250	300
Final V (mL) =	500	500	500	500	500	500
Volume to be tested (10mL) x 3 =	470	470	470	470	470	470
Available vol next dilution (mL) =	OK	OK	OK	OK	OK	OK

- c. Each vial was spiked with 50 μL of the selected internal standard in water to then be analyzed by using GC-SPME-FID technique (see GC-SPME-FID analysis instrument #1)

- **Cleaning**

The laboratory glassware must be clean and dried every time an experiment is performed as follows.

- Three rinses with 7X cleaning solution
- Three rinses with 1.2 M HCL
- Three rinses with Acetone/Methylene chloride 50%-50%.
- Oven dry glassware 400°C for 6 hours.
- Dry and cover with parafilm until use.

- **Labeling**

Every container, beaker, volumetric flask among other glassware, SPE line tubing, etc. used was labeled specifying the date and time (MM/DD/YY, HH:MM format), concentration, the volume of the compounds analyzed, name of the solvent and its derivation.

The SPE line tubing was labeled by wrapping a tape around the hose indicating sample initial conditions, and the other details specified in the label general form.

The vials were marked with the concentration of the compounds analyzed for the calibration curves, while those that were obtained from the eluent were labeled with the number of the sample point, initial concentration and date (MM/DD format).

B.7. Adsorption experiments/Sample preparation

In order to determine the kinetics of adsorption of the Titanium (IV) oxide nanopowder (Aeroxide P25, $\geq 99.5\%$) for each specific compound two procedures were developed at dark conditions depending on the instrument used for their detection. It is important to point out that the stock solution was prepared using only one single compound per experiment to avoid that two or more contaminants were competing for adsorption sites on the TiO_2 surface.

TiO_2 adsorption constants for TCEP, gemfibrozil, and 17β estradiol (SPE-GC-FID).

- a. In a glass carboy (20L capacity), 2L of purified water were added, and then the respective amounts of the compounds listed in table 8, 9 and 10 were also added separately at different carboys and stirred for 60 minutes. Then another 2L of purified water were added to each one, and the solution was stirred for 240 more minutes. Finally, 6L of purified water were added to complete 10L volume into each carboy, and the mixture was stirred for 24h period.

Table B8. Preparation of sample stock solution TCEP.

Compound	Amount
TCEP (μL)	21.75
Total volume of purified water (L) =	10.0
Stock Conc. per contaminant (mgL^{-1})=	3.0

Table B9. Preparation of sample stock solution gemfibrozil.

Compound	Amount
Gemfibrozil (mg)	30.0
Total volume of purified water (L) =	10.0
Stock Conc. per contaminant (mgL^{-1})=	3.0

Table B10. Preparation of sample stock solution 17β estradiol.

Compound	Amount
17 beta estradiol (mg)	30.0
Total volume of purified water (L) =	10
Stock Conc. per contaminant (mgL^{-1})=	3.0

- b. For each compound preparation four bottles were wrapped up with aluminum foil and filled up with 500mL of the each of the stock solutions given at the tables B9 and B10.
- c. According to table B11, different amounts of TiO_2 were added into each bottle to reach the concentrations desired.

Table B11. Desired TiO_2 concentrations for adsorption experiments (TCEP, gemfibrozil, 17β estradiol).

Bottle	1	2	3	4
TiO_2 slurry conc. (gL^{-1})	1.0	3.0	7.0	10.0
Amount of TiO_2 to add (mg)	500	1500	3500	5000

- d. The bottles were capped and left stirring during a period of 24 h to reach the equilibrium concentration.
- e. The 500mL of each bottle were centrifuged for 60 minutes, then passed through a glass vacuum filtration using 47 mm cellulose membrane filter circles of 42 μm pore size to separate the TiO_2 nanoparticles from the water sample. The 500 mL filtered sample were collected in a 1000 mL filter flask and then transferred into a 500 mL beaker ready for SPE loading procedure, and then step 10 of the section B1 was applied.

TiO₂ adsorption constants for 1,4 dioxane and NDMA (GC-SPME-FID).

- From section B1, step 2, two stock solutions were prepared using the same amounts volumes of table B2. One using 1,4 dioxane and the other was using NDMA separately
- For each compound preparation four bottles were wrapped up with aluminum foil and filled up with 98.5 mL of purified water and spiked with 1.5 mL of the respective solution prepared on step 1, then the solutions were stirred for about 60 min to finally reach a concentration of 3 mgL⁻¹.
- According to table B12, different amounts of TiO₂ are added into each bottle to reach the concentrations desired.

Table B12. Desired TiO₂ concentrations for adsorption experiments (1,4 dioxane and NDMA).

Bottle	1	2	3	4
TiO ₂ slurry conc. (gL ⁻¹)	1.0	3.0	7.0	10.0
Amount of TiO ₂ to add (mg)	100	300	700	1000

- The bottles were capped and left stirring during a period of 24 h to reach the equilibrium concentration.
- 10 mL of each bottle were filtered using a syringe filter of 25mm of diameter and 0.45 μm of pore size, and directly filtered volume into the 20 mL vials, and the step 10 of the section B1 was applied to each sample.

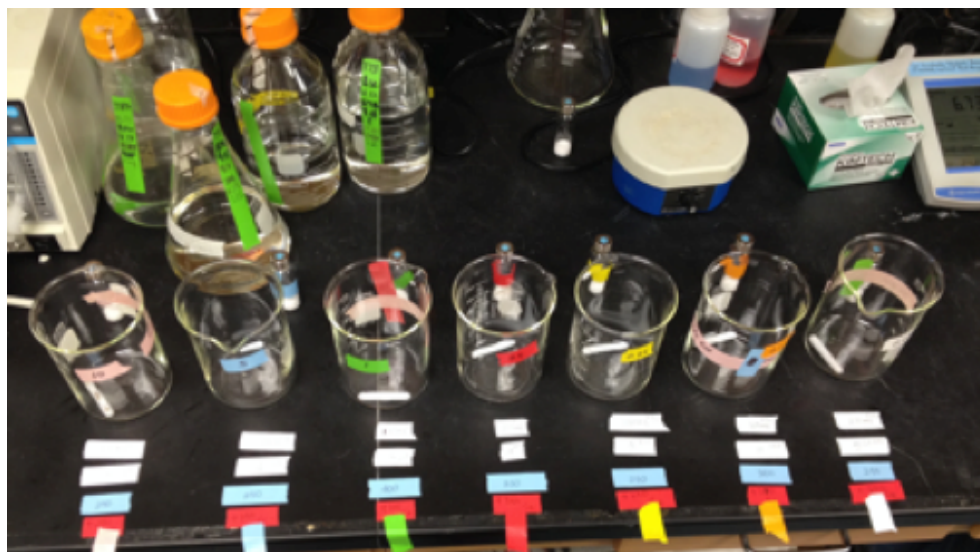
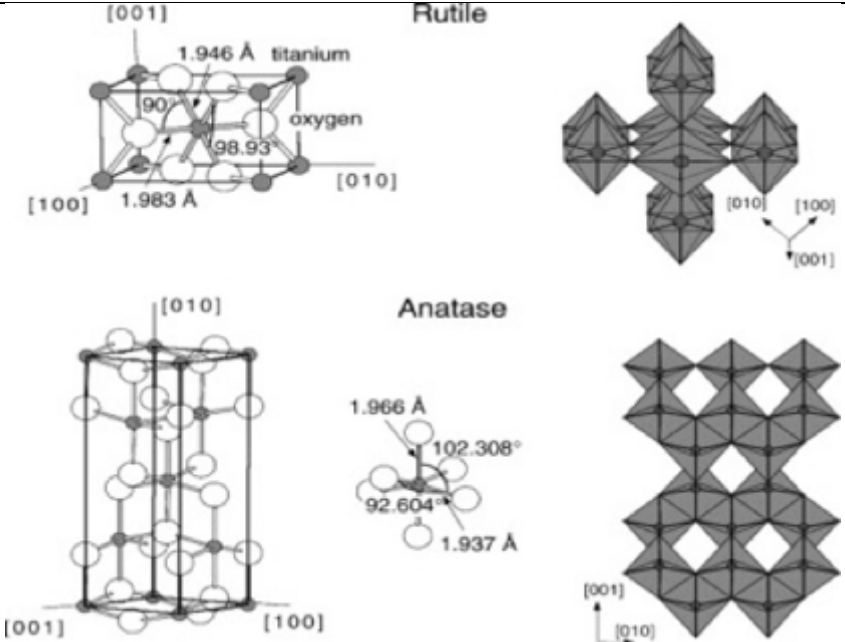


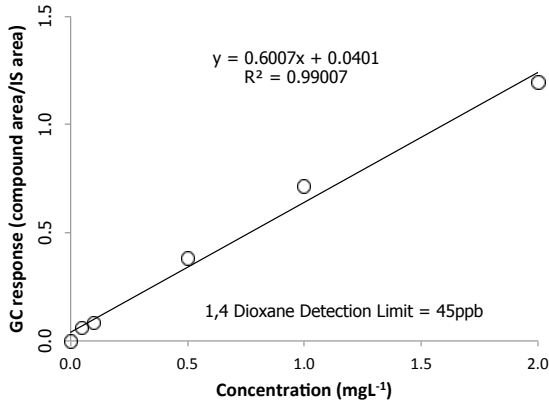
Figure B7. Adsorption experiments.

APPENDIX C: TiO₂ Properties

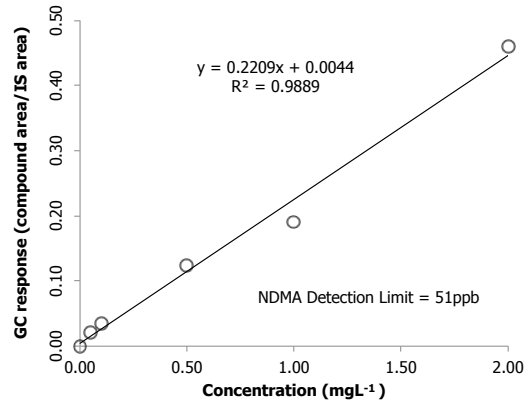
Compound	Titanium (IV) oxide nanopowder (Aeroxide P25, ≥ 99.5%)
CAS No. [121]	13463-67-7
Formula [121]	TiO ₂
MW (g mol⁻¹) [121]	79.87
Structure [121]	 <p>Crystal structures of the two forms of titanium dioxide. (A) Rutile unit cell of titanium dioxide. (B) Anaphase unit cell [75].</p>
Presentation [121]	Powder
Pzc [217]	6.25
Surface area. (m²g⁻¹) [218]	50.0
Dens. (gmL⁻¹) [121]	4.26
XRD [218]	Anatase (75.6%) Rutile (21.6%) Amorphous (2.8%)
Crystallite p.size (nm) [218]	18

APPENDIX D: GC Calibration Curves and Detection Limits

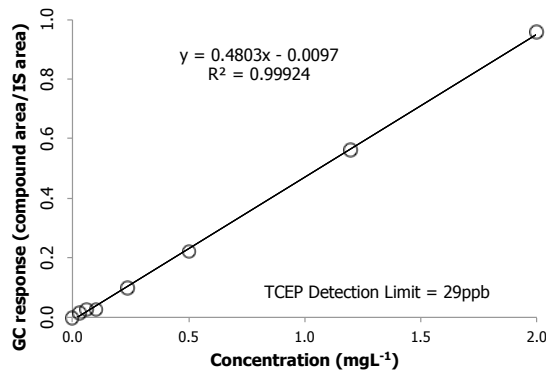
The calibration curves were determined for each compound and are showed in figure B7. The detection limits were calculated using the online Method Detection Limit Calculator by EPA 40 CFR Part 136, APPENDIX B Revision 1.11 [96].



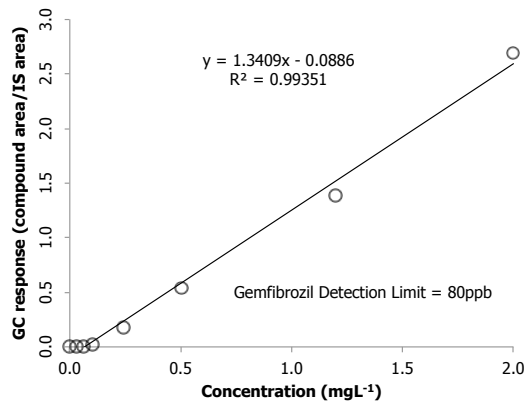
1,4-dioxane



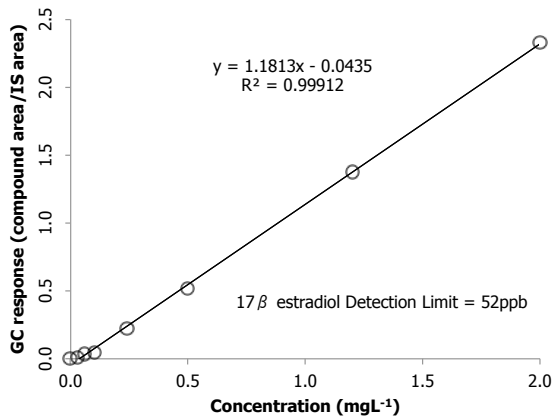
NDMA



TCEP



Gemfibrozil

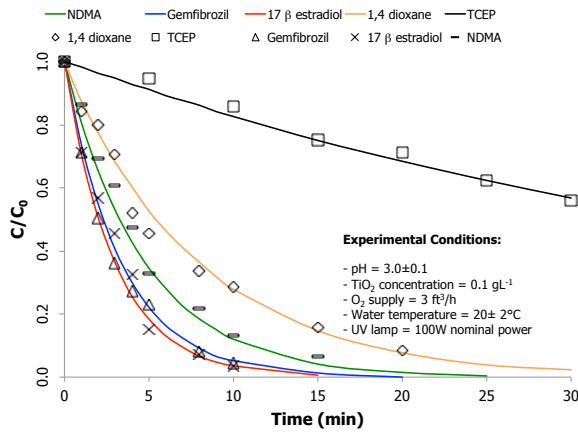


17β estradiol

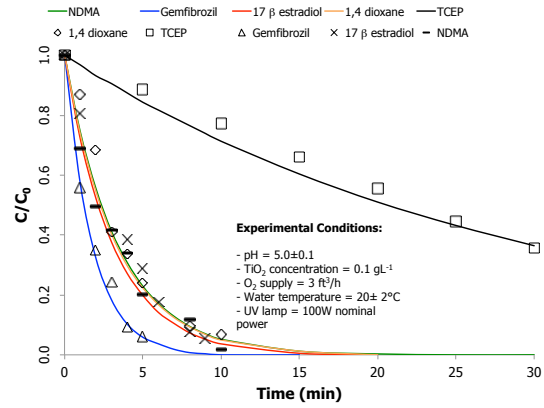
Table D1. Detection Limits (DL) for each compound using GC-FID

Contaminant	DL (µgL ⁻¹)
1,4 dioxane	45
NDMA	51
TCEP	29
Gemfibrozil	80
17β estradiol	52

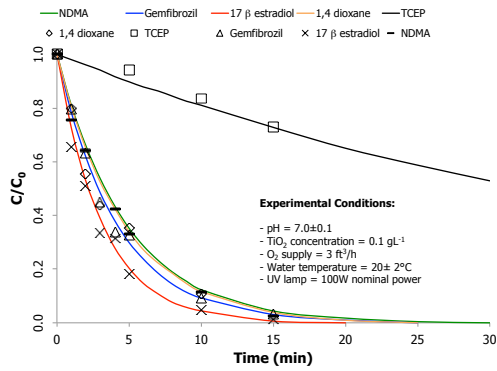
APPENDIX E: UV/TiO₂ Oxidation Results at Different pH Levels (TiO₂ = 0.1 gL⁻¹)



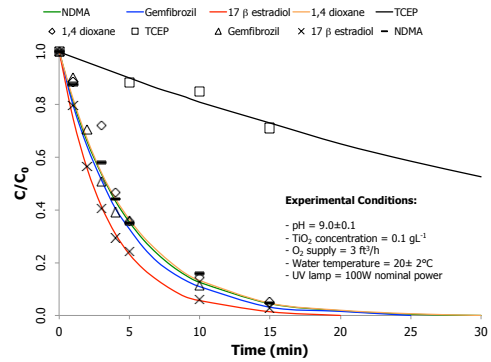
pH = 3



pH = 5

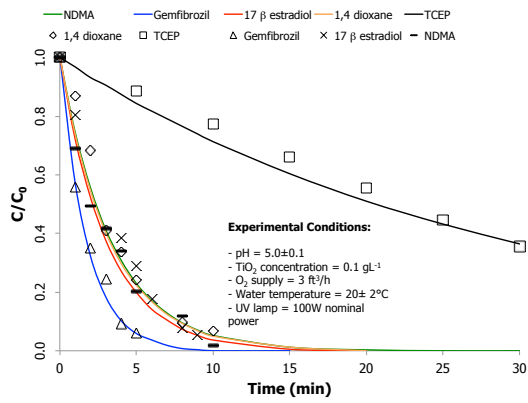


pH = 7

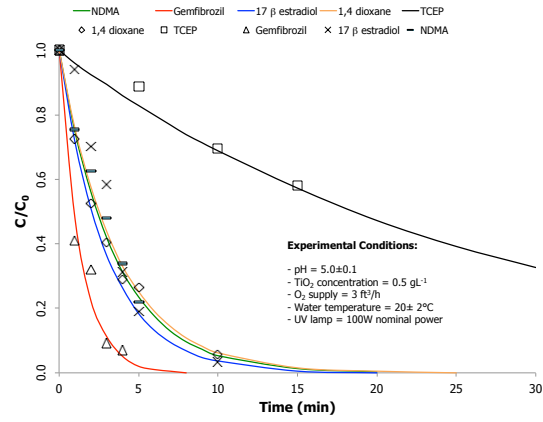


pH = 9

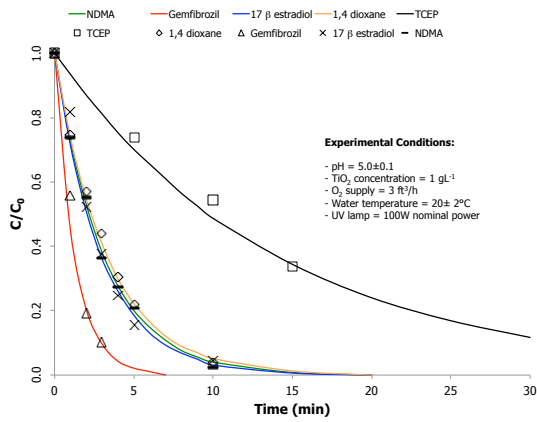
APPENDIX F: UV/TiO₂ Oxidation Results at Different TiO₂ Concentrations (pH = 5)



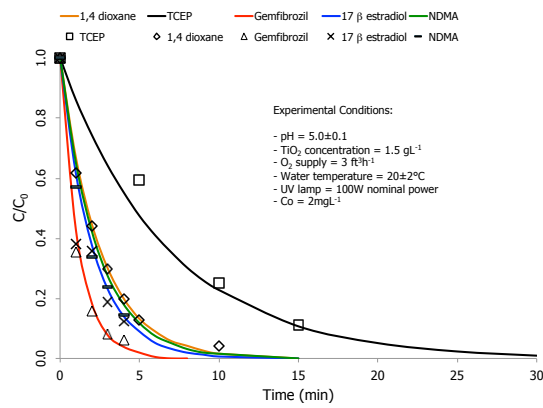
TiO₂ concentration 0.1 gL⁻¹



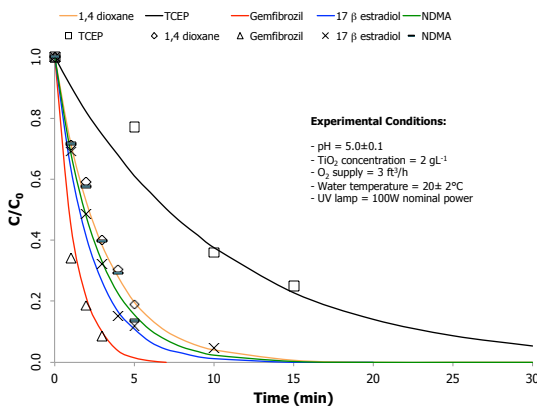
TiO₂ concentration 0.5 gL⁻¹



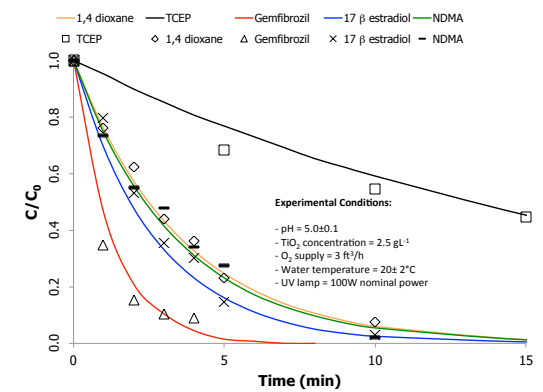
TiO₂ concentration 1.0 gL⁻¹



TiO₂ concentration 1.5 gL⁻¹

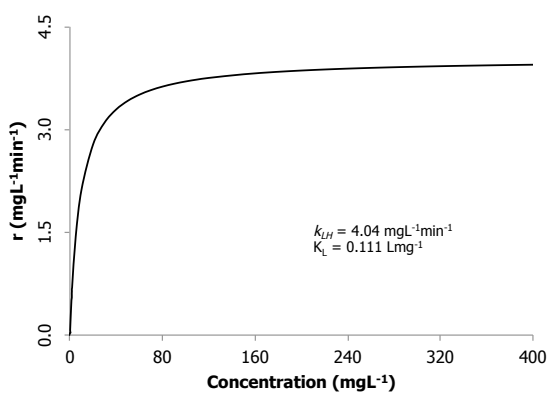


TiO₂ concentration 2.0 gL⁻¹

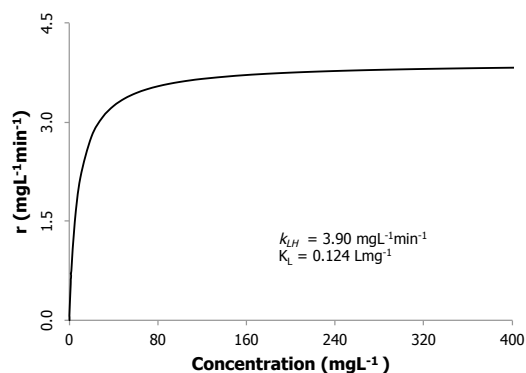


TiO₂ concentration 2.5 gL⁻¹

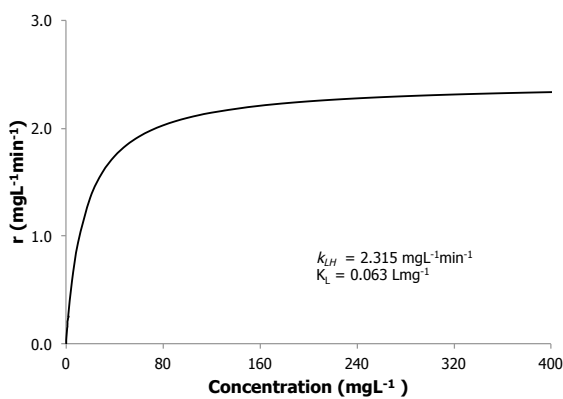
APPENDIX G: The Langmuir-Hinshelwood Kinetics Model Trends



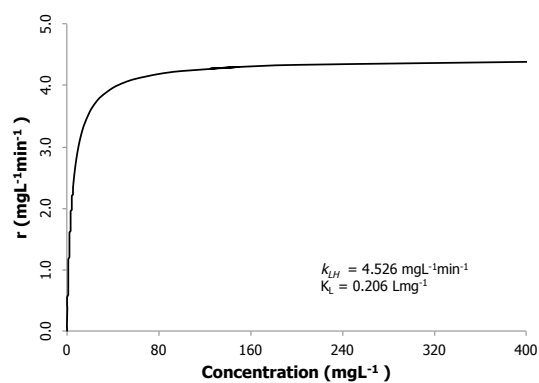
1,4 dioxane



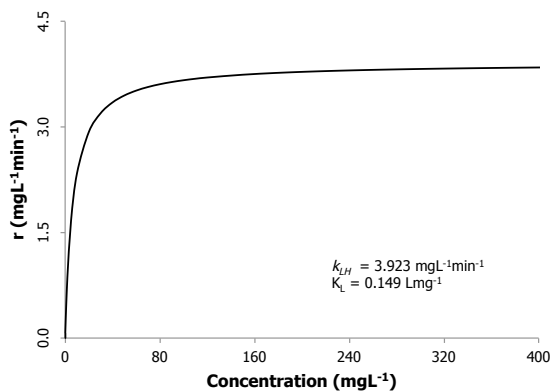
NDMA



TCEP



Gemfibrozil

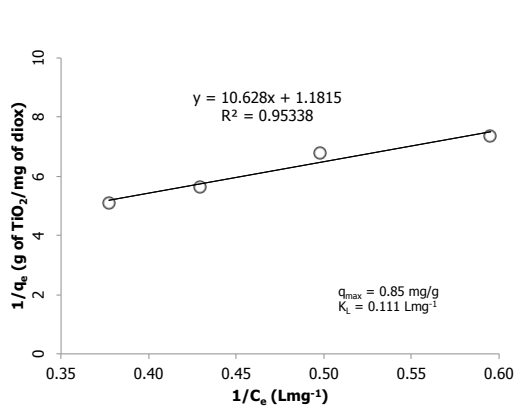


17β estradiol

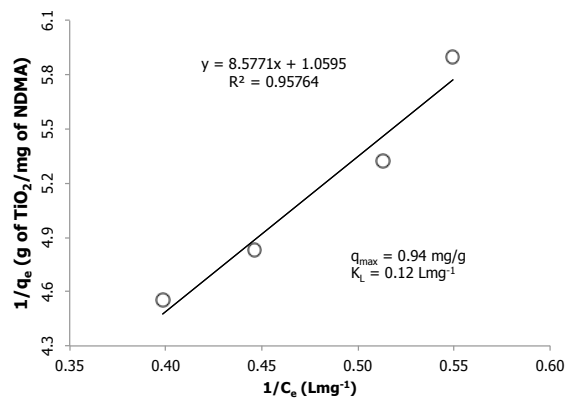
Table G1. Values of K_L and q_{max} for contaminants.

Contaminant	k_{LH} ($\text{mgL}^{-1}\text{g}^{-1}$)
1,4 dioxane	4.04
NDMA	3.90
TCEP	2.315
Gemfibrozil	4.526
17β estradiol	3.923

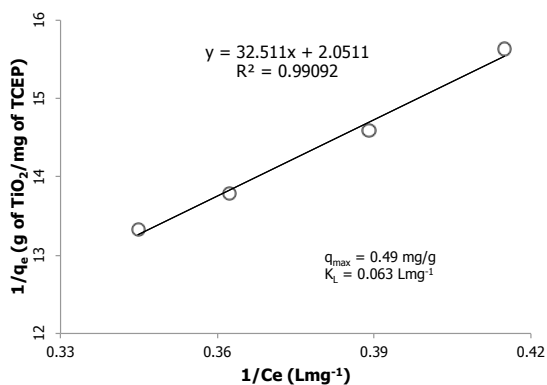
APPENDIX H: Linearized Langmuir Isotherm



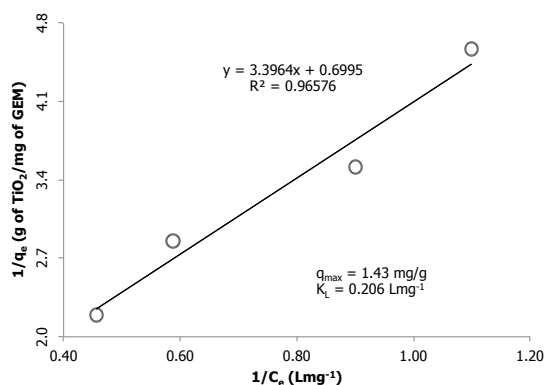
1,4 dioxane



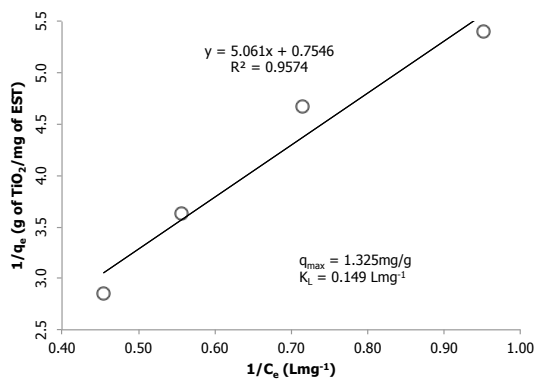
NDMA



TCEP



Gemfibrozil



17β estradiol

Table H1. Values of K_L and q_{\max} for contaminants.

Contaminant	q_{\max} (mgg^{-1})	K_L (Lmg^{-1})
1,4 dioxane	0.850	0.111
NDMA	0.940	0.124
TCEP	0.490	0.063
Gemfibrozil	1.430	0.206
17β estradiol	1.325	0.149

APPENDIX I: Pseudo-First Order Rate Constant Earlier Times – k (min^{-1})

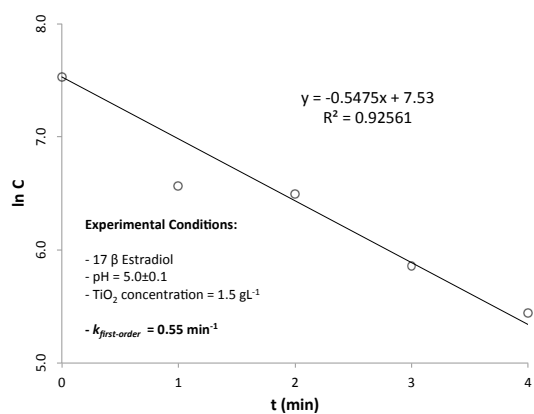
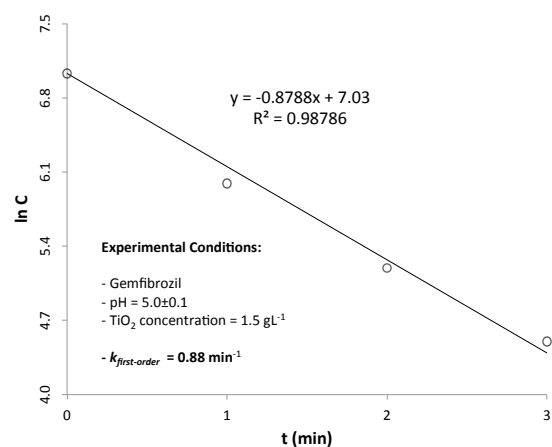
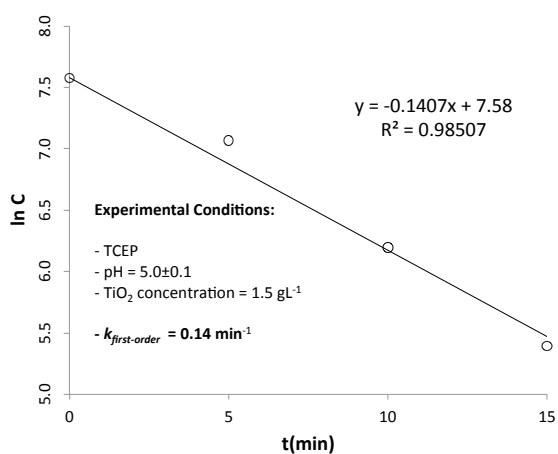
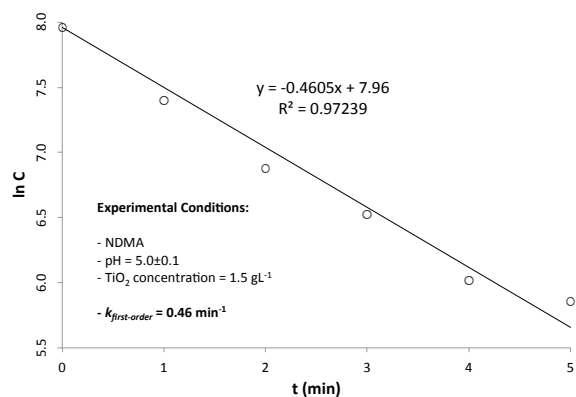
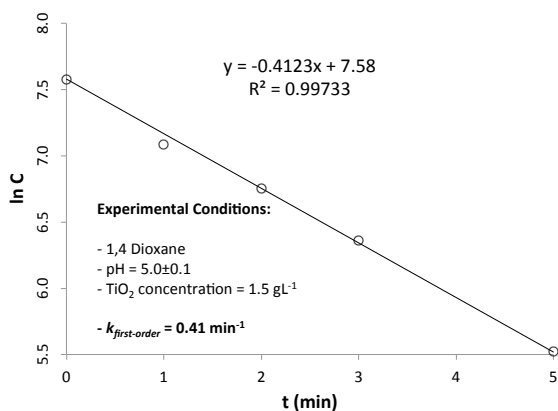
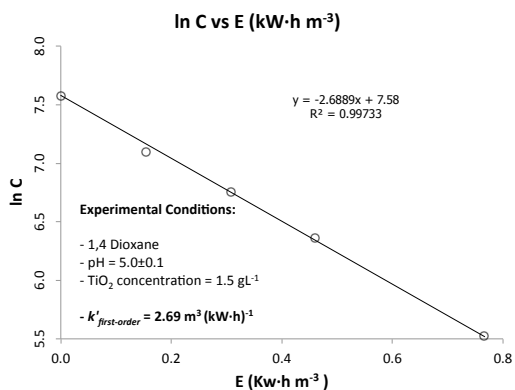


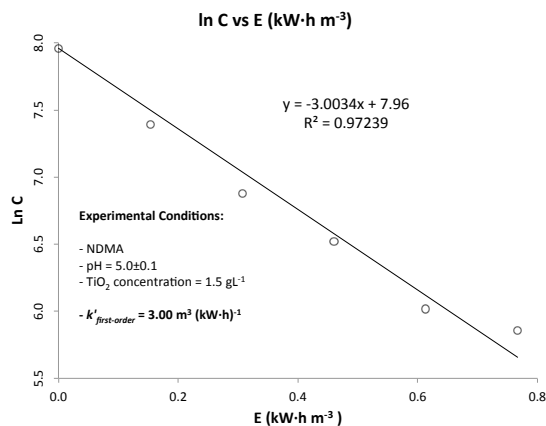
Table II. Values of k at 1.5 gL^{-1} of TiO_2 .

Contaminant	k (min^{-1})
1,4 dioxane	0.41
NDMA	0.46
TCEP	0.14
Gemfibrozil	0.88
17β estradiol	0.55

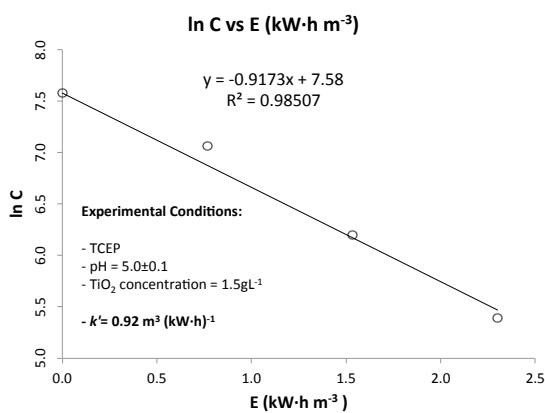
APPENDIX J: Pseudo-First Order Rate Constants Normalized to Energy per Volume -- k' [$m^3(kW \cdot h)^{-1}$]



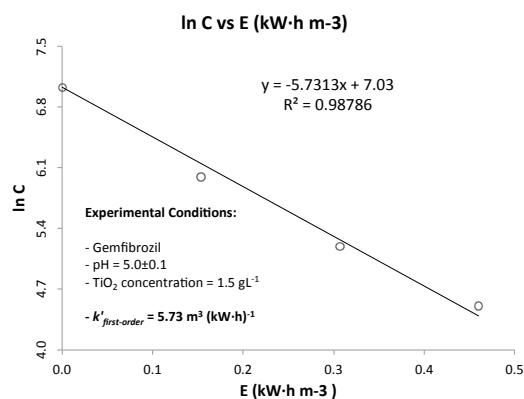
1,4 dioxane



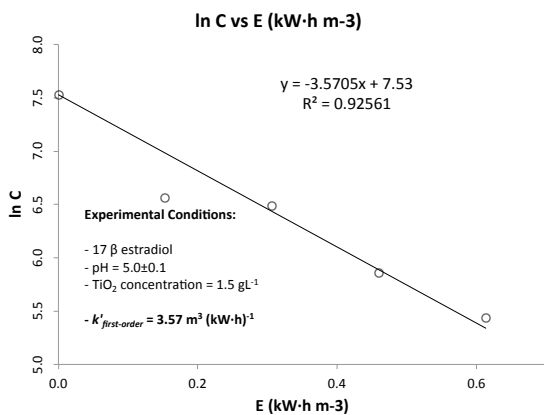
NDMA



TCEP



Gemfibrozil

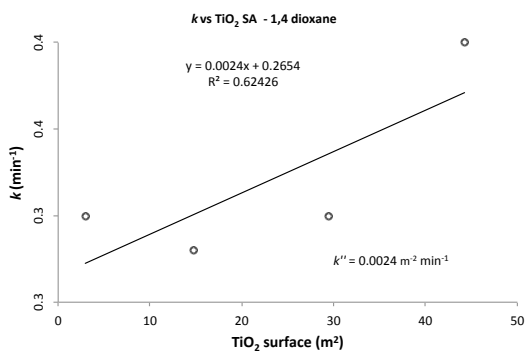


17β estradiol

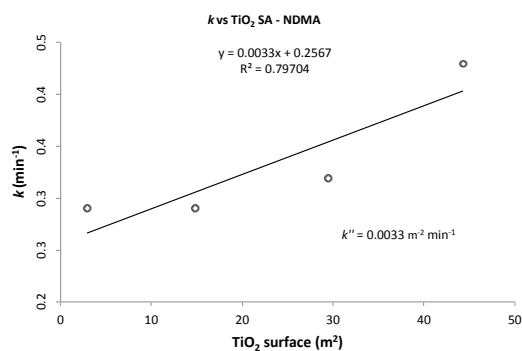
Table J1. Values of k' at 1.5 gL^{-1} of TiO_2 .

Contaminant	k' ($m^3 (kW \cdot h)^{-1}$)
1,4 dioxane	2.69
NDMA	3.00
TCEP	0.92
Gemfibrozil	5.73
17β estradiol	3.57

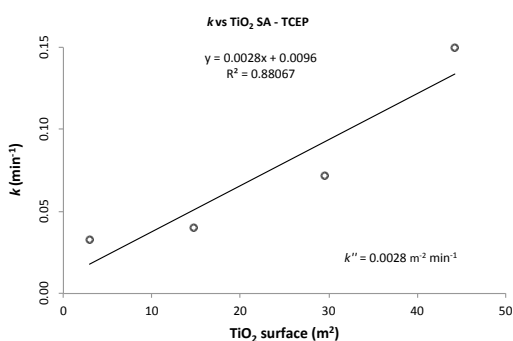
APPENDIX K: Pseudo-First Order Rate Constants Normalized to TiO₂ Surface Area -- k'' (min⁻¹m⁻²)



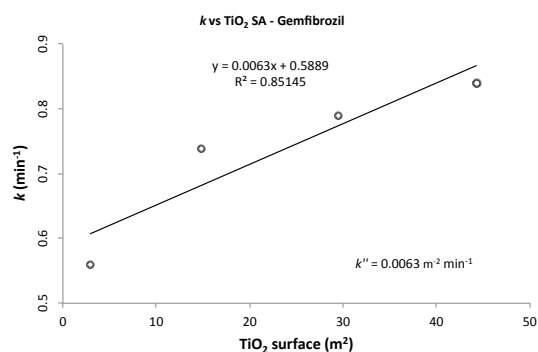
1,4 dioxane



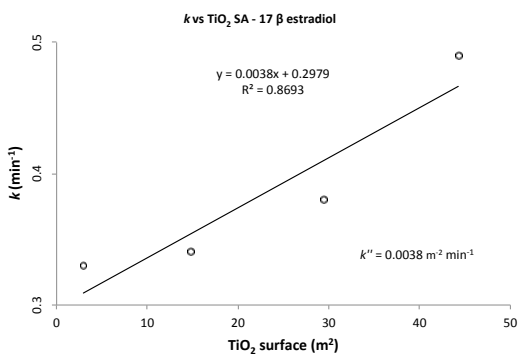
NDMA



TCEP



Gemfibrozil

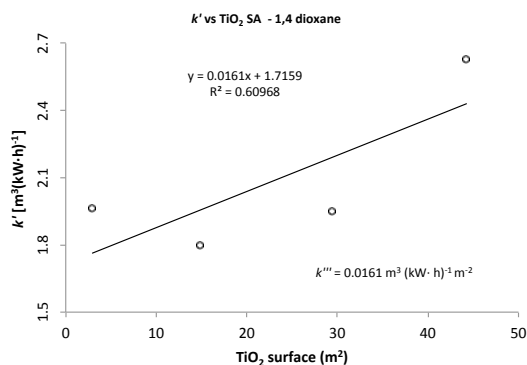


17β estradiol

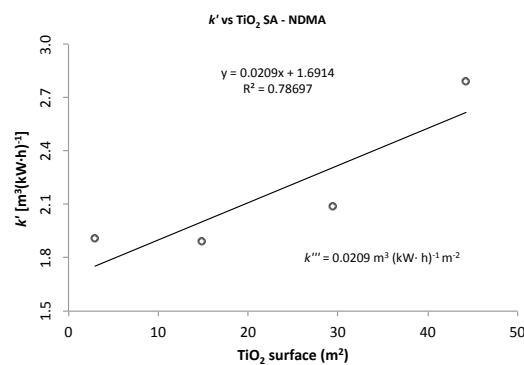
Table K1. Values of k'' at 1.5 gL⁻¹ of TiO₂.

Contaminant	k'' (min ⁻¹ m ⁻²)
1,4 dioxane	0.0024
NDMA	0.0033
TCEP	0.0028
Gemfibrozil	0.0063
17β estradiol	0.0038

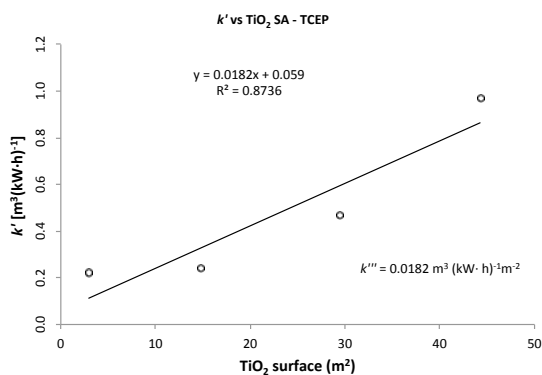
APPENDIX L: Pseudo-First Order Rate Constants Normalized to Energy & TiO₂ Surface Area -- k''' ($\text{m}^3 (\text{kW}\cdot\text{h})^{-1} \text{m}^{-2}$)



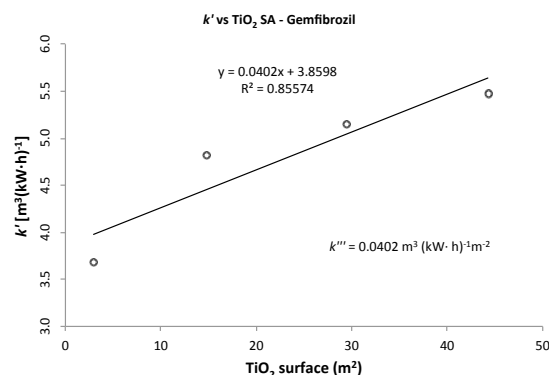
1,4 dioxane



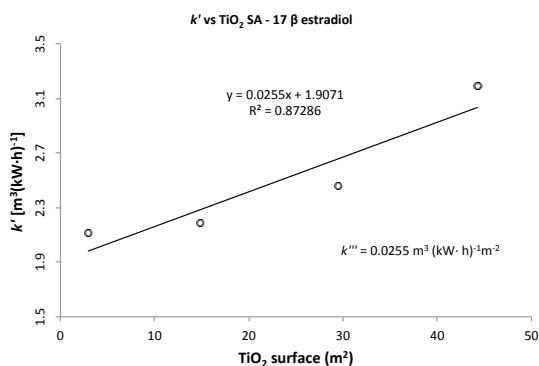
NDMA



TCEP



Gemfibrozil

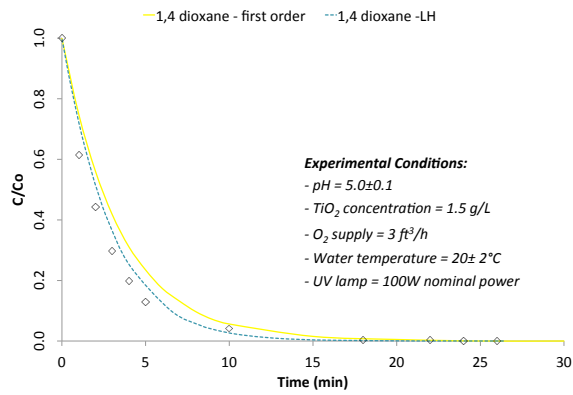


17 β estradiol

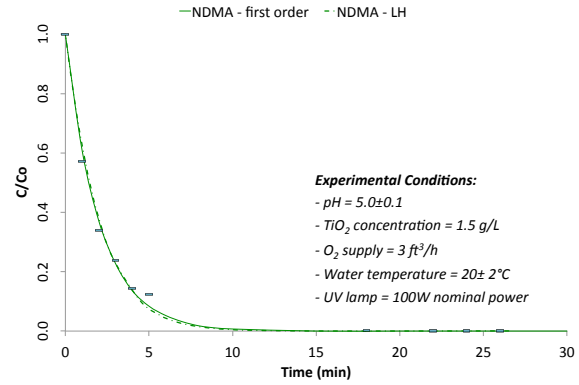
Table L1. Values of k''' at 1.5 gL^{-1} of TiO_2 .

Contaminant	k''' $[\text{m}^3 (\text{kW}\cdot\text{h})^{-1} \text{m}^{-2}]$
1,4 dioxane	0.0161
NDMA	0.0209
TCEP	0.0182
Gemfibrozil	0.0402
17 β estradiol	0.0255

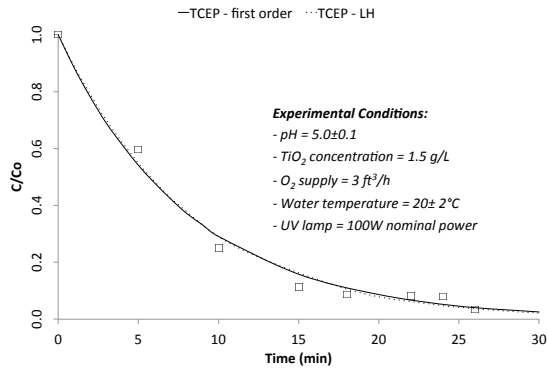
APPENDIX M: Combined Data Plotted as C/C_0 versus Time for Each Compound.



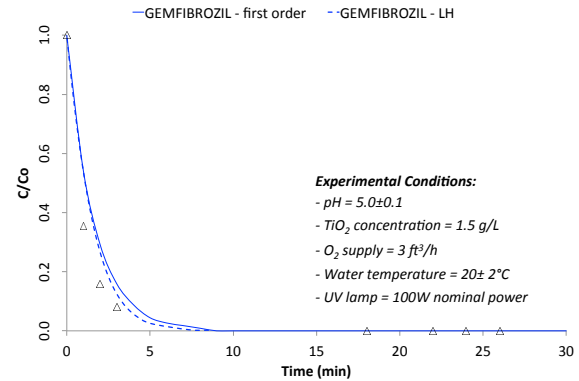
1,4 dioxane



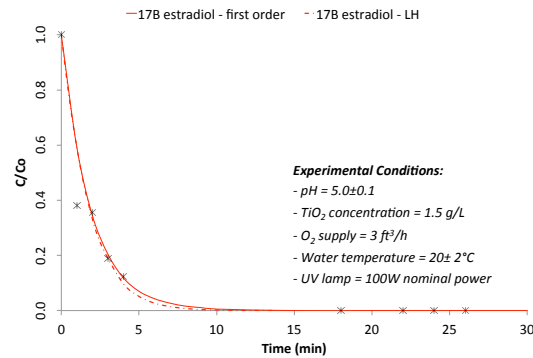
NDMA



TCEP

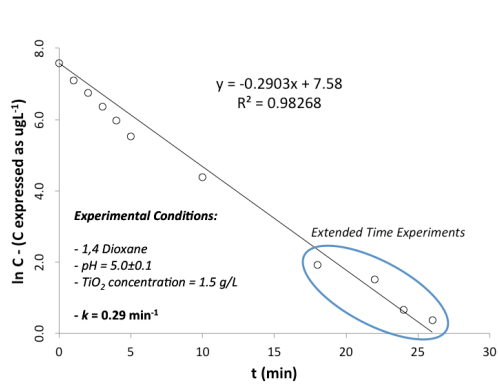


Gemfibrozil

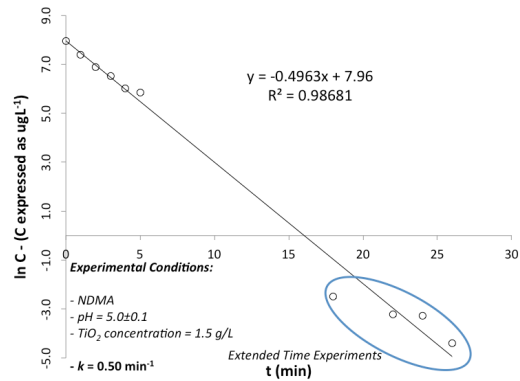


17β estradiol

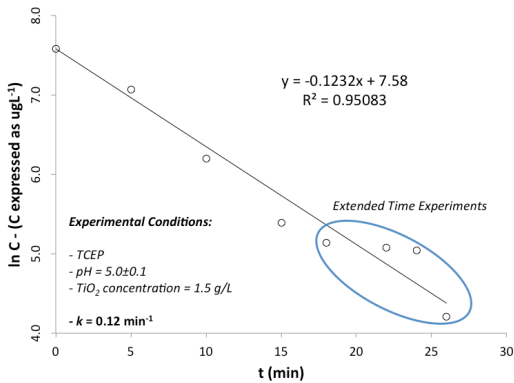
APPENDIX N: Pseudo-First order Rate Constant for Combined Data (early and extended times)



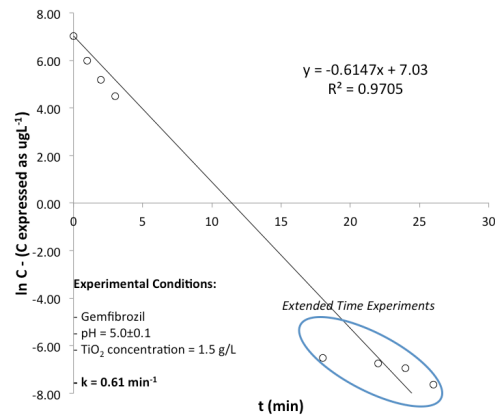
1,4 dioxane



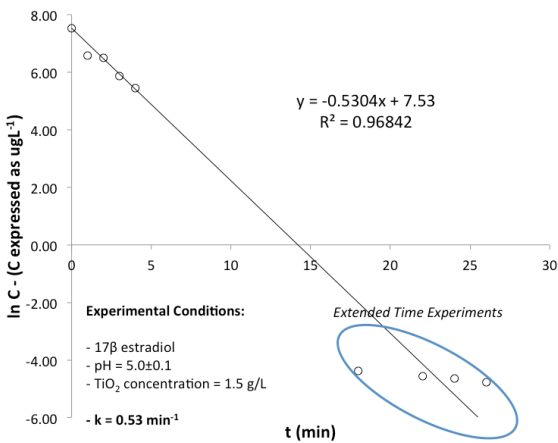
NDMA



TCEP



Gemfibrozil

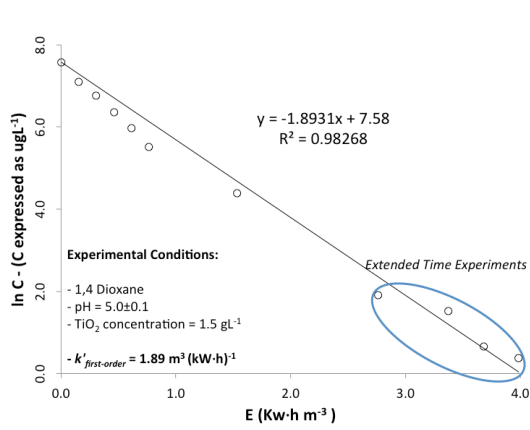


17β estradiol

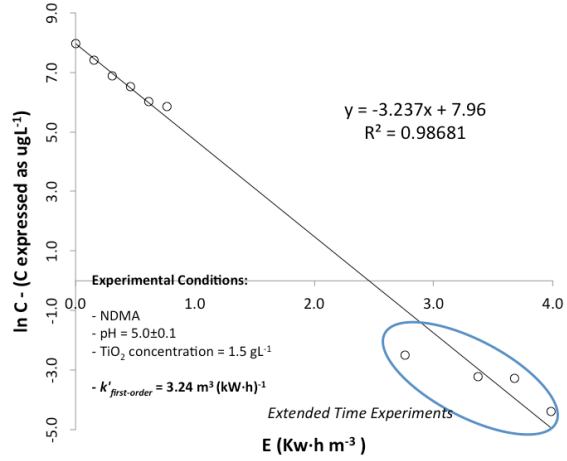
Table N1. Values of k at 1.5 gL⁻¹ of TiO₂.

Contaminant	<i>k</i> (min ⁻¹)
1,4 dioxane	0.29
NDMA	0.50
TCEP	0.12
Gemfibrozil	0.61
17β estradiol	0.53

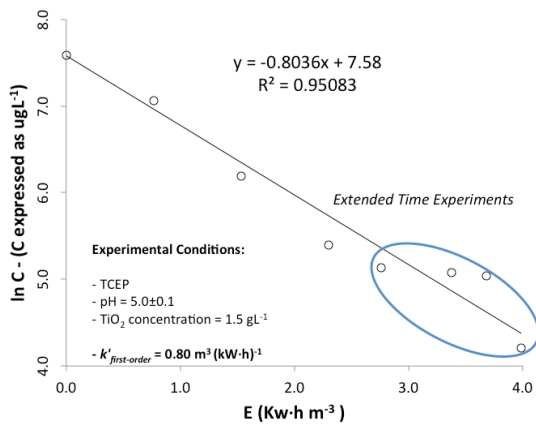
APPENDIX O: Pseudo-First Order Rate Constants Normalized to Energy & TiO₂ Surface Area -- k''' ($m^3 (kW \cdot h)^{-1} m^{-2}$) for Combined Data.



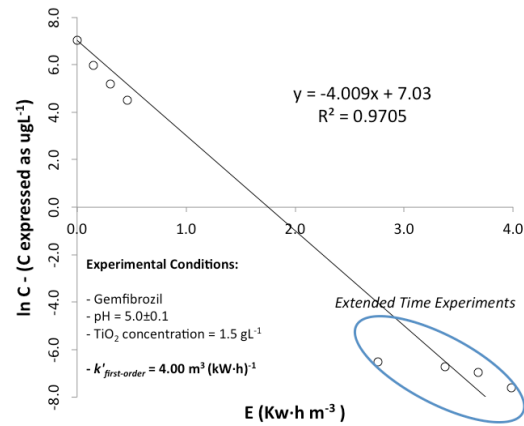
1,4 dioxane



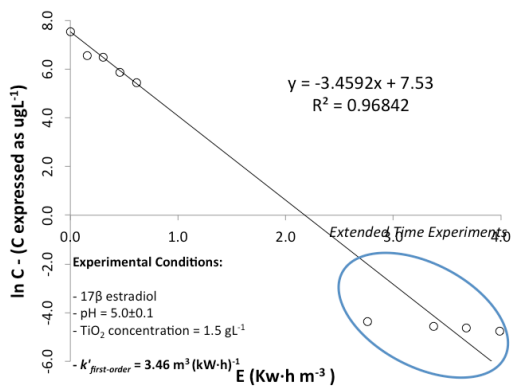
NDMA



TCEP



Gemfibrozil

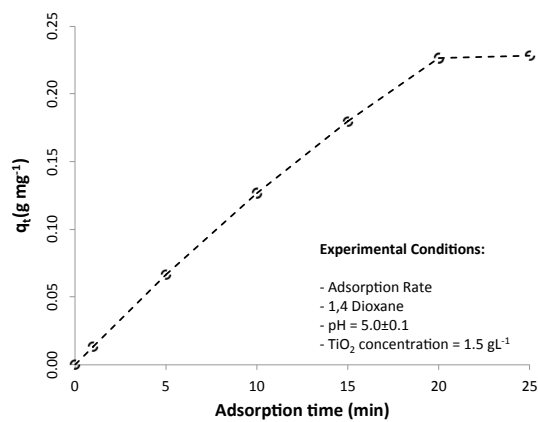


17β estradiol

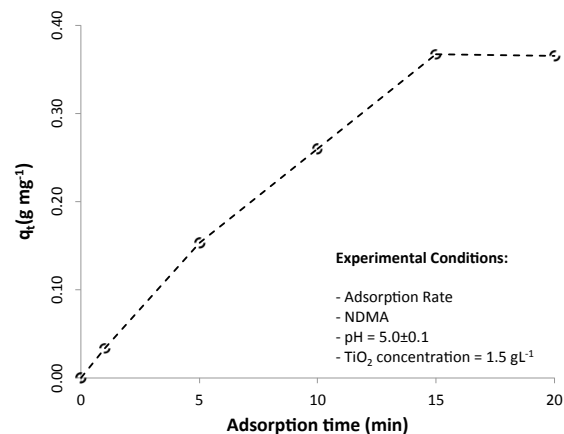
Table O1. Values of k' At 1.5 gL⁻¹ of TiO₂.

Contaminant	k' ($m^3 (kW \cdot h)^{-1}$)
1,4 dioxane	1.89
NDMA	3.24
TCEP	0.80
Gemfibrozil	4.00
17β estradiol	3.46

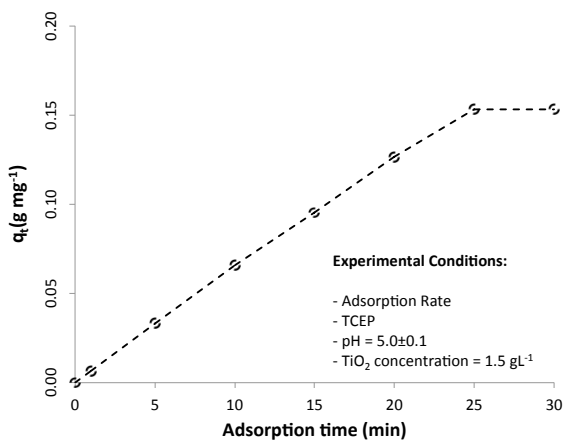
APPENDIX P: Non-linear Adsorption Rate Data (q_t vs t)



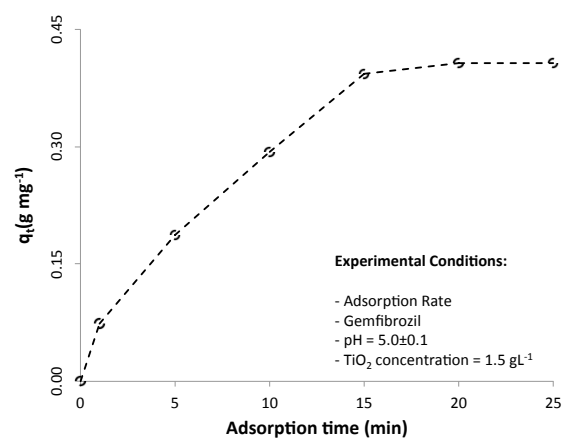
1,4 dioxane



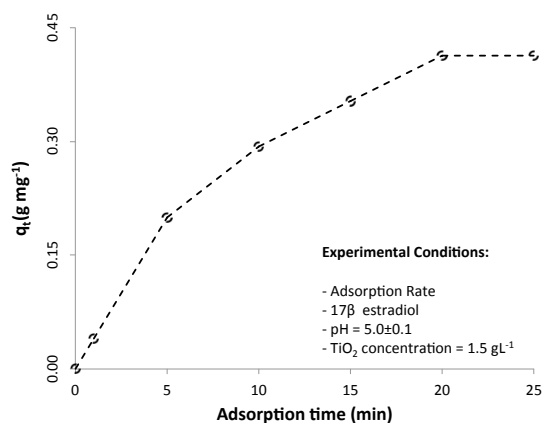
NDMA



TCEP

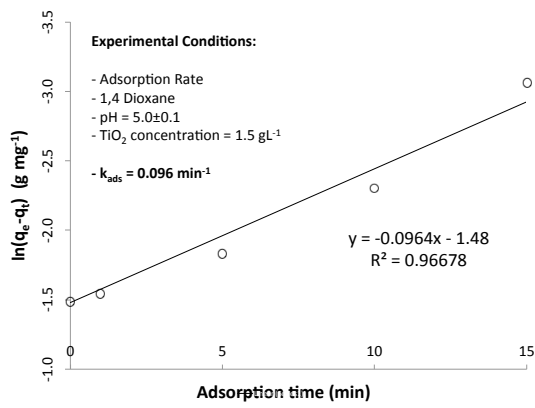


Gemfibrozil

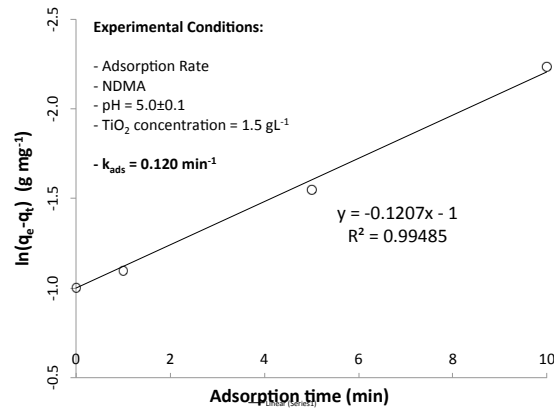


17β estradiol

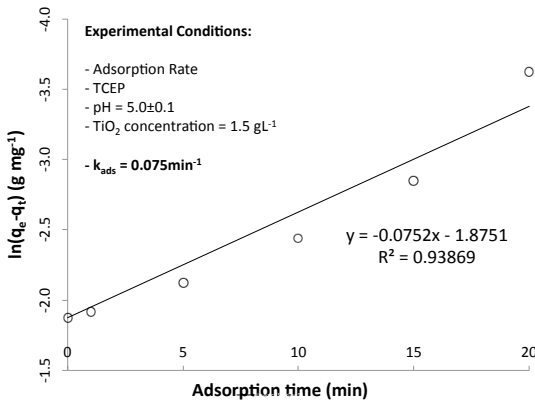
APPENDIX Q: First Order Adsorption Kinetic Constants



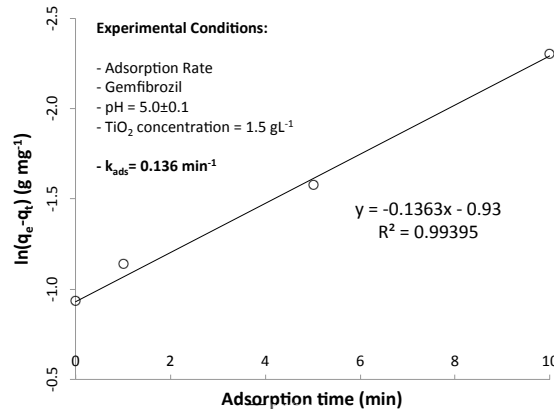
1,4 dioxane



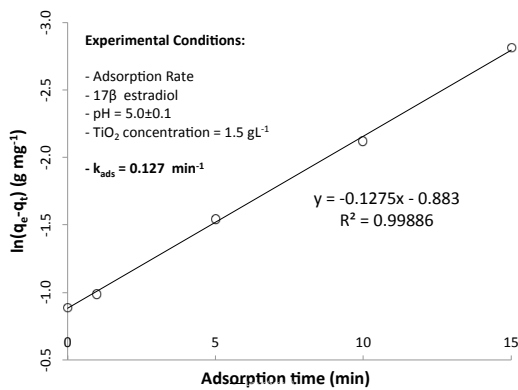
NDMA



TCEP



Gemfibrozil



17β estradiol

Table Q1. Values of k(adsorption) at 1.5 gL⁻¹ of TiO₂.

Contaminant	k_{ads} (min ⁻¹)
1,4 dioxane	0.096
NDMA	0.1207
TCEP	0.075
Gemfibrozil	0.1363
17β estradiol	0.1275

APPENDIX R: Spectral Energy Distribution Lamp series: 7825-30 (Ace Glass, Vineland, NJ, USA)

	Wavelength (Angstroms)	Radiated Energy (Watts)
infrared	13673	0.65
	11287	0.62
	10140	0.85
(yellow)	5780	1.55
(green)	5461	1.35
(blue)	4358	1.08
(violet)	4045	0.75
UVA	3660	1.4
UVA	3341	0.13
UVB	3130	1.02
UVB	3025	0.41
UVB	2967	0.32
UVB	2894	0.1
UVB	2804	0.12
UVC	2753	0.06
UVC	2700	0.07
UVC	2652	0.3
UVC	2571	0.11
UVC	2537	0.34
UVC	2482	0.1
UVC	2400	0.05
UVC	2380	0.03
UVC	2360	0.02
UVC	2320	0.02
UVC	2224	0.04
Total UV radiated	W	4.64
Lamp arc length	in	2.9
Lamp arc length	cm	6.99
lamp diam	cm	0.92
Lamp arc area	cm ²	20.19
Total length lamp	cm	15.56
Well diameter	cm	2.50
Well arc length total area	cm ²	54.86

IX. BIBLIOGRAPHY

1. WATER.ORG, U. International Decade for Action 'WATER FOR LIFE' 2005-2015 2014/11/24]; United Nations, Department of Economic and Social Affairs (UNDESA)]. Available from: <http://www.un.org/waterforlifedecade/scarcity.shtml>.
2. Barnes, K.K., et al., *A national reconnaissance of pharmaceuticals and other organic wastewater contaminants in the United States — I) Groundwater*. Science of The Total Environment, 2008. **402**(2-3): p. 192-200.
3. Fawell, J. and M.J. Nieuwenhuijsen, *Contaminants in drinking water Environmental pollution and health*. British Medical Bulletin, 2003. **68**(1): p. 199-208.
4. Focazio, M.J., et al., *A national reconnaissance for pharmaceuticals and other organic wastewater contaminants in the United States — II) Untreated drinking water sources*. Science of The Total Environment, 2008. **402**(2-3): p. 201-216.
5. Qing Li, Q., et al., *Persistent Organic Pollutants and Adverse Health Effects in Humans*. Journal of Toxicology and Environmental Health, Part A, 2006. **69**(21): p. 1987-2005.
6. Stuart, M., et al., *Review of risk from potential emerging contaminants in UK groundwater*. Science of The Total Environment, 2012. **416**(0): p. 1-21.
7. Castiglioni, S., et al., *Removal of pharmaceuticals in sewage treatment plants in Italy*. Environmental Science & Technology, 2006. **40**(1): p. 357-363
8. Carballa, M., et al., *Behavior of pharmaceuticals, cosmetics and hormones in a sewage treatment plant*. Water research, 2004. **38**(12): p. 2918-2926
9. Comninellis, C., et al., *Advanced oxidation processes for water treatment: advances and trends for R&D*. Journal of Chemical Technology & Biotechnology, 2008. **83**(6): p. 769-776.
10. Teoh, W.Y., J.A. Scott, and R. Amal, *Progress in Heterogeneous Photocatalysis: From Classical Radical Chemistry to Engineering Nanomaterials and Solar Reactors*. The Journal of Physical Chemistry Letters, 2012. **3**(5): p. 629-639.
11. Crittenden, J.C., et al., *MWH's Water Treatment: Principles and Design*. EngineeringPro collection. 2012.
12. Carey, J., J. Lawrence, and H. Tosine, *Photodechlorination of PCB's in the presence of titanium dioxide in aqueous suspensions*. Bulletin of Environmental Contamination and Toxicology, 1976. **16**(6): p. 697-701.
13. Miller, R. and R. Fox, *Treatment of organic contaminants in air by photocatalytic oxidation: A commercialization perspective*. Photocatalytic Purification and Treatment of Water and Air, 1993: p. 573-578.
14. Cabrera, M.I., O.M. Alfano, and A.E. Cassano, *Absorption and scattering coefficients of titanium dioxide particulate suspensions in water*. The Journal of Physical Chemistry, 1996. **100**(51): p. 20043-20050
15. Suri, R.P.S., et al., *Heterogeneous photocatalytic oxidation of hazardous organic contaminants in water*. Water environment research, 1993: p. 665-673
16. Matthews, R.W. and S.R. McEvoy, *Photocatalytic degradation of phenol in the presence of near-UV illuminated titanium dioxide*. Journal of Photochemistry and Photobiology A: Chemistry, 1992. **64**(2): p. 231-246.
17. Sagawe, G., et al., *Photocatalytic reactors for treating water pollution with solar illumination. II: A simplified analysis for flow reactors*. Chemical engineering science, 2003. **58**(12): p. 2601-2615.
18. EPA. *Contaminant Candidate List 3 - CCL 3*. 2009; Available from: <http://water.epa.gov/scitech/drinkingwater/dws/ccl/ccl3.cfm>.
19. CDPH, *California Department of Public Health's Drinking Water Program's; Groundwater Replenishment Reuse DRAFT Regulation*. 2013.

20. EPA, *Technologies for upgrading existing or designing new drinking water treatment facilities / U.S. Environmental Protection Agency*. 1990.
21. Huang, C.P., C. Dong, and Z. Tang, *Advanced chemical oxidation: its present role and potential future in hazardous waste treatment*. Waste management, 1993. **13**(5): p. 361-377
22. Nakada, N., et al., *Removal of selected pharmaceuticals and personal care products (PPCPs) and endocrine-disrupting chemicals (EDCs) during sand filtration and ozonation at a municipal sewage treatment plant*. Water Research, 2007. **41**(19): p. 4373-4382.
23. Kim, I., N. Yamashita, and H. Tanaka, *Performance of UV and UV/H₂O₂ processes for the removal of pharmaceuticals detected in secondary effluent of a sewage treatment plant in Japan*. Journal of Hazardous Materials, 2009. **166**(2-3): p. 1134-1140.
24. Castellote, M. and N. Bengtsson, *Principles of TiO₂ Photocatalysis*, in *Applications of Titanium Dioxide Photocatalysis to Construction Materials*, Y. Ohama and D. Van Gemert, Editors. 2011, Springer Netherlands. p. 5-10.
25. Phillips, J.C., G. Lucovsky, and O. Safari Books, *Bonds and bands in semiconductors*. 2010, [New York, N.Y.] (222 East 46th Street, New York, NY 10017): Momentum Press.
26. Yu, P.Y., et al., *Fundamentals of semiconductors: physics and materials properties*. 2001, New York: Springer.
27. Braslavsky, S.E., *Glossary of terms used in photochemistry, 3rd edition*. Pure Appl. Chem., IUPAC 2007. **79**(3): p. 293-465.
28. Chong, M.N., et al., *Recent developments in photocatalytic water treatment technology: A review*. Water Research, 2010. **44**(10): p. 2997-3027.
29. Konstantinou, I.K., V.A. Sakkas, and T.A. Albanis, *Photocatalytic degradation of propachlor in aqueous TiO₂ suspensions. Determination of the reaction pathway and identification of intermediate products by various analytical methods*. Water Research, 2002. **36**(11): p. 2733-2742.
30. Herrmann, J.M., *Heterogeneous photocatalysis: state of the art and present applications In honor of Pr. R.L. Burwell Jr. (1912-2003), Former Head of Ipatieff Laboratories, Northwestern University, Evanston (Ill)*. Topics in Catalysis, 2005. **34**(1-4): p. 49-65.
31. Linsebigler, A.L., G. Lu, and J.T. Yates, *Photocatalysis on TiO₂ Surfaces: Principles, Mechanisms, and Selected Results*. Chemical Reviews, 1995. **95**(3): p. 735-758.
32. Kaneko, M. and I. Okura, *Photocatalysis: Science and Technology*. Biological and Medical Physics Series. 2010: Springer.
33. Calvert, J.G., Pitts, J. N., *Experimental Methods in Photochemistry in Photochemistry in John Wiley & Sons, Inc*. 1966: New York. p. 686-798.
34. Ollis, D.F., E. Pelizzetti, and N. Serpone, *Photocatalyzed destruction of water contaminants*. Environmental Science & Technology, 1991. **25**(9): p. 1522-1529.
35. Hoffmann, M.R., et al., *Environmental Applications of Semiconductor Photocatalysis*. Chemical Reviews, 1995. **95**(1): p. 69-96.
36. Center for Environmental Research, I., *Handbook: advanced photochemical oxidation processes*. EPA 625/R. 1999: Center for Environmental Research Information, National Risk Management Research Laboratory, Office of Research and Development, U.S. Environmental Protection Agency.
37. Valente, J.P.S., P.M. Padilha, and A.O. Florentino, *Studies on the adsorption and kinetics of photodegradation of a model compound for heterogeneous photocatalysis onto TiO₂*. Chemosphere, 2006. **64**(7): p. 1128-1133.
38. Henderson, M.A., *A Surface Science Perspective on TiO₂ Photocatalysis*. Surface Science Reports, 66(6-7):185-297, 2011. **66**(6-7): p. 185-297.
39. Tang, H., et al., *Photoluminescence in TiO₂ anatase single crystals*. Solid State Communications, 1993. **87**(9): p. 847-850.

40. Vinu, R.a.M., Giridhar *Environmental remediation by photocatalysis*. Journal of the Indian Institute of Science, 2010. **90**(2): p. 189-230.
41. Chong, M.N., et al., *Optimisation of an annular photoreactor process for degradation of Congo Red using a newly synthesized titania impregnated kaolinite nano-photocatalyst*. Separation and Purification Technology, 2009. **67**(3): p. 355-363.
42. Malato, S., et al., *Decontamination and disinfection of water by solar photocatalysis: Recent overview and trends*. Catalysis Today, 2009. **147**(1): p. 1-59.
43. Gaya, U.I. and A.H. Abdullah, *Heterogeneous photocatalytic degradation of organic contaminants over titanium dioxide: A review of fundamentals, progress and problems*. Journal of Photochemistry and Photobiology C: Photochemistry Reviews, 2008. **9**(1): p. 1-12.
44. Ray, A.K., *Design, modelling and experimentation of a new large-scale photocatalytic reactor for water treatment*. Chemical Engineering Science, 1999. **54**(15): p. 3113-3125.
45. Ballari, M.d.l.M., O.M. Alfano, and A.E. Cassano, *Mass transfer limitations in slurry photocatalytic reactors: Experimental validation*. Chemical Engineering Science, 2010. **65**(17): p. 4931-4942.
46. Brandi, R.J., et al., *Absolute quantum yields in photocatalytic slurry reactors*. Chemical Engineering Science, 2003. **58**(3-6): p. 979-985.
47. Camera-Roda, G., F. Santarelli, and M. Panico, *Study and optimization of an annular photocatalytic slurry reactor*. Photochemical & Photobiological Sciences, 2009. **8**(5): p. 712-718.
48. Wu, C.-H., H.-W. Chang, and J.-M. Chern, *Basic dye decomposition kinetics in a photocatalytic slurry reactor*. Journal of Hazardous Materials, 2006. **137**(1): p. 336-343.
49. Qi, N., et al., *CFD modelling of hydrodynamics and degradation kinetics in an annular slurry photocatalytic reactor for wastewater treatment*. Chemical Engineering Journal, 2011. **172**(1): p. 84-95.
50. Alfano, O.M., et al., *Photocatalysis in water environments using artificial and solar light*. Catalysis Today, 2000. **58**(2-3): p. 199-230.
51. Parent, Y., et al., *Solar photocatalytic processes for the purification of water: state of development and barriers to commercialization*. Solar Energy, 1996. **56**(5): p. 429-437.
52. Zhang, T.C., et al., *Nanotechnologies for Water Environment Applications*. 2009: American Society of Civil Engineers.
53. Torimoto, T., et al., *Effects of adsorbents used as supports for titanium dioxide loading on photocatalytic degradation of propylamide*. Environmental science & technology, 1996. **30**(4): p. 1275-1281.
54. Hofstadler, K., et al., *New reactor design for photocatalytic wastewater treatment with TiO₂ immobilized on fused-silica glass fibers: photomineralization of 4-chlorophenol*. Environmental science & technology, 1994. **28**(4): p. 670-674.
55. Peill, N.J. and M.R. Hoffmann, *Development and Optimization of a TiO₂-Coated Fiber-Optic Cable Reactor: Photocatalytic Degradation of 4-Chlorophenol*. Environmental science & technology, 1995. **29**(12): p. 2974-2981.
56. Zhang, Y., et al., *Fixed-bed photocatalysts for solar decontamination of water*. Environmental science & technology, 1994. **28**(3): p. 435-442.
57. Fernandez, A., et al., *Preparation and characterization of TiO₂ photocatalysts supported on various rigid supports (glass, quartz and stainless steel). Comparative studies of photocatalytic activity in water purification*. Applied Catalysis B: Environmental, 1995. **7**(1): p. 49-63.
58. Al-Ekabi, H. and N. Serpone, *Kinetics studies in heterogeneous photocatalysis. I. Photocatalytic degradation of chlorinated phenols in aerated aqueous solutions over titania supported on a glass matrix*. The Journal of Physical Chemistry, 1988. **92**(20): p. 5726-5731.

59. Zhang, Z., et al., *Role of particle size in nanocrystalline TiO₂-based photocatalysts*. The Journal of Physical Chemistry B, 1998. **102**(52): p. 10871-10878.
60. Barni, B., et al., *Pilot-plant-scale photodegradation of phenol in aqueous solution by photocatalytic membranes immobilizing titanium dioxide (PHOTOPERM® process)*. Chemosphere, 1995. **30**(10): p. 1861-1874.
61. Pozzo, R.L., et al., *The performance in a fluidized bed reactor of photocatalysts immobilized onto inert supports*. Catalysis Today, 2000. **62**(2): p. 175-187.
62. Satoh, N., et al., *Quantum size effect in TiO₂ nanoparticles prepared by finely controlled metal assembly on dendrimer templates*. Nature Nanotechnology, 2008. **3**(2): p. 106-111.
63. Byrne, J.A., et al., *Immobilisation of TiO₂ powder for the treatment of polluted water*. Applied Catalysis B: Environmental, 1998. **17**(1): p. 25-36.
64. Ha, H.Y. and M.A. Anderson, *Photocatalytic degradation of formic acid via metal-supported titania*. Journal of Environmental Engineering, 1996. **122**(3): p. 217-221.
65. Gorokhovskii, A.V., et al., *Ceramic membranes for photocatalytic water purification*. Glass and Ceramics, 2011. **68**(5): p. 187-190.
66. Low, G.K.C. and R.W. Matthews, *Flow-injection determination of organic contaminants in water using an ultraviolet-mediated titanium dioxide film reactor*. Analytica chimica acta, 1990. **231**: p. 13-20.
67. Porkodi, K. and S.D. Arokiamary, *Synthesis and spectroscopic characterization of nanostructured anatase titania: A photocatalyst*. Materials Characterization, 2007. **58**(6): p. 495-503.
68. Anderson, M.A., M.J. Gieselmann, and Q. Xu, *Titania and alumina ceramic membranes*. Journal of Membrane Science, 1988. **39**(3): p. 243-258.
69. Bertoni, G., et al., *Quantification of crystalline and amorphous content in porous samples from electron energy loss spectroscopy*. Ultramicroscopy, 2006. **106**(7): p. 630-635.
70. Carp, O., C.L. Huisman, and A. Reller, *Photoinduced reactivity of titanium dioxide*. Progress in Solid State Chemistry, 2004. **32**(1-2): p. 33-177.
71. Deng, X., Y. Yue, and Z. Gao, *Gas-phase photo-oxidation of organic compounds over nanosized TiO₂ photocatalysts by various preparations*. Applied Catalysis B: Environmental, 2002. **39**(2): p. 135-147.
72. Watson, S.S., et al., *The effect of preparation method on the photoactivity of crystalline titanium dioxide particles*. Chemical Engineering Journal, 2003. **95**(1-3): p. 213-220.
73. Suttiponparnit, K., et al., *Role of Surface Area, Primary Particle Size, and Crystal Phase on Titanium Dioxide Nanoparticle Dispersion Properties*. Nanoscale Research Letters, 2011. **6**(1): p. 1-8.
74. O'Hayre, R., et al., *The Influence of TiO₂ Particle Size in TiO₂/CuInS₂ Nanocomposite Solar Cells*. Advanced Functional Materials, 2006. **16**(12): p. 1566-1576.
75. Austin, R.H. and S.-f. Lim, *The Sackler Colloquium on promises and perils in nanotechnology for medicine*. Proceedings of the National Academy of Sciences, 2008. **105**(45): p. 17217-17221.
76. Hurum, D.C., et al., *Explaining the Enhanced Photocatalytic Activity of Degussa P25 Mixed-Phase TiO₂ Using EPR*. The Journal of Physical Chemistry B, 2003. **107**(19): p. 4545-4549.
77. Emeline, A.V., V. Ryabchuk, and N. Serpone, *Factors affecting the efficiency of a photocatalyzed process in aqueous metal-oxide dispersions: Prospect of distinguishing between two kinetic models*. Journal of Photochemistry and Photobiology A: Chemistry, 2000. **133**(1-2): p. 89-97.
78. Gora, A., et al., *Photocatalytic oxidation of herbicides in single-component and multicomponent systems: Reaction kinetics analysis*. Applied Catalysis B, Environmental, 2006. **65**(1): p. 1-10.

79. Khataee, A.R., M. Fathinia, and S. Aber, *Kinetic Modeling of Liquid Phase Photocatalysis on Supported TiO₂ Nanoparticles in a Rectangular Flat-Plate Photoreactor*. Industrial & Engineering Chemistry Research, 2010. **49**(24): p. 12358-12364.
80. Mehrvar, M., et al., *Non-linear parameter estimation for a dynamic model in photocatalytic reaction engineering*. Chemical Engineering Science, 2000. **55**(21): p. 4885-4891.
81. Molinari, R., A. Caruso, and L. Palmisano, *3.07 - Photocatalytic Processes in Membrane Reactors*, in *Comprehensive Membrane Science and Engineering*, E. Drioli and L. Giorno, Editors. 2010, Elsevier: Oxford. p. 165-193.
82. Serpone, N., *Brief introductory remarks on heterogeneous photocatalysis*. Solar Energy Materials and Solar Cells, 1995. **38**(1-4): p. 369-379.
83. Salaices, M., B. Serrano, and H.I. de Lasa, *Photocatalytic conversion of phenolic compounds in slurry reactors*. Chemical Engineering Science, 2004. **59**(1): p. 3-15.
84. Ortiz-Gomez, A., et al., *Photocatalytic Oxidation of Phenol: Reaction Network, Kinetic Modeling, and Parameter Estimation*. Industrial & Engineering Chemistry Research, 2007. **46**(23): p. 7394-7409.
85. Hernández-Alonso, M.a.D., et al., *Ozone enhanced activity of aqueous titanium dioxide suspensions for photocatalytic oxidation of free cyanide ions*. Applied Catalysis B: Environmental, 2002. **39**(3): p. 257-267.
86. Aris, A., et al., *Influence of varying reacting conditions in the degradation of azo dye using immobilized TiO₂ photocatalyst*. Water Science & Technology, 2002. **46**(9): p. 255-262.
87. Cassano, A.E. and O.M. Alfano, *Reaction engineering of suspended solid heterogeneous photocatalytic reactors*. Catalysis Today, 2000. **58**(2-3): p. 167-197.
88. Li puma, G., *Dimensionless Analysis of Photocatalytic Reactors Using Suspended Solid Photocatalysts*. Chemical Engineering Research and Design, 2005. **83**(7): p. 820-826.
89. Barceló, D. and A. Alastuey, *Emerging Organic Contaminants and Human Health*. The Handbook of Environmental Chemistry. 2012: Springer.
90. Bhandari, A., et al., *Contaminants of emerging environmental concern*. 2009, Reston, Va: American Society of Civil Engineers.
91. Pal, A., et al., *Impacts of emerging organic contaminants on freshwater resources: Review of recent occurrences, sources, fate and effects*. Science of The Total Environment, 2010. **408**(24): p. 6062-6069.
92. Tyler, C., S. Jobling, and J.P. Sumpter, *Endocrine disruption in wildlife: a critical review of the evidence*. CRC Critical Reviews in Toxicology, 1998. **28**(4): p. 319-361.
93. Bull, R.J., A.R. Foundation, and A. United States. Environmental Protection, *Use of Toxicological and Chemical Models to Prioritize DBP Research*. 2006: AWWA Research Foundation.
94. Mohr, T.K.G. and J.A. Stickney, *Environmental Investigation and Remediation: 1,4-Dioxane and other Solvent Stabilizers*. 2010: CRC Press.
95. Mazurkiewicz, J. and P. Tomasik, *Why 1, 4-dioxane is a water-structure breaker*. Journal of molecular liquids, 2006. **126**(1): p. 111-116
96. Chemiasoft. http://www.chemiasoft.com/chemd/mdl_epa.
97. U.S. Environmental Protection Agency. *Integrated Risk Information System (IRIS) on 1,4-Dioxane*. National Center for Environmental Assessment, Office of Research and Development, Washington, DC. 1999.
98. Fetter, C.W. and C.W. Fetter Jr, *Contaminant hydrogeology*. Vol. 500. 1999: Prentice hall Upper Saddle River, NJ.
99. Fishbein, L., *Potential Industrial Carcinogens and Mutagens*. Studies in Environmental Science. 2011: Elsevier Science.
100. Nyer, E.K., *In Situ Treatment Technology, Second Edition*. Environmental science and engineering series. 2000: Taylor & Francis.

101. Schaechter, M., *Encyclopedia of Microbiology*. 2009: Elsevier Science.
102. Maurino, V., et al., *Light-assisted 1, 4-dioxane degradation*. *Chemosphere*, 1997. **35**(11): p. 2675-2688.
103. Stefan, M.I. and J.R. Bolton, *Mechanism of the degradation of 1, 4-dioxane in dilute aqueous solution using the UV/hydrogen peroxide process*. *Environmental science & technology*, 1998. **32**(11): p. 1588-1595.
104. '99 Rubber Conference: G-Mex Centre, Manchester : June 7/8/9 and 10 : the International Rubber Exhibition and Conference : Conference Book of Papers, ed. C.C. Limited. 1999: Rapra Technology Limited.
105. Schäfer, A.I., et al., *Micropollutants in water recycling: a case study of N-Nitrosodimethylamine (NDMA) exposure from water versus food*. *Sustainability Science and Engineering*, 2010. **2**: p. 203-228
106. *US EPA 2001 Western Groundwater Operable Unit OU-3, Aerojet Sacramento Site, Rancho Cordova, California*.
107. Knosmiller, S., et al., *Genotoxic effects of nitrosamines and cooked food mutagens in various organs of mice and their modification by dietary factors*. *Food and Cancer Prevention: Chemical and Biological Aspects of Anticarcinogens and Antimutagens*, Royal Society of Chemistry, Cambridge, 1993: p. 47-53.
108. Andrews, R.C., et al., *Impact of Chlorine Dioxide on Transmission, Treatment, and Distribution System Performance*. 2005: AWWA Research Foundation, American Water Works Association.
109. Nawrocki, J. and P. Andrzejewski, *Nitrosamines and water*. *Journal of Hazardous Materials*, 2011. **189**(1-2): p. 1-18.
110. Lv, J., Y. Li, and Y. Song, *Reinvestigation on the ozonation of N-nitrosodimethylamine: Influencing factors and degradation mechanism*. *Water research*, 2013. **47**(14): p. 4993-5002
111. Lee, C., J. Yoon, and U. Von Gunten, *Oxidative degradation of N-nitrosodimethylamine by conventional ozonation and the advanced oxidation process ozone/hydrogen peroxide*. *Water Research*, 2007. **41**(3): p. 581-590.
112. Reemtsma, T., J.B. Quintana, and R. Rodil, *Organophosphorus flame retardants and plasticizers in water and air I. Occurrence and fate*. *TrAC Trends in Analytical Chemistry*, 2008. **27**(9): p. 727-737.
113. Barnes, K.K., et al., *A national reconnaissance of pharmaceuticals and other organic wastewater contaminants in the United States—I) Groundwater*. *Science of the Total Environment*, 2008. **402**(2): p. 192-200.
114. Fries, E. and W. Püttmann, *Occurrence of organophosphate esters in surface water and ground water in Germany*. *Journal of Environmental Monitoring*, 2001. **3**(6): p. 621-626.
115. *Agency for Toxic Substances and Disease Registry (ATSDR) - MRLs. (2009). "Minimal Risk Levels for Hazardous Substances (MRLs). Sigma-Aldrich, Sigmaaldrich, 2011.*
116. *Sigma-Aldrich, Sigmaaldrich, 2011.*
117. *Atsdr, U.S., Agency for toxic substances and disease registry. Case Studies in Environmental Medicine./*<http://www.atsdr.cdc.gov/HEC/CSEM/csem.html> S, 2009.
118. Martínez-Carballo, E., et al., *Determination of selected organophosphate esters in the aquatic environment of Austria*. *Science of the total environment*, 2007. **388**(1): p. 290-299
119. Larson, R.A. and E.J.U. Weber, *Reaction Mechanisms in Environmental Organic Chemistry*. 1994: Taylor & Francis.
120. Ruan, X.-C., et al., *Photodegradation of Tri (2-chloroethyl) Phosphate in Aqueous Solution by UV/H₂O₂*. *Water, Air, & Soil Pollution*, 2013. **224**(1): p. 1-10
121. Aldrich, S.; Available from: <http://www.sigmaaldrich.com/>.

122. Bendz, D., et al., *Occurrence and fate of pharmaceutically active compounds in the environment, a case study: Høje River in Sweden*. Journal of Hazardous Materials, 2005. **122**(3): p. 195-204.
123. Heberer, T., *Occurrence, fate, and removal of pharmaceutical residues in the aquatic environment: a review of recent research data*. Toxicology letters, 2002. **131**(1): p. 5-17.
124. Araujo, L., et al., *Persistence of gemfibrozil, naproxen and mefenamic acid in natural waters*. Environmental Chemistry Letters, 2011. **9**(1): p. 13-18.
125. Daughton, C.G. and T.A. Ternes, *Pharmaceuticals and personal care products in the environment: agents of subtle change?* Environmental health perspectives, 1999. **107**(Suppl 6): p. 907.
126. Mimeault, C., et al., *The human lipid regulator, gemfibrozil bioconcentrates and reduces testosterone in the goldfish, Carassius auratus*. Aquatic Toxicology, 2005. **73**(1): p. 44-54.
127. Metcalfe, C.D., et al., *Estrogenic potency of chemicals detected in sewage treatment plant effluents as determined by in vivo assays with Japanese medaka (Oryzias latipes)*. Environmental Toxicology and Chemistry, 2001. **20**(2): p. 297-308
128. Murai, T., H. Iwabuchi, and T. Ikeda, *Identification of gemfibrozil metabolites, produced as positional isomers in human liver microsomes, by on-line analyses using liquid chromatography/mass spectrometry and liquid chromatography/nuclear magnetic resonance spectroscopy*. JOURNAL-MASS SPECTROMETRY SOCIETY OF JAPAN, 2004. **52**: p. 277-283.
129. Pubchem. Available from:
<http://pubchem.ncbi.nlm.nih.gov/summary/summary.cgi?cid=5757>.
130. Bhandari, A., et al., *Contaminants of Emerging Environmental Concern*. 2009: American Society of Civil Engineers.
131. Minkin, M.J. and C.V. Wright, *A Woman's Guide to Menopause & Perimenopause*. Yale University Press health & wellness. 2005: Yale University Press.
132. Bistan, M., et al., *The photocatalytic degradation of 17 α -ethynylestradiol by pure and carbon nanotubes modified TiO₂ under UVC illumination*. Central European Journal of Chemistry, 2012. **10**(4): p. 1137-1148.
133. Ohko, Y., et al., *17 β -Estradiol degradation by TiO₂ photocatalysis as a means of reducing estrogenic activity*. Environmental science & technology, 2002. **36**(19): p. 4175-4181.
134. (EPA), E.P.A. *MDL, 40 CFR Part 136. APPENDIX B, revision 1.11*. 2011; Available from:
http://www.chemiasoft.com/chemd/mdl_epa.
135. Wong, C.C. and W. Chu, *The direct photolysis and photocatalytic degradation of alachlor at different TiO₂ and UV sources*. Chemosphere, 2003. **50**(8): p. 981-987.
136. Brandi, R.J., et al., *A Laboratory Reactor for Photocatalytic Studies in Slurry Operation*. Journal of Advanced Oxidation Technologies, 2002. **5**(2): p. 175-185.
137. Wang, L.K., et al., *Environmental Bioengineering: Volume 11*. 2010: Humana Press.
138. *Marvin 15.3.9.0 (master-2684), 201n (2015), ChemAxon* (<http://www.chemaxon.com>).
139. Combourieu, B., et al., *Thiomorpholine and morpholine oxidation by a cytochrome P450 in Mycobacterium aurum MO1. Evidence of the intermediates by in situ 1H NMR*. Biodegradation, 1998. **9**(6): p. 433-442
140. Watson, G.K., C. Houghton, and R.B. Cain, *Microbial metabolism of the pyridine ring. The hydroxylation of 4-hydroxypyridine to pyridine-3, 4-diol (3, 4-dihydroxypyridine) by 4-hydroxypyridine 3-hydroxylase*. Biochem. J, 1974. **140**: p. 265-276.
141. Turnbull, M., <http://eawag-bbd.ethz.ch/servlets/rule.jsp?rule=bt0351>. EAWAG-BBD biotransformation rule, ruleID# bt0351, 2015.
142. Turnbull, M., <http://eawag-bbd.ethz.ch/servlets/rule.jsp?rule=bt0352>. EAWAG-BBD biotransformation rule, ruleID# bt0352., 2010.

143. Shaw, J.P. and S. Harayama, *Purification and characterisation of the NADH: acceptor reductase component of xylene monooxygenase encoded by the TOL plasmid pWVO of Pseudomonas putida mt-2*. European Journal of Biochemistry, 1992. **209**(1): p. 51-61
144. Tojo, G. and M. Fernandez, *Oxidation of Alcohols to Aldehydes and Ketones: A Guide to Current Common Practice*. 2006: Springer.
145. Keat, M.J. and D.J. Hopper, *Aromatic aldehyde dehydrogenase from Pseudomonas putida NCIB 9869*. Biochem Soc Trans, 1975. **3**(3): p. 385-386.
146. Mahajan, M.C., P.S. Phale, and C.S. Vaidyanathan, *Evidence for the involvement of multiple pathways in the biodegradation of 1-and 2-methylnaphthalene by Pseudomonas putida CSV86*. Archives of microbiology, 1994. **161**(5): p. 425-433
147. Poelarends, G.J., et al., *Degradation of 1, 3-dichloropropene by Pseudomonas cichorii 170*. Applied and environmental microbiology, 1998. **64**(8): p. 2931-2936
148. Hiser, L., M.E. Basson, and J. Rine, *ERG10 from Saccharomyces cerevisiae encodes acetoacetyl-CoA thiolase*. Journal of Biological Chemistry, 1994. **269**(50): p. 31383-31389
149. Campos-García, J., et al., *The branched-chain dodecylbenzene sulfonate degradation pathway of Pseudomonas aeruginosa W51D involves a novel route for degradation of the surfactant lateral alkyl chain*. Applied and environmental microbiology, 1999. **65**(8): p. 3730-3734
150. Enroth, C., et al., *The crystal structure of phenol hydroxylase in complex with FAD and phenol provides evidence for a concerted conformational change in the enzyme and its cofactor during catalysis*. Structure, 1998. **6**(5): p. 605-617.
151. Hernáez, M.J., et al., *Identification of a hydratase and a class II aldolase involved in biodegradation of the organic solvent tetralin*. Applied and environmental microbiology, 2002. **68**(10): p. 4841-4846
152. Armstrong, S.M. and T.R. Patel, *Microbial degradation of phloroglucinol and other polyphenolic compounds*. Journal of basic microbiology, 1994. **34**(2): p. 123-135.
153. Grant, D.J.W. and J.C. Patel, *The non-oxidative decarboxylation of p-hydroxybenzoic acid, gentisic acid, protocatechuic acid and gallic acid by Klebsiella aerogenes (Aerobacter aerogenes)*. Antonie van Leeuwenhoek, 1969. **35**(1): p. 325-343
154. Casellas, M., et al., *New metabolites in the degradation of fluorene by Arthrobacter sp. strain F101*. Applied and environmental microbiology, 1997. **63**(3): p. 819-826.
155. Zhao, Y., J. Hu, and W. Jin, *Transformation of oxidation products and reduction of estrogenic activity of 17 β -estradiol by a heterogeneous photo-Fenton reaction*. Environmental science & technology, 2008. **42**(14): p. 5277-5284
156. Kasprzyk-Hordern, B., *Chemistry of alumina, reactions in aqueous solution and its application in water treatment*. Advances in colloid and interface science, 2004. **110**(1): p. 19-48
157. Byrne, J.A. and P. Fernández-Ibáñez, *Solar Photocatalytic Treatment of Wastewater*. Wastewater Treatment: Advanced Processes and Technologies, 2012: p. 37
158. Yoon, S.-H. and J.H. Lee, *Oxidation mechanism of As (III) in the UV/TiO₂ system: evidence for a direct hole oxidation mechanism*. Environmental science & technology, 2005. **39**(24): p. 9695-9701
159. Molinari, R., et al., *Heterogeneous photocatalytic degradation of pharmaceuticals in water by using polycrystalline TiO₂ and a nanofiltration membrane reactor*. Catalysis Today, 2006. **118**(1): p. 205-213
160. Comerton, A.M., et al., *Membrane adsorption of endocrine disrupting compounds and pharmaceutically active compounds*. Journal of Membrane Science, 2007. **303**(1): p. 267-277
161. Kabasakalian, P., E. Britt, and M.D. Yudis, *Solubility of some steroids in water*. Journal of pharmaceutical sciences, 1966. **55**(6): p. 642-642
162. Delleur, J.W., *The Handbook of Groundwater Engineering, Second Edition*. 2006: CRC Press.
163. Milne, G.W., *Gardner's Commercially Important Chemicals: Synonyms, Trade Names, and Properties*. 2005: Wiley.

164. Mohr, T.K.G., *Solvent stabilizers*. Santa Clara Valley Water District, White Paper, 2001.
165. Inagaki, S.U., *Orbitals in Chemistry*. 2009: Springer.
166. Draber, W. and T.U. Fujita, *Rational Approaches to Structure, Activity, and Ecotoxicology of Agrochemicals*. 1992: Taylor & Francis.
167. McGuire, M.J., I.H. Suffet, and J.V. Radziul, *Assessment of unit processes for the removal of trace organic compounds from drinking water*. Journal (American Water Works Association), 1978: p. 565-572.
168. Kwon, S.C., et al., *Treatment characteristic of 1,4-dioxane by ozone-based advanced oxidation processes*. Journal of Industrial and Engineering Chemistry, 2012.
169. Zenker, M.J., R.C. Borden, and M.A. Barlaz, *Occurrence and treatment of 1, 4-dioxane in aqueous environments*. Environmental Engineering Science, 2003. **20**(5): p. 423-432.
170. Nakajima, A., et al., *Sonophotocatalytic destruction of 1, 4-dioxane in aqueous systems by HF-treated TiO₂ powder*. Journal of Photochemistry and Photobiology A: Chemistry, 2004. **167**(2): p. 75-79
171. Kishimoto, N., et al., *Applicability of ozonation combined with electrolysis to 1, 4-dioxane removal from wastewater containing radical scavengers*. Ozone: Science and Engineering, 2007. **29**(1): p. 13-22.
172. Bliss, J., *MS thesis "Treatment of 1,4-dioxane in Water: Sustainable Treatment Options"*, WPI. 2014.
173. Otto, M. and S. Nagaraja, *Treatment technologies for 1,4-Dioxane: Fundamentals and field applications*. Remediation Journal, 2007. **17**(3): p. 81-88.
174. Safarzadeh-Amiri, A., J.R. Bolton, and S.R. Cater, *Ferrioxalate-mediated photodegradation of organic pollutants in contaminated water*. Water Research, 1997. **31**(4): p. 787-798.
175. Jobb, B., *Removal of N-nitrosodimethylamine(NDMA) from the Ohsweken(Six Nations) water supply: Interim report*. 1993.
176. Jobb, D.B., et al. *A study of the occurrence and inhibition of formation of N-nitrosodimethylamine (NDMA) in the Ohsweken water supply Winnipeg, Manitoba, Canada*. . 1992.
177. Landsman, N.A., et al., *Free radical chemistry of advanced oxidation process removal of nitrosamines in water*. Environmental science & technology, 2007. **41**(16): p. 5818-5823.
178. Reinhard, M., et al., *From effluent to new water: Performance evaluation and quality assurance*. CHIMIA International Journal for Chemistry, 2003. **57**(9): p. 561-566.
179. Sharpless, C.M. and K.G. Linden, *Experimental and model comparisons of low-and medium-pressure Hg lamps for the direct and H₂O₂ assisted UV photodegradation of N-nitrosodimethylamine in simulated drinking water*. Environmental science & technology, 2003. **37**(9): p. 1933-1940.
180. Lee, C., et al., *UV Photolytic Mechanism of N-Nitrosodimethylamine in Water: Dual Pathways to Methylamine versus Dimethylamine*. Environmental Science & Technology, 2005. **39**(7): p. 2101-2106.
181. Mitch, W.A., et al., *N-nitrosodimethylamine (NDMA) as a drinking water contaminant: a review*. Environmental Engineering Science, 2003. **20**(5): p. 389-404.
182. Lee, C., et al., *Oxidation of N-nitrosodimethylamine (NDMA) precursors with ozone and chlorine dioxide: kinetics and effect on NDMA formation potential*. Environmental science & technology, 2007. **41**(6): p. 2056.
183. Plumlee, M.H., et al., *N-nitrosodimethylamine (NDMA) removal by reverse osmosis and UV treatment and analysis via LC-MS/MS*. Water Research, 2008. **42**(1): p. 347-355.
184. Jong-Oh Kim, et al., *Removal of refractory compounds by ultraviolet and anodized TiO₂ metal membrane with reactive nano-sized cylindrical tubes on its surface*. Desalination and Water Treatment, 2011. **34**(1-3): p. 304-308.

185. Stefan, M.I. and J.R. Bolton, *UV direct photolysis of N-nitrosodimethylamine (NDMA): Kinetic and product study*. Helvetica Chimica Acta, 2002. **85**(5): p. 1416-1426.
186. Liang, S., et al., *Use of pulsed-UV processes NDMA to destroy*. Journal-American Water Works Association, 2003. **95**(9): p. 121-131.
187. Votruba, M.J., *MS thesis "Ozonation of Tris-2-Chloroethyl Phosphate (TCEP) in Water"*, WPI. 2013.
188. Pisarenko, A.N., et al., *Effects of ozone and ozone/peroxide on trace organic contaminants and NDMA in drinking water and water reuse applications*. Water research, 2012. **46**(2): p. 316-326.
189. Snyder, S.A., et al., *Ozone Oxidation of Endocrine Disruptors and Pharmaceuticals in Surface Water and Wastewater*. Ozone: Science & Engineering, 2006. **28**(6): p. 445-460.
190. Benotti, M.J., et al., *Evaluation of a photocatalytic reactor membrane pilot system for the removal of pharmaceuticals and endocrine disrupting compounds from water*. Water Research, 2009. **43**(6): p. 1513-1522.
191. Nguyen, H., *MS thesis "Advanced Oxidation of Tris-2-Chloroethyl Phosphate (TCEP) in Water"*, WPI. 2011.
192. Westerhoff, P., et al., *Fate of endocrine-disruptor, pharmaceutical, and personal care product chemicals during simulated drinking water treatment processes*. Environmental Science & Technology, 2005. **39**(17): p. 6649-6663.
193. Kim, S.D., et al., *Occurrence and removal of pharmaceuticals and endocrine disruptors in South Korean surface, drinking, and waste waters*. Water research, 2007. **41**(5): p. 1013-1021.
194. Molinari, R., et al., *Photo assisted fenton in a batch and a membrane reactor for degradation of drugs in water*. Separation Science and Technology, 2007. **42**(7): p. 1597-1611
195. Snyder, S.A., et al., *Role of membranes and activated carbon in the removal of endocrine disruptors and pharmaceuticals*. Desalination, 2007. **202**(1-3): p. 156-181.
196. Molinari, R., et al., *Degradation of the drugs Gemfibrozil and Tamoxifen in pressurized and de-pressurized membrane photoreactors using suspended polycrystalline TiO₂ as catalyst*. Journal of Membrane Science, 2008. **319**(1): p. 54-63.
197. Kim, S.-E., H. Yamada, and H. Tsuno, *Evaluation of estrogenicity for 17 β -estradiol decomposition during ozonation*. Ozone: Science and Engineering, 2004. **26**(6): p. 563-571.
198. Coleman, H.M., et al., *Photocatalytic degradation of 17- β -oestradiol on immobilised TiO₂*. Applied Catalysis B: Environmental, 2000. **24**(1): p. L1-L5.
199. Yurdakal, S., et al., *Photodegradation of pharmaceutical drugs in aqueous TiO₂ suspensions: Mechanism and kinetics*. Catalysis Today, 2007. **129**(1): p. 9-15.
200. Loebl, H., G. Stein, and J. Weiss, *89. Chemical actions of ionising radiations on aqueous solutions. Part VIII. Hydroxylation of benzoic acid by free radicals produced by X-rays*. Journal of the Chemical Society (Resumed), 1951: p. 405-407.
201. Johnson, G.R.A., G. Stein, and J. Weiss, *724. Some free-radical reactions of chlorobenzene. The action of the hydrogen peroxide-ferrous salt reagent and of X-rays on aqueous solutions of chlorobenzene*. J. Chem. Soc., 1951: p. 3275-3278
202. Kodama, S. and S. Yagi, *Photocatalytic hydrogenation, decomposition and isomerization reactions of alkenes over TiO₂-adsorbed water*. J. Chem. Soc., Faraday Trans., 1992. **88**(12): p. 1685-1690
203. Guisnet, M., N.S. Gnep, and S. Morin, *Mechanisms of xylene isomerization over acidic solid catalysts*. Microporous and mesoporous materials, 2000. **35**: p. 47-59
204. Riyas, S., G. Krishnan, and P.N. Mohan Das, *Liquid phase photooxidation of toluene in the presence of transition metal oxide doped titania*. Journal of the Brazilian Chemical Society, 2008. **19**(5): p. 1023-1032

205. Terzian, R. and N. Serpone, *Heterogeneous photocatalyzed oxidation of creosote components: mineralization of xylenols by illuminated TiO₂ in oxygenated aqueous media*. Journal of Photochemistry and Photobiology A: Chemistry, 1995. **89**(2): p. 163-175
206. Huang, M.Q., et al., *Low-Molecular Weight and Oligomeric Components in Secondary Organic Aerosol from the Photooxidation of p-Xylene*. Journal of the Chinese Chemical Society, 2008. **55**(2): p. 456-463
207. Park, H. and W. Choi, *Photocatalytic conversion of benzene to phenol using modified TiO₂ and polyoxometalates*. Catalysis Today, 2005. **101**(3): p. 291-297
208. Koenig, G., et al., *Chloroacetic acids*. Ullmann's Encyclopedia of Industrial Chemistry
209. Afzal Pasha, M., K. Manjula, and V. Puttaramgowda Jayashankara, *Titanium Dioxide-Mediated Friedel-Crafts Acylation of Aromatic Compounds in Solvent-Free Condition under Microwave Irradiation*. Synthesis and Reactivity in Inorganic and Metal-Organic Chemistry, 2006. **36**(4): p. 321-324
210. Salvatore, R.N., C.H. Yoon, and K.W. Jung, *Synthesis of secondary amines*. Tetrahedron, 2001. **57**(37): p. 7785-7811
211. Bruckner, R. and M.U. Harmata, *Organic Mechanisms: Reactions, Stereochemistry and Synthesis*. 2010: Spektrum Akademischer Verlag GmbH.
212. Katritzky, A.R., D.L. Ostercamp, and T.I. Yousaf, *The mechanisms of heterocyclic ring closures*. Tetrahedron, 1987. **43**(22): p. 5171-5186
213. Chemspider. Available from: <http://www.chemspider.com/>.
214. Sangster, J., *Octanol-Water Partition Coefficients: Fundamentals and Physical Chemistry*. Wiley Series in Solutions Chemistry. 1997: Wiley.
215. Spero, J.M., B. DeVito, and L. Theodore, *Regulatory Chemicals Handbook*. Chemical Industries. 2000: Taylor & Francis.
216. Sigma Aldrich. <http://www.sigmaaldrich.com/analytical-chromatography/sample-preparation/spe/tube-configuration-guide.html>.
217. Nudelman, N., *Química sustentable*. 2004: Ediciones UNL.
218. Sogaard, E., *Chemistry of Advanced Environmental Purification Processes of Water: Fundamentals and Applications*. 2014: Elsevier Science.